Analytical Methods for Energy Storage Design in Hybrid Renewable Systems

Han Kun Ren

Oriel College

University of Oxford

A thesis submitted for the degree of

Doctor of Philosophy

Michaelmas 2024

Abstract

The need for storage design stems from rising greenhouse gas emissions, a key contributor to climate change. A significant portion of global greenhouse gas emissions originates from the energy sector due to fossil fuel usage. An alternative to fossil fuels is renewable energy. Renewable generation produces no emissions during operation and have lower life-cycle emissions compared to fossil fuel power plants. However, renewables are weather-dependent, leading to intermittent and non-dispatchable generation. This intermittency induces instability in the electricity system, while the lack of dispatchability results in curtailed generation and unmet demand. These challenges can be effectively managed through energy storage. Storage captures surplus energy during periods of high generation, and releases that energy during low generation, resulting in a more consistent generation output that can match the demand. Proper storage design ensures that storage can effectively manage renewable intermittency and provide dispatchability.

The thesis explores storage design, encompassing storage sizing, storage and solar sizing, and storage sizing and placement. First, an analytical method is proposed to size storage based on its largest cumulative charge or discharge. The method is applied to two case studies. The first study demonstrates that optimally sized storage does not have wasted capacity due to over-sizing, nor does it cause energy deficits due to under-sizing. The second study finds that increasing the storage size has diminishing returns on the additional storage energy provided to the system. Second, the thesis proposes a hybridized techno-economic method to size solar photovoltaic and lithium battery storage. The hybridized method uses an analytical method to define the size search space, and then employs an enumerative approach to explore the search space to find the lowest-cost system sizing. The method is applied to a solar-battery microgrid case study, which finds that solar and storage will take up a greater portion of the energy system as their costs come down, but the electricity grid remains essential for providing cost-effective flexibility. Third, the thesis proposes an analytical method for sizing and placing energy storage. The method uses optimal power flow to decide the power dispatch at each location. Then, the analytical method is employed to size and place storage based on the power dispatch. The method is applied to a case study on a village with wind and solar generation. The study finds that storage tends to be placed near large generation, large demand, or lines with high power flow. These works contribute to the purpose of the thesis, which is to gain a better understanding of storage design in the context of hybrid renewable systems.

Acknowledgements

There are inflection points in life where a single event can alter one's course. One such moment occurred on an early morning when I interviewed for a Master's in Energy Systems at the University of Oxford. Little did I know that my interviewers, David Wallom and Malcolm McCulloch, would become my mentors for the next five years, shaping my life trajectory in more ways than I could have imagined. For that, I am profoundly grateful. Thank you for giving me the opportunity, and thank you for changing my life.

David, I am grateful for your constant guidance and support. Thank you for your steadfast patience, thank you for the lunchtime chats, and thank you for all the time you have dedicated to me despite your busy schedule. Thank you for starting the Master's in Energy Systems, and I know you will change the lives of many more aspiring students. Most importantly, thank you for showing me the beautiful world of academia.

Malcolm, I am thankful for your sound advice and fresh ideas. Thank you for the workshops, for showing me your new Tesla, and for the office snacks. Most importantly, thank you for starting the Energy Systems Accelerator, which provided a space for our groups to gather under one roof, enabling me to meet many amazing people in your group.

I would also like to thank the postdoctoral researchers in our group: Devki Nanda Jha, Maomao Hu, and Weiqi Hua. You were not only my mentors in the office, but also my friends outside the office. The fond memories from our trips together are ones I will treasure. Although it was sad to see you leave Oxford, I am so happy that all of you have moved on to the next stages of your lives, and become professors at prestigious universities.

To the DPhil students and researchers in our group: Sara Abdelaziz, Rohan Agrawal, Andy Bowery, Martin Higgins, Maitha Al Shimmari, Katya Soegiharto, Sarah Sparrow, and Weijia Yang, thank you for your friendship. You have greatly enriched my experience at Oxford. I would also like to thank Graeme Smith, Steven Williams, and Judy Dendy for your contributions in supporting the Oxford e-Research Centre.

To the friends I have met along the way during my education and work, thank you all for being part of my life. A special thank you to Bolin Gao, Clarence Li, Calvin Kuang, and Adrian Lambert for our travels together and the many fond memories we have created. Your companionship, laughter, and support have made this journey all the more meaningful.

Lastly, I would like to thank my parents, thank you for supporting me throughout my life. I left home to pursue my dreams, and when I returned afterward, the wrinkles on my mom's face and the white hair on my dad's head really saddened me. Although time will inevitably pass, I hope you both remain safe and healthy. In the next stage of my life, I wish to spend more time with you, and to support you as you have supported me throughout my life. Perhaps no words can fully express how I feel, but thank you for being my parents.

Contents

List of Figures

List of Tables

Nomenclature

α	multiplier
$\bar{x}$	mean value
Δt	time interval (hour)
ϵ	permissible difference limit
η	storage power efficiency
η_c	charge efficiency
η_d	discharge efficiency
ϕ	transformer phase shift angle ($\circ$)
ρ	degradation factor
σ	storage energy leakage rate (%/hour)
τ	transformer tap ratio
θ	voltage angle
θ_{ref}	reference bus voltage angle ($\circ$)
b	binary decision variable
B_{ij}	susceptance element of bus admittance matrix
$\mathbf{C}$	critical point matrix
C^0	generator cost constant coefficient
C^1	generator cost linear coefficient
C^2	generator cost quadratic coefficient
C^{GR}	grid electricity import's annual cost (GBP)
C^{PV}	solar PV system's annualized cost (GBP)
C^S	storage size cost coefficient
C^{ST}	storage system's annualized cost (GBP)
C_c	charge C-rating
C_d	discharge C-rating
D	demand power (kW)
$\mathbf{D}$	difference matrix
D_{tot}	annual electricity demand (kWh)

DoD	depth of discharge (%)
DoD_{max}	maximum depth of discharge (%)
DoD_{min}	minimum depth of discharge (%)
E	storage size (kWh)
E^{GR}	grid electricity import (kWh)
E^{PV}	solar PV capacity (kW)
E^{PV}_{max}	maximum solar PV capacity (kW)
E^{S}	storage size (kWh)
E^{S}_{max}	maximum storage size (kWh)
E_{thru}	annual energy throughput (kWh/year)
E_{tot}	storage's total energy capacity (kWh)
E^{S}_{tot}	storage's total energy capacity (kWh)
F^{PV}_{min}	minimum solar PV capacity factor
F^{PV}_{t}	solar PV capacity factor
G_{ij}	conductance element of bus admittance matrix
G	generation power (kW)
I	branch current flow
i	bus index
I^{PV}	solar PV system's installed cost per capacity (GBP/kW)
I^{S}	storage system's installed cost per capacity (GBP/kWh)
I_{max}	maximum branch current flow limit
$\mathbf{I}_{bus}$	bus current flow vector
ij	branch index
K^{GR}	grid electricity price (GBP/kWh)
$\mathbf{L}$	lower triangular matrix
$LCOE$	levelized cost of electricity (GBP/kWh)
M	large number
N	storage cycle life (cycle)
n	transformer turn ratio
n^{PV}	solar PV system's lifespan (year)
n^{S}	storage system's lifespan (year)

O^{PV}	solar PV system's annual operation and maintenance cost per capacity (GBP/kW)
O^{S}	storage system's annual operation and maintenance cost per capacity (GBP/kWh)
P^{G}	generator active power (kW)
P^{L}	load demand active power (kW)
P^{PV}	solar PV generation power (kW)
P^{S}	storage active power (kW)
P_c	storage maximum charge rate (kW)
P_c^S	allowable storage charge power (kW)
P_d	storage maximum discharge rate (kW)
P_d^S	allowable storage discharge power (kW)
P_i	bus active power injection
P_{low}^S	storage lower power limit (kW)
P_{max}^G	maximum generator active power limit (kW)
P_{max}^S	maximum storage power limit (kW)
P_{min}^G	minimum generator active power limit (kW)
P_{min}^S	minimum storage power limit (kW)
P_{up}^S	storage upper power limit (kW)
Q^{G}	generator reactive power (kVAR)
Q^{L}	load demand reactive power (kW)
Q^{S}	storage reactive power (kW)
Q_i	bus reactive power injection
Q_{max}^G	maximum generator reactive power limit (kW)
Q_{min}^G	minimum generator reactive power limit (kW)
r	discount rate (%)
r_n	randomized data from normal distribution
r_u	randomized data from uniform distribution
s	standard deviation
S	storage energy level (kWh)
$\mathbf{S}$	critical storage level vector

S_0	starting storage level (kWh)
$\mathbf{S}_{bus}$	bus apparent power injection vector
S_i	bus apparent power injection
S_{low}	lower storage energy limit (kWh)
S_{max}	maximum storage energy limit (kWh)
S_{min}	minimum storage energy limit (kWh)
S_{t_n}	critical storage level (kWh)
S_T	ending storage level (kWh)
S_{up}	upper storage energy limit (kWh)
S_s	sustainable starting or ending storage level (kWh)
SOC	state of charge (%)
T	time at the end of the design time horizon (hour)
t	time step in the first design time horizon (hour)
t'	time step in the second design time horizon (hour)
T_{cal}	storage calendar life (year)
T_{life}	storage lifespan (year)
t_n	time at critical point (hour)
V	voltage magnitude (V)
$\mathbf{V}$	bus voltage magnitude vector
V_{max}	maximum bus voltage magnitude limit (V)
V_{min}	minimum bus voltage magnitude limit (V)
V_{ref}	reference bus voltage magnitude (V)
x	historical data
y	branch series admittance
Y	admittance element of the bus admittance matrix
$\mathbf{Y}_{br}$	branch admittance matrix
$\mathbf{Y}_{bus}$	bus admittance matrix
y^s	bus shunt admittance
y^{sh}	branch shunt admittance
$\mathbf{1}$	all-ones vector

1 Introduction

Contents

1.1 Background

In recent years, we have witnessed record-breaking heat waves, devastating forest fires, more frequent hurricanes, and catastrophic floods, along with irregular snowstorms causing electricity blackouts [1]. It is hard to deny that our climate is changing, leading to more frequent extreme weather events. Greenhouse gas emissions have long been recognized as the primary driver of climate change. The Paris Agreement has drawn the world's attention to dealing with climate change [2]. The agreement explicitly calls for the reduction of greenhouse gas emissions, with the aim of limiting the temperature increase to less than 2°C above pre-industrial levels. Many signatory nations to the agreement have vowed to become carbon-neutral by 2050. However, current data show that more than 73% of our emissions come from the energy sector due to fossil fuels [3]. As the world continues to develop, so too will our hunger for energy.

Renewable energy provides an emission-free alternative to fossil fuels. Renewable generation, such as solar and wind, produces no emissions during operation, and has lower life-cycle emissions than fossil fuel power plants [4]. The renewable industry has seen tremendous growth in recent years. In many countries, solar farms already produce electricity significantly cheaper than fossil fuel power plants [5]. Renewable energy is not only becoming more cost-effective, but also less constrained by geographical limitations. Solar and wind energy are available anywhere, making them suitable for remote communities, where the electricity grid cannot reach [6]. The benefits in terms of environmental impact, economics, and accessibility provide renewable energy with a unique advantage over fossil fuels. Embracing renewable energy will not only reduce our reliance on fossil fuels, but also alleviate the environmental impact associated with their use.

However, renewable sources, such as solar and wind, are weather-dependent, meaning they can only generate energy when the wind blows or when the sun shines [7]. These renewables cannot generate energy consistently, and their intermittent generation poses a challenge for electrical systems designed to operate at specific voltage and frequency levels [8]. The intermittency could destabilize the grid.

Moreover, many renewables lack natural energy storage, which means they are not dispatchable and cannot control generation to match demand [9]. The lack of dispatchability creates mismatches between generation and demand, resulting in curtailed generation and unmet demand. The intermittency and non-dispatchability pose major challenges in integrating renewables with existing energy systems.

Energy storage can mitigate renewable intermittency and non-dispatchability. Storage regulates renewable intermittency by capturing surplus energy during high generation periods and releasing that energy during low generation, resulting in a more consistent generation output [10]. Additionally, storage can discharge the stored energy to supplement periods of excess demand, effectively providing dispatchability to renewables. Proper storage design ensures sufficient capacity for charging and discharging energy as needed. Moreover, proper design prevents unutilized or wasted storage, minimizes system losses, and maintains a reasonable system cost.

1.2 Motivation

Storage design is crucial to ensuring the proper functioning of energy storage in hybrid renewable systems. There are four main approaches for energy storage design: enumerative, mathematical optimization, meta-heuristic optimization, and analytical. The enumerative approach systematically iterates through system sizes within a defined search range, simulating the system at each iteration to find the lowest-cost system size [11]. The meta-heuristic approach is similar to the enumerative approach, with the difference being that, instead of iterating through the entire search space, meta-heuristic algorithms smartly navigate the search space to find the optimal solution [12]. The mathematical optimization approach uses optimization algorithms to optimize storage design based on objective and constraint equations describing the energy system [13]. The analytical approach utilizes storage models to construct the storage energy profile and subsequently determines the storage size based on the storage profile [14].

The enumerative approach is simple to implement, but it is calculation-intensive, making it unsuitable for problems with a large solution space. Meta-heuristic

methods are also easy to implement and can handle complex non-convex models. However, most meta-heuristic algorithms are stochastic, which makes them relatively slow and unable to guarantee global optimality. In contrast, some mathematical optimization methods are faster and can guarantee global optimality, but they struggle with non-linear and non-convex models. Analytical methods offer a balance of strengths. They are faster than meta-heuristic methods and can handle non-linear and non-convex models. Moreover, they converge to the global optimum when coupled with convex models and can converge to near-optimal solutions when coupled with non-convex models. Their design approach is physics-based, which makes them more explainable and enables a deeper understanding of the reasoning behind the design. This is in contrast to other approaches, which find solutions through trial and error or complex black-box algorithms.

A limited number of analytical methods are available for storage design, and they exhibit limitations that hinder their broad applicability. Some analytical methods may fail when dealing with erratic storage profiles, while others do not yield optimal sizing and placement. Some analytical methods are only designed for energy systems with over-generation, making them unsuitable for other systems. Additionally, most analytical methods do not consider storage energy leakage, which can impact long-term storage sizing. Some methods also neglect storage power limits, resulting in designs with unrealistic power requirements. Some analytical methods do not require equal starting and ending storage levels, rendering the storage profile non-repeatable for future time horizons. The lack of repeatability means the storage size is valid only for the current time horizon and not for future time horizons. The thesis aims to address these issues and provide a better understanding of energy storage design in hybrid renewable systems.

1.3 Contribution

Chapter 3 presents an analytical method to optimally size energy storage. The method first constructs a temporal storage profile of stored energy based on how the storage is charged and discharged in response to generation and demand. The

storage is sized according to the largest cumulative charge or discharge in the profile. The major contributions made in this chapter are as follows:

- The proposed sizing algorithm is based on a new theory that storage should be sized according to the largest cumulative charge or discharge it is expected to experience, depending on whether it is accumulating or depleting energy over the design time horizon.
- The proposed method has a fast calculation speed when applied to a reasonably sized dataset, calculates the optimal size that maximizes storage energy utilization, and can handle non-linear models.
- The proposed method yields the optimal storage size that maximizes storage energy utilization while eliminating unutilized storage capacity. When the system operates under a conventional operation strategy, maximizing storage utilization can also maximize renewable consumption.
- The method is extended iteratively to account for depth of discharge, maximum charge and discharge rates, and storage leakage. Storage leakage is often ignored in other analytical methods but is shown to affect long-term storage sizing.

Chapter 4 presents a hybridized techno-economic method to size solar PV (photovoltaic) and lithium storage systems. The hybridized method uses an analytical method to calculate the maximum storage and solar sizes. The maximum sizes are used to define the search space, and an enumerative approach is employed to systematically iterate through the search space to find the lowest-cost system sizing. The contributions of this chapter are summarized as follows:

- Novel analytical method that calculates maximum solar and storage system sizes, which are used to define the size search space boundary. The bounded search space guarantees optimal sizing while reducing the number of search iterations.

- The design space explores the relationship between solar capacity, storage capacity, and the amount of grid electricity imports required to support the demand.

- Most studies do not account for the future trend of solar PV and lithium battery composition in the energy system. This study analyzes that trend using solar and battery system cost projections.

Chapter 5 presents a hybridized analytical and mathematical optimization method for sizing and placing energy storage. The method uses optimal power flow to determine the power dispatch at each location. The storage power dispatch is used to construct the storage profile, and an analytical method is employed to size and place storage based on the profiles. The major contributions made in this chapter are as follows:

- The proposed method yields the optimal storage size and placement, achieving the smallest total storage size that minimizes generator costs. The generator cost is minimized by maximizing storage utilization, and the small storage size is achieved by eliminating wasted storage capacity through the analytical method.

- The proposed method is faster than meta-heuristic methods, handles non-convex models better than mathematical optimization methods, and demonstrates effective convergence to optimal sizing and placement.

- The proposed method is a technical approach that operates without requiring storage cost data. This stands in contrast to other methods, where errors in storage cost estimates can lead to inaccuracies in storage sizing and placement.

1.4 Publication

The work in this thesis is based on research carried out during the DPhil. Parts of this work have been published in the following papers. Below are the published

and planned publications associated with each chapter and their corresponding CRediT (Contributor Roles Taxonomy) author statement:

Chapter 3: Han Kun Ren, Masao Ashtine, Malcolm McCulloch, David Wallom. (2023). An analytical method for sizing energy storage in microgrid systems to maximize renewable consumption and minimize unused storage capacity. Journal of Energy Storage, 68, 107735.

- Han Kun Ren: Conceptualization, Methodology, Software, Validation, Formal Analysis, Investigation, Writing – original draft, Visualization.
- Masaō Ashtine: Writing – review & editing.
- Malcolm McCulloch: Writing – review & editing, Supervision.
- David Wallom: Conceptualization, Resources, Data Curation, Writing – review & editing, Supervision.

Chapter 4: Han Kun Ren, Malcolm McCulloch, David Wallom. (2022). Optimal sizing of solar photovoltaic and lithium battery storage to reduce grid electricity reliance in buildings. ECEEE 2022 Summer Study on Energy Efficiency: Agents of Change, 1199-1208.

- Han Kun Ren: Conceptualization, Methodology, Software, Validation, Formal Analysis, Investigation, Writing – original draft, Visualization.
- Malcolm McCulloch: Conceptualization, Writing – review & editing, Supervision.
- David Wallom: Conceptualization, Resources, Data Curation, Writing – review & editing, Supervision, Funding acquisition.

Chapter 5: Han Kun Ren, Malcolm McCulloch, David Wallom. Energy storage capacity sizing and site placement in renewable systems using optimal power flow to minimize generator cost and maximize storage utilization.

- Han Kun Ren: Conceptualization, Methodology, Software, Validation, Formal Analysis, Investigation, Writing – original draft, Visualization.
- Malcolm McCulloch: Writing – review & editing, Supervision.
- David Wallom: Conceptualization, Resources, Data Curation, Writing – review & editing, Supervision, Project Administration.

1.5 Thesis Outline

The thesis is structured in six chapters, and the remainder of the thesis is organized as follows:

Chapter 2 provides a review of background information and relevant literature on storage design. This chapter introduces the electricity system and provides relevant background on the major components within the hybrid renewable system: generation, demand, and storage. The design criteria for the hybrid renewable system are reviewed. Literature reviews are presented for each of the four main approaches to energy storage design: enumerative, mathematical optimization, meta-heuristic optimization, and analytical approaches. The main approaches are compared, and the current gap within the literature on the analytical approach is discussed.

Chapter 3 proposes an analytical method to optimally size energy storage. The proposed method yields the optimal storage size that maximizes storage utilization while eliminating unutilized storage capacity. The method is extended iteratively to account for storage lifespan models. Monte Carlo simulation is also introduced to account for uncertainties in generation and demand. The proposed method is benchmarked against mathematical, meta-heuristic, and enumerative optimizations. It is then applied to two solar-battery case studies, one with surplus renewable generation, and the other with excess electricity demand.

Chapter 4 presents a hybridized techno-economic method to optimally size solar PV and energy storage. The hybridized method uses an analytical method to calculate the maximum storage and solar sizes. The maximum sizes are used to define the search space, and an enumerative approach is employed to systematically

iterate through the search space to find the lowest-cost system sizing. The hybridized method is applied to a case study on a solar-battery microgrid system based on the city of Oxford. The study explores the characteristics of the design space and also explores the future composition of the hybrid renewable system using cost projections.

Chapter 5 proposes an analytical method for sizing and placing energy storage, with the objective of maximizing storage utilization and minimizing generator costs. The method uses optimal power flow to determine the power dispatch. Storage is then sized and placed using an analytical method based on the dispatch. The proposed method is benchmarked against both meta-heuristic and mathematical optimization methods using the IEEE (Institute of Electrical and Electronics Engineers) Reliability Test System. The method is applied to a case study on a carbon-neutral village with wind and solar generation.

Chapter 6 summarizes the works presented in the thesis, and explains how the works fit together to contribute to the main theme of the thesis, which is to gain a better understanding of storage design in the context of hybrid renewable systems. Moreover, the chapter suggests potential extensions and improvements for each work in this thesis. The suggestions include algorithm improvements, method extensions, and case study extensions.

Please note that all figures in this thesis are presented as vector graphics, which can be zoomed in for enhanced clarity without resolution loss. Moreover, the code used in this thesis is available at [15].

2
Literature Review

Contents

2.1 Introduction

The literature review chapter provides background information and relevant literature on storage design. This chapter introduces the electricity system and provides relevant background on the major components within the system: generation, demand, and storage. Additionally, the chapter provides reviews of the literature on energy storage design and explores the research gap within the literature.

The chapter is structured as follows: Section 2.2 introduces the grid electricity system and the three main types of microgrid systems. Section 2.3 discusses the six types of renewable generation: solar, wind, marine, hydro, bioenergy, and geothermal. Moreover, this section discusses the three main approaches for modelling renewable generation: physical models, machine learning models, and hybrid models. Section 2.4 presents four types of electricity demand: residential, commercial, industrial, and transport. Similar to renewable generation modelling, this section discusses the three main approaches for modelling electricity demand. Section 2.5 outlines the three main types of energy storage: short-term, mid-term, and long-term storage. Section 2.6 discusses the four types of criteria for designing energy storage: technical, economic, social, and environmental. Section 2.7 discusses the four main approaches for energy storage design: enumerative, mathematical optimization, meta-heuristic optimization, and analytical approaches. Finally, Section 2.8 compares the four main approaches for energy storage design and discusses the current gap in the literature regarding the analytical approach.

2.2 Electricity System

The electricity grid system is designed to generate, transmit, and distribute electrical power. Its purpose is to deliver electricity from generators to end-users, such as homes and buildings. However, the integration of renewables into the existing grid system poses numerous challenges, which is why there is a growing interest in microgrid systems.

2.2.1 Power Grid System

The electricity grid transports energy from generators to meet load demand. Typically, power is generated by large power plants, including renewable power plants, in three phases with a frequency matching that of the grid. The grid operates at either 50 or 60 Hertz, with three phases that are 120^o apart [16]. Each grid section operates at a specific voltage, with higher voltages used during transmission to reduce losses. The voltage is stepped up using transformers, and power is transported via the transmission grid. Then, the voltage is stepped down using transformers at substations [17]. The power is subsequently distributed through the distribution grid. Some large consumers tap directly into the distribution grid, while transformers further step down the voltage for smaller consumers. Smaller consumers, such as houses, typically tap into only one of the three phases. Incorporating renewables may require extensive upgrades to the existing grid system [18].

2.2.2 Microgrid System

In recent years, there has been a growing interest in incorporating renewables and storage within localized electricity systems called microgrids. Microgrids offer several advantages compared to conventional grid systems. First, microgrids offer greater resilience. They offer the ability to operate in island mode, meaning they can operate independently from the grid system during a grid outage [19]. Second, microgrids offer cost reduction through local generation, reducing the need for extensive transmission and distribution infrastructure [20]. Third, microgrids are more accessible. They can power remote communities such as island nations [21]. There are three main approaches to setting up a microgrid system: AC-coupled, DC-coupled, and hybrid-coupled. The advantages and disadvantages of each setup are summarized in Table 2.1 [22].

An example of an AC-coupled microgrid is shown in Fig. 2.1. All generation and demand units are connected to a common AC bus [23]. The grid regulates the AC bus' frequency and voltage [24]. All components connected to the bus have to convert their power to the standard frequency and voltage. For DC generators, such as solar

System Setup	Advantage	Disadvantage
AC coupled	• Good reliability, faults are easily detected • Standardized equipment with economy of scale • Easy grid connection	• Power quality issues such as reactive power and harmonic distortion • Frequency synchronization is required
DC coupled	• No power quality issues • Single wire connection • No synchronization	• No standardization and economy of scale
Hybrid coupled	• Allow both AC and DC load to connect directly • No synchronization	• Experimental with higher cost • Control is more complex with both AC and DC

Table 2.1: Microgrid system setup comparison.

PVs, the DC power needs to be converted to 3-phase AC power via an inverter [25]. For AC generators, such as wind turbines, the AC power needs to be converted to 3-phase AC with standard voltage and frequency via a converter [26]. Energy storage needs a bi-directional DC and 3-phase AC converter for both charging and discharging power [27]. Large AC demand, such as an industrial complex, can tap directly into the AC bus for 3-phase AC power. For smaller AC demand, such as homes, they can tap into one of the three phases. For DC load, a rectifier is needed to convert the 3-phase AC power to DC power with an appropriate voltage [28].

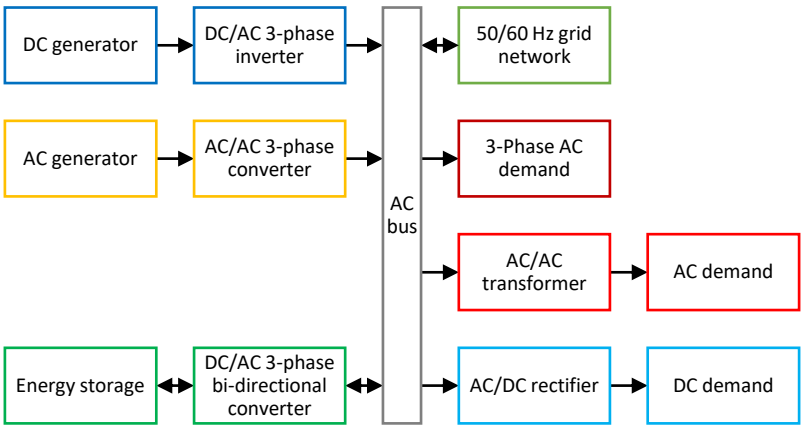

Figure 2.1: AC-coupled hybrid renewable microgrid setup example.

An example of a DC-coupled microgrid is shown in Fig. 2.2. All components are connected to a common DC bus [22]. The DC bus has a standard voltage, and all connecting components must convert to this voltage [29]. DC generators, such as solar PVs, use a DC-to-DC converter to get the appropriate voltage [30]. For AC generators, such as wind turbines, a 3-phase AC-to-DC rectifier is needed to convert AC power to the appropriate DC power [31]. Energy storage needs a bi-directional DC-to-DC converter to convert power to the appropriate voltages [32]. Large DC demand can directly tap into the DC bus, while smaller DC demand requires a DC-to-DC converter to step down the voltage. For AC demand, a DC-to-AC inverter is needed to convert DC power into appropriate AC power [33].

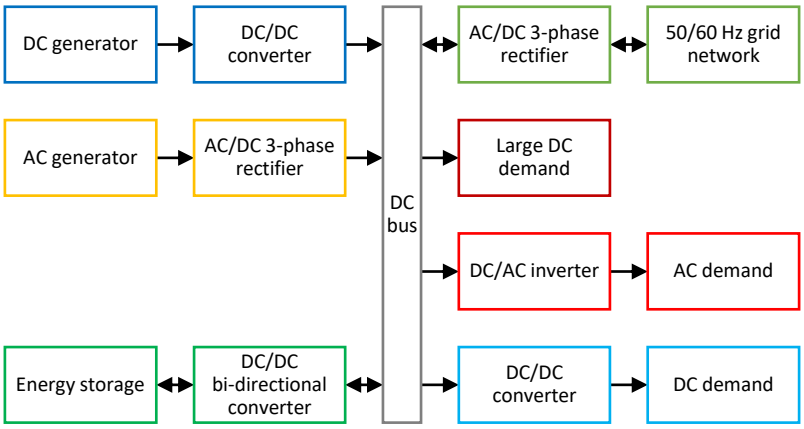

Figure 2.2: DC-coupled hybrid renewable microgrid setup example.

An example of a hybrid-coupled microgrid is shown in Fig. 2.3. The hybrid-coupled microgrid has both AC and DC buses, and they are connected via a bi-directional AC-to-DC converter [28]. AC demand and generators are connected to the AC bus, while DC demand and generators are connected to the DC bus [34]. DC generators, such as solar PVs, are connected to the DC bus via DC-to-DC converters to get the appropriate voltage [35]. Similarly, AC generators, such as wind turbines, are connected to the AC bus via AC-to-AC converters to get the appropriate voltage and frequency [22]. Energy storage is connected to the DC bus through a bi-directional DC-to-DC converter [36]. Large AC and DC demands are connected directly to their respective buses, while smaller demand need AC-to-AC or DC-to-DC converters to step down the voltage.

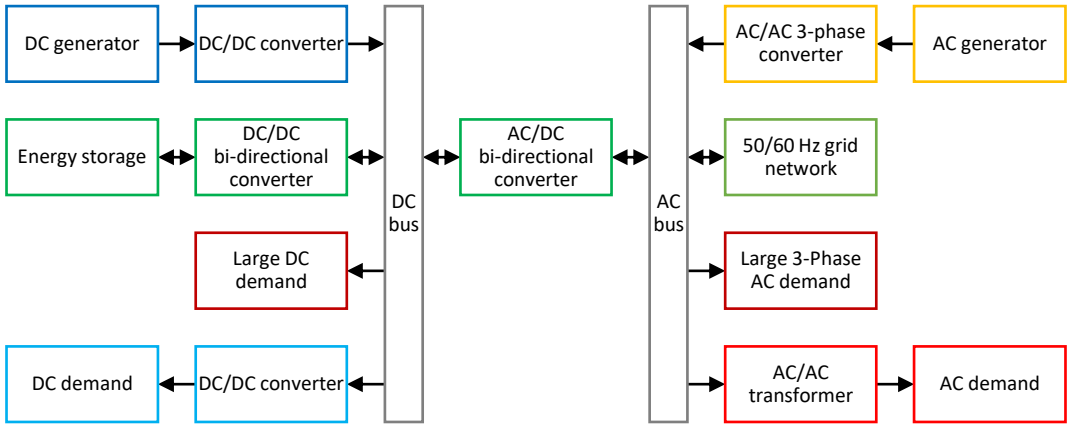

Figure 2.3: AC and DC-coupled hybrid renewable microgrid setup example.

2.3 Renewable Generation

All renewables can trace their energy source from the Sun, the Moon, or the Earth. Renewables generate electricity using two methods: electricity generators or photovoltaic cells. An overview of renewables and how they generate electricity is shown in Fig. 2.4 [37].

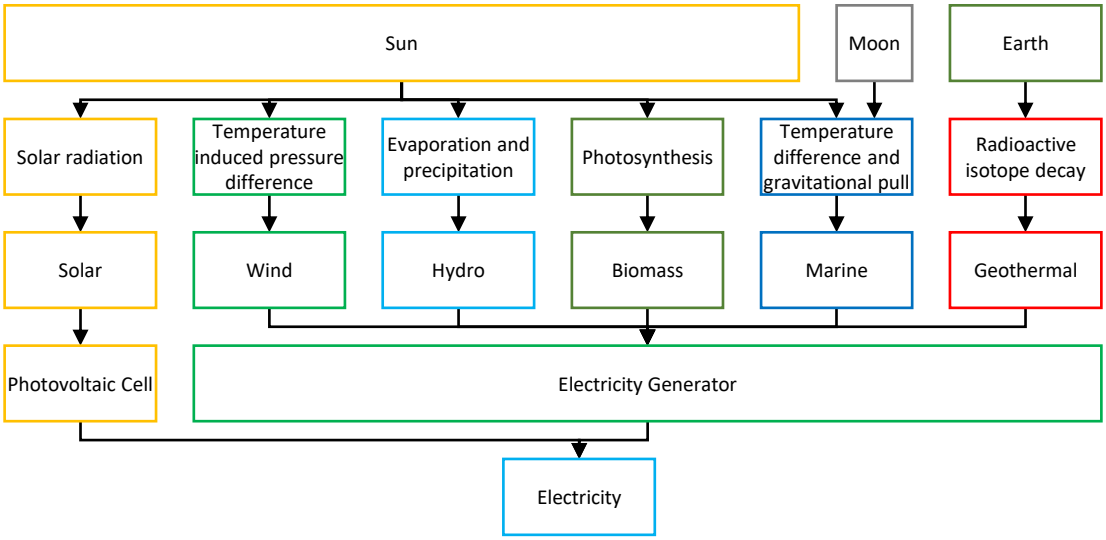

Figure 2.4: Renewable generation overview.

2.3.1 Electricity Generation Method

Renewables employ two primary methods to generate electricity: electricity generators and photovoltaic cells, with the majority relying on electricity generators [38].

An electric generator works according to Faraday's Law of Induction, which says that as a conductor moves through a magnetic field, an electrical current is induced within the conductor. Based on this law, if a wire spins between two magnets, the spinning motion in the magnetic field will induce a current flow within the wire [16]. Renewables generate electricity by spinning a turbine using wind, water, or pressurized gas. The turbine is connected to an electricity generator. The spinning turbine drives the spinning motion of magnets within the generator. The spinning magnets induce electricity current in the wire, generating electricity.

A solar photovoltaic cell has two main parts: a n-type (negative-type) layer and a p-type (positive-type) layer. The n-type layer consists of silicon doped with impurities that have excess electrons. The p-type layer consists of silicon doped with impurities that have electron deficits, or an excess of holes where electrons should be [39]. When the two layers touch, excess electrons from the n-type layer migrate to the nearby region in the p-type layer, leaving behind holes. The migration creates a depletion zone, where the n-type side of the depletion zone is slightly positive due to the holes left behind, while the p-type side is slightly negative due to the migrated electrons. The slightly positive and negative difference creates an electric field in the depletion zone. When photons from solar radiation strike the depletion zone, the energy of the photons excites electrons, causing them to transition from the valence band to the conduction band and creating electron-hole pairs [16]. The electric field in the depletion zone forces the electron into the n-type layer, which already has excess electrons. On the other hand, holes are forced towards the p-type layer, where there is already an excess of holes. The continuous addition of electrons in the n-type layer, and the addition of holes in the positive-type layer creates potential differences between the two layers. As such, electrons will actively flow from the n-type layer to the p-type layer if these two layers are connected with an external wire. This flow of electrons within that wire is electricity.

2.3.2 Renewable Generation Type

Renewables are categorized as dispatchable and non-dispatchable. Non-dispatchable renewables, such as solar, wind, and marine energy, lack natural energy storage. They require pairing with energy storage devices, like batteries, to achieve dispatchable generation. In contrast, dispatchable renewables, including hydro, bionergy, and geothermal, possess natural energy storage mechanisms [40]. Hydropower, for example, utilizes water reservoirs created by dams to store potential energy [41]. Biofuels serve as a form of natural chemical energy storage, while geothermal relies on the constant heat reservoir within the Earth [42]. This inherent storage capacity enables dispatchable renewables to adjust their generation in response to demand fluctuations, provided they have a sufficient ramp rate, meaning they can effectively ramp up or down their power output. When the ramp rate of dispatchable renewables is insufficient to match fluctuating demand, fast-responding energy storage systems, such as supercapacitors and batteries, can be used to supplement the supply [43].

Solar energy harnesses sunlight to generate electricity through two main methods: solar photovoltaics and concentrated solar [44]. In solar photovoltaics, photons from solar radiation excite electrons within the photovoltaic cell, creating electricity [45]. Alternatively, in concentrated solar systems, mirrors reflect and concentrate sunlight onto a single spot [46]. The concentrated sunlight then heats water into steam, and the pressurized steam drives a turbine to generate electricity.

Wind energy also depends on solar radiation. Solar radiation heats up the Earth differently. Some parts of the Earth, such as the Arctic, reflect solar radiation and stay cold [47]. While other parts, such as forests, absorb solar radiation and heat up [48]. This creates regions with temperature differences. Regions with higher temperatures heat up the air, and warm air has lower pressure. On the other hand, colder regions cool the air, and cold air has higher pressure. The pressure difference induces airflow from high-pressure regions to low-pressure regions, and this movement of air is perceived as wind [49]. Wind's kinetic energy can spin turbines connected to electricity generators, converting kinetic energy into electricity [50]. Wind power

is categorized into onshore and offshore. Typically, offshore wind turbines are more expensive but generate more energy due to the stronger winds at sea [51].

Marine energy is composed of wave and tidal energy. Wave energy originates from solar radiation, which creates temperature-induced pressure differences between regions, generating wind. As the wind moves across the ocean, it forms waves on the ocean surface [52]. The kinetic energy from these waves can be harnessed and converted into electricity using an electricity generator [53]. On the other hand, tidal energy is influenced by both the Sun and the Moon. Gravitational pulls from the Sun and Moon give rise to tides [54]. When the tide rises, water is pushed inland, and as it falls, water recedes. This rhythmic movement of water can be utilized to rotate turbines, ultimately generating electricity [55].

Hydropower also derives its energy from solar radiation. Solar radiation heats up water, leading to its evaporation into air moisture. Subsequently, as the air cools, the moisture condenses into rain droplets. The land channels the rain into rivers. Dams are constructed on rivers to direct water flow through hydro turbines. This flow of water spins the turbine to generate electricity [56]. Hydropower is categorized into hydro dams and run-of-the-river hydro plants. Run-of-the-river hydro plants utilize the kinetic energy of river flow to produce electricity. In contrast, hydro dams convert the gravitational energy of water into kinetic energy to generate electricity [57]. The gravitational potential energy, or the weight of the water, exerts pressure on itself as it enters the turbine. This pressure propels the water through the turbine, spinning it to generate electricity [58]. The hydropower dam forms a water reservoir behind it, acting as a natural energy storage system that stores potential energy [59]. This setup enables dispatchable hydropower, where water can be released on demand to generate electricity.

Bioenergy is one of the most versatile renewable sources [60]. Through photosynthesis, plants harness solar radiation to produce glucose, which fuels their growth [61]. These plants are harvested and turned into biofuels. The biofuels are combusted to heat water into steam [62]. The pressurized steam then drives turbines to generate electricity. Beyond plant-based sources, organic wastes also contribute to

bioenergy. Anaerobic digestion plants employ microorganisms to consume organic wastes, converting them into biogas [63]. This biogas can be burned to heat water into steam, which, in turn, drives turbines to produce electricity. Bioenergy exhibits versatility in its applications, particularly in hard-to-decarbonize sectors like aviation, where high-energy-density fuels are needed [64].

Geothermal energy derives its power from the Earth. The decay of radioactive materials within the Earth releases energy, which heats the Earth [65]. Geothermal wells tap into this heat reservoir to generate energy. For electricity generation, a higher temperature is required, so geothermal power plants are strategically located in geologically active areas where lava is closer to the surface [66]. This proximity allows geothermal wells to reach the necessary temperature at relatively shallow depths. Fluid is pumped into the wells to be heated [67]. The heated fluid is then used to heat water into steam, which in turn spins a turbine, generating electricity [68].

2.3.3 Renewable Generation Profile

For the aforementioned renewables, their idealized daily generation profile in the UK is shown in Fig. 2.5. Note that the capacity factor relates the actual generation to the rated generation. Solar begins to generate energy at sunrise, then peaks at noon, and falls in the afternoon, before fully stopping at sunset [69]. However, cloud coverage can cause solar generation to rise and fall during the day [70]. For some locations, such as the UK, wind generation is typically higher during the day and lower at night [71]. However, the daily wind generation is highly random and dependent on the local environment. Tidal generation peaks twice a day, due to tides rising and falling two times a day. The timing of the tidal peak varies throughout the month, depending on the moon's position. For dispatchable renewables, including hydro, bioenergy, and geothermal, their daily generation profile is shown as constant, based on their average capacity factor. However, since they are dispatchable, they can be controlled to follow the electricity demand pattern.

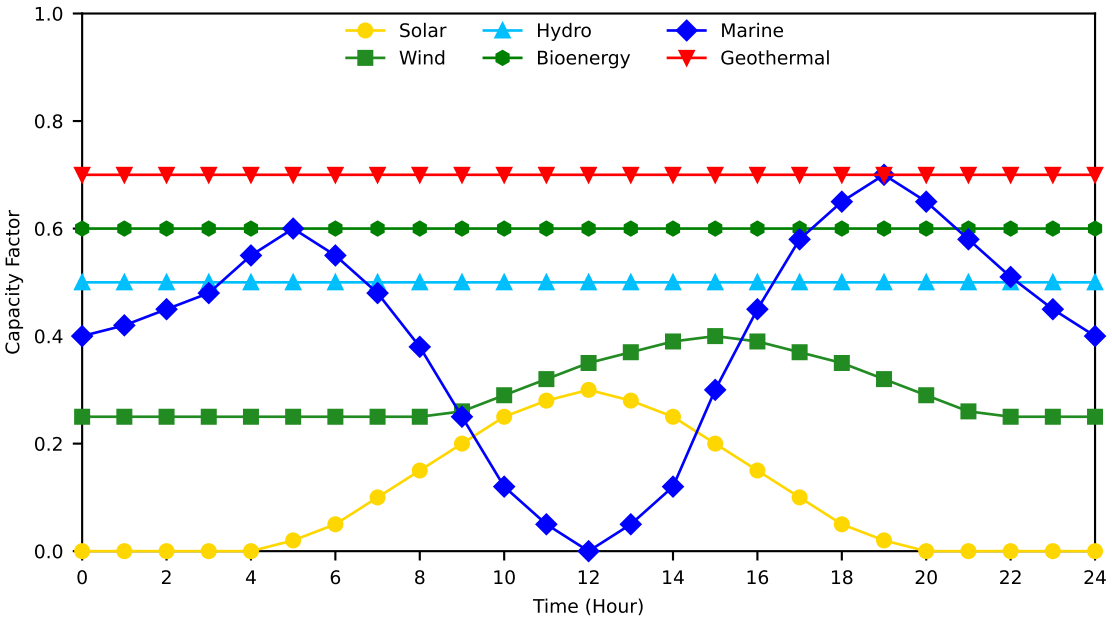

Figure 2.5: Idealized daily profile of renewable generation capacity factors in the UK for each hour in a day.

The idealized annual generation profile for renewables in the UK is shown in Fig. 2.6. Solar generation is at its lowest during winter and peaks in the summer [72]. This seasonal fluctuation is attributed to the shorter daylight hours in winter and the longer daylight hours in summer. Notably, the generation reaches its minimum during the winter solstice, which has the shortest daylight hours in the year, while it peaks during the summer solstice, the longest day of the year. On the other hand, wind generation peaks during the winter and is lower during the summer [73]. One contributing factor is the greater temperature gradients during winter, driven by moving cold fronts, leading to higher wind speeds.

The annual generation profile of wind exhibits a high degree of complementarity with solar [74]. When wind generation is high, solar generation tends to be low, and vice versa. This complementary relationship makes wind and solar a suitable combination for achieving more consistent generation [75]. Tidal generation peaks twice a month, occurring during the new moon and full moon, when the moon is closest to Earth, resulting in the highest tides [76]. Hydropower generation is influenced by the seasons, producing more energy during the rainy season and less during the dry season [77]. Bioenergy maintains a relatively constant generation

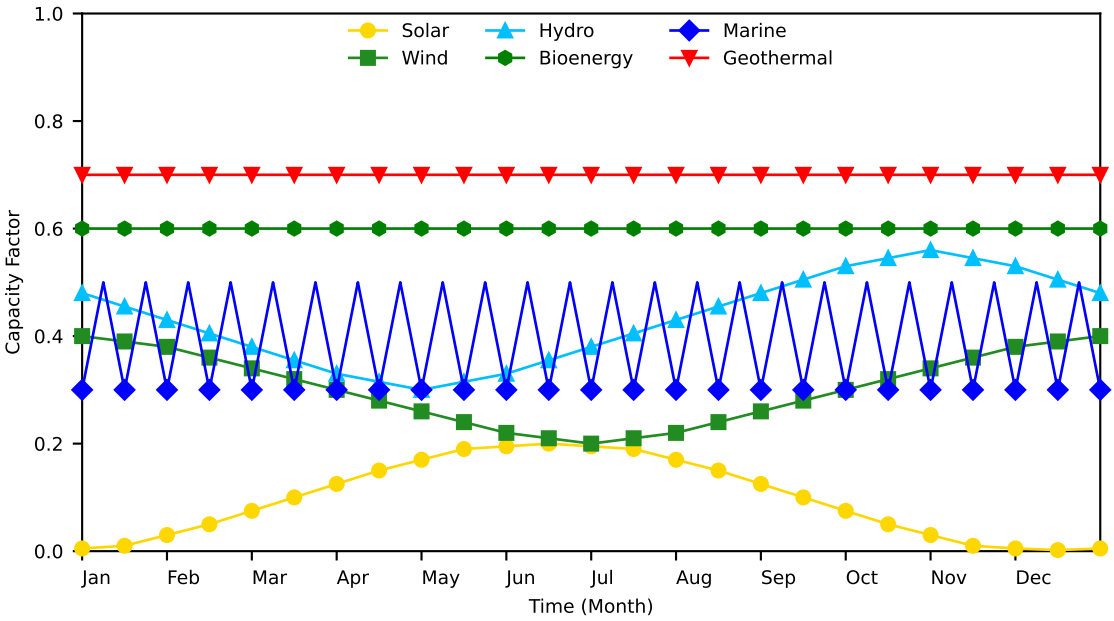

Figure 2.6: Idealized annual profile of renewable generation capacity factors in the UK for each month in a year.

capacity throughout the year. Similarly, geothermal generation remains stable due to the Earth's consistent internal temperature across seasons, enabling a steady power output.

2.3.4 Renewable Generation Model

Renewable generation data are not always available, prompting the development of generation models. Renewable generation is modelled via three main methods: physical model, machine learning, and hybrids of the two [78].

The physical model uses physics-based equations to calculate the renewable generation. An example is the solar generation model developed by Pfenninger and Staffell. The model uses retro-perspective analysis to calculate and refine its results [79]. The model first obtains solar irradiance and temperature data from NASA's MERRA database. The temperature data is then fed into Huld's temperature-dependent solar PV efficiency curve to determine the solar panel efficiency [80]. The irradiance data is processed into direct irradiance and diffused irradiance using the Boland-Ridley-Lauret model [81]. The direct and diffused irradiances are then scaled according to the incline of the solar panel. Finally, the solar power output

is calculated using the panel efficiency, direct irradiance, and diffused irradiance. The advantage of physical models is that the internal workings are known, making them easier to modify. The downside is that the models can get quite complex, and their complexity only increases as the model becomes more accurate.

The machine-learning model uses data to model the generation output. Examples of machine learning models include statistical and deep learning models. Generation modelling mainly uses past generation and meteorological data [82]. For example, a solar generation model uses data such as solar irradiation, temperature, humidity, and wind speed [13]. A popular statistical method is SVM (Support Vector Machine), which performs just as well as deep learning methods such as RNN (Recurrent Neural Network) [83]. SVM maps input data into higher dimensions using a kernel function. Then uses linear regression in the higher dimension to find the hyperplane that fits the data. The hyperplane is used to predict generation based on the input. Then the prediction is transformed from the higher dimension to the original dimension to produce the result. The advantage of machine learning models is that they can produce highly accurate results [84]. However, the downside is that they might not work sometimes, as their internal workings are not physics-based.

The hybrid model combines both physical and machine learning models. For example, a machine learning model can be employed to model meteorological data, such as temperature and solar irradiation. These meteorological data can then be fed into a physical model, such as that by Pfenninger and Staffell, to determine the solar generation [79]. The advantage of hybrid models is that they can be highly accurate. The disadvantage is that they can be highly complex, involving both physical and machine learning models.

2.4 Electricity Demand

The purpose of designing energy storage is to assist renewable generation in meeting the demand. Energy demand is typically categorized into four sectors: residential, commercial, industrial, and transport, each with its own unique characteristics [85].

2.4.1 Electricity Demand Type

Understanding demand profiles is crucial for designers to choose the right combination of renewable and storage. For instance, commercial demand tends to peak during the day, aligning well with the solar generation profile. On the other hand, residential demand is lower during the day but increases in the evening. In such cases, energy storage can help align solar generation with demand. The electricity demand profiles in the UK are shown in Fig. 2.7 [86].

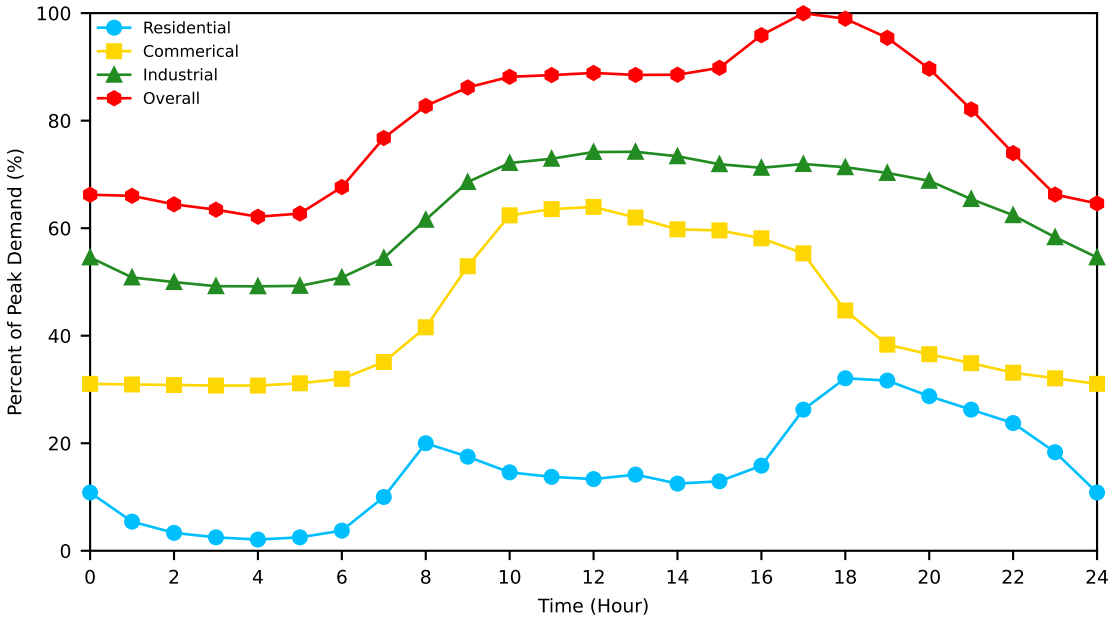

Figure 2.7: Electricity demand profiles for residential, commercial, industrial sectors, and overall electricity demand for each hour of the day.

The residential electricity demand profile exhibits a "duck curve" pattern [87]. The demand is lowest at night. Then, it rises in the morning as people wake up and have breakfast. The demand then dips until another rise at noon, when people have lunch. It then dips in the afternoon, before peaking in the evening, when people start to have dinner and watch TV. At night, the demand drops to its lowest level. In contrast to residential demand, commercial demand follows the typical commercial hours [88]. The demand is the lowest at night and rises in the morning as commercial activities begin. It stays peaked until noontime, after which it dips a little in the afternoon. When the commercial hours end, the

demand drops to the lowest level again. Industrial demand is similar to commercial demand, except it has much higher energy intensity [89]. Transport demand is not shown in the figure because the sector is still reliant on fossil fuels, leaving little data on the electricity demand. However, it is anticipated that electric vehicle will contribute to increased electricity demand during the evening [90]. This is because most people finish using their car by evening and park it for charging, resulting in an expected rise in electricity demand during that period. The overall electricity demand combines the common characteristics of all sectors [91]. The demand is the lowest at night, and starts to rise in the morning. It remains relatively steady until the afternoon, when it experiences a peak as people begin to return home. The demand then drops to the lowest level again at night.

2.4.2 Electricity Demand Model

Since demand data are not always available, various techniques have been developed to model demand based on other accessible data. Demand modelling is typically categorized into three main methods: physical models, machine learning, and a hybrid approach that combines both [92].

Physical models are physics-based, where the internal workings are known. The models typically use data on equipment and appliances, building materials, occupant behaviour, and climate conditions. ASHRAE has a system for calculating heating and cooling loads based on building design, occupancy, and outside environment [93]. Electricity consumption is then calculated based on the heating and cooling loads. Other electrical demand, such as lighting and appliances, are calculated based on the appliances' energy rating and occupant behaviour.

Machine learning models, such as statistical and deep learning models, model demand based on relevant data [94]. Relevant data include outdoor and indoor climate conditions, occupant schedules, and building characteristics [83]. An example of a statistical model is the Elexon electricity demand profiles, which were used for electricity settlement. The model sampled half-hourly data from consumers in Great Britain. These demand data were correlated to temperature, sunset

time, and day of the week using linear regression [86]. Before digital meters were introduced, electricity suppliers would read meters periodically and use Elexon profiles to determine the half-hourly demand between meter readings. The supplier would then use the half-hourly demand profile to charge the customer accordingly.

The RNN (Recurrent Neural Network) is an example of a deep learning model. Like other neural networks, RNN consists of multiple layers of nodes, separated into the input, hidden, and output layers [95]. Nodes in the input layer process data coming into the neural network. The processed data then goes to the hidden layers. The hidden layer nodes activate differently based on the data and how they were trained. The hidden layer nodes send activation signals to the output layer. Nodes in the output layer process the signals and calculate the result. The difference between RNN and other neural networks is that nodes in the hidden layer have memory and can retain information from previous inputs [96]. In essence, the memory feature allows RNN to accurately model sequential data, and since demand data is inherently sequential, RNN proves particularly effective in this context.

Hybrid models combine physical and machine learning models, and this area of research is still relatively new. An example of a hybrid approach involves machine learning to learn occupant schedules. The occupant schedule is then fed into a physical model to calculate the energy demand.

2.5 Storage

Energy storage enables non-dispatchable generation to meet the demand. Energy storage is divided into short-term, mid-term, and long-term storage [97]. The division depends on how fast the storage can discharge and how long it can hold the energy. A fast discharge rate is required for short-term storage, while a low energy leakage rate is needed for long-term storage [98].

2.5.1 Short-term Storage

An example of short-term storage is the flywheel, which converts kinetic energy into electricity and vice versa [99]. The flywheel is a large and heavy disk that

spins in a low-friction environment [100]. When charging, electricity powers a motor to spin the flywheel. When discharging, the spinning flywheel connects to a generator, and the spinning momentum drives the generator to produce electricity. The flywheel is good for short-term storage because it can discharge energy almost instantaneously. Furthermore, the flywheel directly uses 3-phase AC power, and its spinning momentum can help regulate the grid frequency [101]. However, the flywheel is unsuitable for long-term storage, because it loses its spinning momentum relatively quickly.

2.5.2 Mid-term Storage

Batteries are energy storage devices that convert chemical energy to electricity. A battery has two main parts: the cathode and the anode [102]. During discharge, the anode's electrode reacts with the electrolyte to produce electrons and positive ions. The electrons are directed out of the battery as electricity. Subsequently, electrons return to the cathode due to the lower electric potential. Reactions occur at the cathode's electrode, where electrons and positive ions recombine. When the battery is charging, this process is reversed, and electrons and positive ions are returned to the anode. Batteries are suitable for mid-term storage, as they can be discharged instantaneously, and their energy leakage is negligible within the timeframe of mid-term storage [103].

2.5.3 Long-term Storage

A promising long-term energy storage device is Power-to-Gas [104]. When charging, electricity powers an electrolyzer to separate water into hydrogen and oxygen [105]. The hydrogen is then stored in pressurized tanks for later use. During discharge, hydrogen is used in fuel cells to produce electricity, and the hydrogen ions combine with oxygen ions to produce water [36]. Alternatively, hydrogen can be burned to create heat, heating water into steam. Then, the pressurized steam drives turbines to produce electricity. While Power-to-Gas has a longer response time, the energy

leakage during storage is minimal, as energy is stored as hydrogen in tanks. This makes Power-to-Gas suitable for long-term energy storage [106].

2.6 Design Criteria

Storage and renewable design is an optimization process, and optimization needs objectives and constraints. Constraints filter out unsuitable solutions, while the objective selects the best solution. In storage design, there are four types of constraint or objective criteria: technical, economic, environmental, and social [107].

2.6.1 Technical

Technical criteria typically focus on the design's ability to meet demand, measured as the percentage of unmet demand relative to the total demand. Various applications exhibit distinct demand patterns. For instance, residential homes generally have low demand during the day but higher demand in the evening. In contrast, commercial buildings experience increased demand during the day and lower demand at night [86]. As a result, the storage and renewable sizes vary to accommodate these diverse demands. Additionally, some renewables, like hydro, are location-specific, leading to the choice of renewable being location-dependent.

2.6.2 Economical

Economic criteria center on the cost of the design, typically measured using the annualized cost. The system cost includes the capital cost of constructing the system, along with operational and maintenance costs [108]. Capital costs generally occur at the beginning of the lifecycle, while operational and maintenance costs are spread throughout the lifecycle. Due to the varying lifecycle lengths of different components, some may require more frequent replacement, resulting in higher capital costs. Annualizing the costs by distributing them across the lifecycle facilitates meaningful cost comparisons. The majority of storage sizing papers focus on technical and economic objectives [28].

2.6.3 Environmental

Environmental criteria centers around the environmental impacts of the design, typically measured in lifecycle greenhouse gas emissions [109]. Given that most renewables generate energy without emissions, it is crucial to consider the overall emissions throughout the lifecycle. This includes emissions during various stages: raw material extraction, manufacturing, distribution, use, and disposal [110]. A retrospective lifecycle analysis can provide a comprehensive understanding of the emissions associated with each type of renewable and storage.

2.6.4 Social

Social criteria concentrate on the design's social impacts, encompassing various measurements such as job creation, income, education, and life expectancy, as well as factors like noise, visual, and land use [110]. Social objectives are diverse, so oftentimes, design is focused on improving specific social criteria. For instance, minimizing land use impact may exclude renewables requiring large land areas, such as bioenergy and solar farms, while encouraging others like marine energy and offshore wind farms. In another scenario, minimizing noise may discourage loud wind turbines but promote passive solar PVs.

2.7 Design Method

The four main approaches for storage design are: enumerative, meta-heuristic optimization, mathematical optimization, and analytical [11]. Moreover, hybridizing the approaches is also an active research area [111]. The enumerative approach is only applied to storage sizing, while the remaining approaches can be applied to both storage sizing and placement. Both meta-heuristic and mathematical approaches have been extensively studied, while less research is available for the analytical approach.

2.7.1 Enumerative

The enumerative approach systematically iterates through system sizes within a defined search range. At each iteration, the system is simulated, and system sizes that do not meet the criteria are discarded. Those that meet the criteria are saved, and their system cost is calculated. The lowest-cost system is then selected as the optimal design [11]. While the enumerative approach is used for storage sizing, it is rarely applied to both storage sizing and placement due to the complexity of the solution space. The enumerative approach cannot process complex solution spaces in a timely manner.

Yang *et al.* used an enumerative method to size solar PV (photovoltaics), wind turbines, and battery banks for a telecommunication relay station [112]. The method iterates through ranges of solar, wind, and battery capacities. At each iteration, the system is simulated, and the occurrence of unmet demand is calculated in terms of LPSP (Loss of Power Supply Probability). The cost for system sizes meeting a specific LPSP is calculated, and the lowest-cost system size is selected.

Borowy proposed a hybridized enumerative and analytical method to size solar PV with batteries [113]. The enumerative method iterates through solar and battery capacity ranges, and calculates the LPSP. Then, an analytical equation models the solar and battery capacities relationship at a specific LPSP. The analytical equation is solved with a cost equation to yield the lowest-cost sizing. Similar to Borowy's approach, Jakhrani *et al.* also used an enumerative-analytical approach to size solar-battery systems [114].

Cabral *et al.* used a probabilistic-enumerative method to size a solar-battery system [115]. The study used the Markov chain and probabilistic beta distribution to create solar generation profiles. The profiles are fed into an iterative method, yielding solar and battery sizes based on the LPSP requirement, following which the lowest-cost size is selected as optimal. The study found the addition of the probabilistic method yielded a smaller storage size with acceptable LPSP. Similarly, Zhu *et al.* also used a probabilistic-enumerative method to size a solar-battery system [116]. The study sized storage to reduce solar power back-feeding the grid.

Bartolucci *et al.* used the enumerative method to size battery and fuel-cell with solar generation [117]. The study found that battery is more economical than fuel-cell when coupled with solar generation. Furthermore, the study showed increasing battery size has a diminishing return on battery energy provided to the system. Zhang *et al.* used the enumerative method to size a grid-connected solar-battery system [118]. The study found that sizing to maximize renewable consumption will result in a lower initial investment, but a longer payback period.

The HOMER (Hybrid Optimization of Multiple Energy Resources) software sizes hybrid renewables using an enumerative approach. Ma *et al.* used HOMER to assess the feasibility of a solar-wind-battery system for a remote island [119]. The study found that the island's existing diesel power system can be fully replaced by the solar-wind-battery system. Halabi *et al.* used HOMER to size a solar-diesel-battery system for a village [120]. The study found that battery is mainly used as backup power due to the higher cost.

2.7.2 Heuristic Optimization

The meta-heuristic approach is similar to the enumerative approach. The difference is that, instead of iterating through the entire search space, meta-heuristic algorithms intelligently navigate the search space using exploration and exploitation to find the optimal solution [12]. However, most meta-heuristic algorithms cannot guarantee a global optimum due to their stochastic nature.

Two of the most popular machine learning algorithms are particle swarm and genetic algorithms [121]. Particle swarm optimization begins by generating a population of random solutions [122]. Each individual particle is then evaluated based on its objective cost. The solution with the lowest objective cost is designated as the global best position, while the lowest objective cost experienced by each particle is recorded as its personal best position. Subsequently, particles move to new positions influenced by three factors: momentum from the previous movement, attraction to the global best position, and attraction to the personal best position. The particles are re-positioned according to these influences, and the solution at

the new position is evaluated. Following this, updates are made to the momentum, global best position, and personal best position, and the process is repeated. After several iterations, the best solution is selected as the optimal.

The genetic algorithm starts with a randomly generated population [123]. Individuals within the population are evaluated based on their objective cost. The top portion of the population is selected as parents, and they undergo crossover and mutation processes to produce offspring. The offspring then replace a portion of the old population to form a new population. The process is then repeated with the new population. After several iterations, the best solution is selected as the optimal.

These algorithms have two main components in common: exploitation and exploration [124]. Exploitation refers to the convergence towards the optimal solution. In the particle swarm algorithm, the particles try to move toward the most optimal position they know. In the genetic algorithm, only solutions close to the optimum are passed on to the next iteration. Exploration is the ability to escape local optima. A local optimum represents a solution that is better than nearby alternatives, but not necessarily the best solution. The particle swarm algorithm achieves exploration through momentum, where particles may randomly overshoot while trying to reach the optimal. The genetic algorithm accomplishes this through mutation, which generates new solutions randomly to explore beyond the current set.

In a subsequent paper by Yang *et al.*, the solar-wind-battery sizing method is refined using a genetic algorithm and more accurate models [125]. This method underwent benchmarking against a real system, demonstrating that the sized storage adequately supported the demand. Zhang *et al.* also employed a genetic algorithm to size a grid-connected solar-battery system [126]. The study proposed three operation strategies: conventional, demand shifting, and a hybrid of conventional and peak-shaving. The hybrid strategy exhibited superior performance in terms of cost and self-sufficiency. In another study by Zhang *et al.*, hydrogen and battery storage were compared in a solar-storage system [127]. The study revealed that the battery system is more cost-effective, while the hydrogen system provides higher power quality.

Shabani *et al.* also used a genetic algorithm to size a solar-wind-storage system [128]. The study concluded that combining wind and solar generation reduces storage size requirements. Saini and Gidwani employed a genetic algorithm to size a solar-battery system [129]. Their study found that optimal sizing and placement of storage can mitigate over-voltage, reduce power loss, and enhance solar PV penetration.

Lai *et al.* used seven optimization algorithms to size an anaerobic digestion plant with solar and storage [108]. The study found that particle swarm optimization with the interior point method is the most suitable algorithm. Fares *et al.* compared ten meta-heuristic algorithms for sizing storage in a solar-wind-battery system [130]. The study found that simulated annealing offers the best compromise between accuracy and speed.

Maleki *et al.* employed the probabilistic Monte Carlo simulation with a particle swarm algorithm to size a solar-wind-battery system [131]. The Monte Carlo simulation generated a distribution of storage sizes, and the final sizing was selected based on the mean value of the distribution. The study found the wind-battery system has the lowest cost due to the lower storage requirement.

Falama *et al.* used the firefly algorithm to size battery and hydrogen storage with solar generation [132]. The objective was to minimize the cost of energy and LPSP. The study found that the solar-battery system is more economically profitable, given the prohibitively high cost of hydrogen fuel cells.

Farsadi *et al.* used a genetic algorithm to place energy storage, with the objective of minimizing system loss [133]. The study found that adding storage can worsen system loss in low-demand systems, whereas in high-demand systems, adding storage reduced system loss.

Jannesar *et al.* used a genetic algorithm to size and place battery storage [134]. The method utilized linear programming for energy dispatch. The energy system was simulated based on the energy dispatch, and the system cost was calculated. The system cost included energy arbitrage, environmental emissions, system loss, transmission fees, and storage costs. The system cost was fed to a genetic algorithm to optimize storage size and placement. The result showed that storage improved

the voltage profile and reduced reverse power flow. Salee and Wirasanti also used a genetic algorithm to size and place battery storage [135]. The method simulated the system via AC OPF to calculate system loss. The system loss was then fed into a genetic algorithm to optimize for voltage deviation and power loss reductions. The results showed optimal storage size and placement achieved the objective.

Hashem *et al.* employed power loss sensitivity analysis and a genetic algorithm to size and place superconducting magnetic energy storage [136]. The method initially utilized power loss sensitivity analysis to narrow down potential sites for storage placement. Subsequently, a genetic algorithm optimized both storage size and placement to minimize system interruption and line overload.

Neagu *et al.* utilized the particle swarm algorithm for storage sizing and placement [137]. The method used a conventional operation strategy to compute storage energy levels and used power flow analysis to calculate system loss. It was tested in a microgrid system with consumers and prosumers featuring solar PV generation. The study demonstrated that storage reduced both system loss and voltage deviation.

Ghaffari *et al.* applied the crow search algorithm to optimally size and place battery energy storage, wind, and solar [138]. The objective was to reduce cost, power loss, flicker emission, and voltage deviation. The study concluded that optimal storage size and placement can effectively reduce both power loss and voltage deviation.

Mohamad *et al.* proposed a two-part method to size and place battery energy storage [139]. In the first part, storage placement was optimized by minimizing the number of units needed to connect all buses. The second part involved distributing the storage capacity across potential sites with the goal of reducing solar generation curtailment. The study revealed that storage was strategically placed near congested lines, and increasing line capacity and storage C-rating effectively reduced solar curtailment. Nick *et al.* also presented a two-part method for sizing and placing storage [140]. The objective was to minimize voltage deviation, system loss, and energy cost. In the first part, a genetic algorithm was employed for sizing and

placing storage. The second part utilized second-order cone programming to perform AC OPF (Optimal Power Flow), simulating the system and calculating the objective cost. The study accounted for the growth in load, PV capacity, and fuel cost. The result showed that optimal storage size and placement effectively reduced voltage deviation, system loss, and energy cost.

2.7.3 Mathematical Optimization

The mathematical programming approach includes classical optimization algorithms, such as linear programming and gradient descent algorithms [13]. These algorithms optimize storage size based on objective and constraint equations describing the energy system. Generally, there are four core constraints for storage design [141]. The first constraint states that the future storage level is equal to the current storage level plus the change in stored energy due to charging or discharging. The second constraint requires that charge and discharge rates must be within the storage's power limits. The third constraint requires that storage levels must remain within the storage's energy limits. The final constraint states that storage levels at the start and end of the design time horizon must be equal.

Chen *et al.* used mixed-integer linear programming to size storage [142]. The method first calculates the minimum storage size via the minimum of the total charged or discharged energy. This minimum size forms a part of the constraints, which are then fed into mixed-integer linear programming to calculate the storage size.

Atia and Yamada adpoted a probabilistic approach with mixed-integer linear programming to size a grid-connected solar-wind-battery system [143]. The study used the normal distribution to model solar generation and demand, and the Weibull distribution to model wind generation. The study found that storage can generate more profit with highly varied electricity pricing, and demand flexibility can reduce the storage requirement.

Al-Ghussain *et al.* utilized the generalized reduced gradient algorithm to size hydrogen fuel cell and pumped hydro in a solar-wind-storage system [144]. The

study found that hydrogen fuel cells can fill the power gap when pumped hydro is starting up, consequently increasing renewable consumption.

Bose *et al.* used convex optimization to place energy storage optimally [145]. The method assumed a total storage capacity and distributed that capacity via convex optimization. The method was implemented in an IEEE 14 bus system with peak-normalized demand and generation data. The study found that larger storage capacities with higher charge and discharge rates enhance the system's peak shaving ability. It also found that storage was placed near large demand, congested lines, and low-cost generators.

Elsir *et al.* introduced a mixed-integer linear programming method for sizing and placing storage [146]. The sizing objective aimed to minimize storage cost, while the placement objective targeted minimizing generator cost, renewable curtailment, and load curtailment. The study showed that optimally sized and placed storage led to reduced operational costs and load shedding.

Opathella *et al.* used mixed-integer linear programming to size and place storage and generators [147]. The method used DC OPF for power dispatch, considering generator downtime, loss of load probability, demand growth, and investment year. The objective was to reduce capital, generation, and grid import costs. The study optimized the investment schedule for each storage and generator, and demonstrated that the optimal storage size and placement improved grid flexibility and reliability. Pena *et al.* also used mixed-integer linear programming to size and place storage with generators and hydropower [148]. The objective was to minimize the cost of battery, generators, and hydropower. The method utilized a modified DC OPF to simulate power dispatch while accounting for line loss. The study found that storage reduced system costs by reducing generator dispatch. Moreover, power loss affected sizing but did not affect placement.

In another study by Nick *et al.*, mixed-integer second-order cone programming was used to size and place storage [149]. The method used K-means clustering to obtain demand and generation profiles, and a linearized capability curve to model the relationship between active and reactive powers. The method also accounted

for the growth in load demand, PV capacity, and fuel cost. The objective was to minimize system cost, power losses, voltage deviation, current flow deviation, and demand curtailment. The results showed that the optimization improved all objectives and eliminated load curtailment.

Karanki and Xu used power loss sensitivity analysis and the particle swarm algorithm to size and place storage [150]. First, power loss sensitivity analysis is used to determine storage placement. Then, the particle swarm algorithm is used to determine storage size and operation. The study showed that optimal storage size and placement reduced system loss. Similarly, Rathore and Patidar used a particle swarm algorithm with active power loss sensitivity analysis to size and place gravity storage [151]. The study found that sizing and placing many smaller storage units could better reduce power loss and voltage fluctuation. Moreover, combining wind and solar could more effectively minimize power loss and voltage fluctuation than individually using wind or solar.

2.7.4 Analytical

The analytical approach involves modelling the relationship between renewable size and system behavior, followed by sizing based on the desired behavior [152]. In the context of storage sizing, this approach utilizes storage models to construct the storage energy profile and subsequently determines the storage size based on that profile [14]. While this approach can find the optimal solution, the analytical model can become increasingly complex as more elements are added to the renewable system.

Cao *et al.* proposed an analytical method for sizing batteries to smooth wind power output [153]. The method first constructed the storage level profile. Then, the method sized storage based on the difference between the initial and the maximum change in storage level.

Neto *et al.* introduced an analytical-probabilistic method for sizing dual battery storage systems [154]. This method utilized a probabilistic model to calculate the distribution of energy and power deficits. The storage was sized based on these

deficits. The study optimized storage operation, with the smaller secondary battery operated to reduce the degradation of the primary battery. The findings indicated that optimal sizing and operation of the dual battery setup extended the primary battery's useful life and reduced the overall system cost.

Arun *et al.* proposed an analytical method for sizing storage in a solar-diesel-battery system [155]. The storage profile was constrained to positive values, with starting and ending storage levels required to be equal. The sizing was then determined based on the highest storage level in the profile. Norbu and Bandyopadhyay also employed Arun's storage sizing method to reduce unmet demand [156]. Bandyopadhyay enhanced Arun's method by iteratively shifting the storage profile to meet constraints [157]. Initially, the storage profile was shifted upwards to eliminate negative storage levels. Then, the latter section was shifted downward to ensure equal starting and ending storage levels. The storage was sized based on the highest storage level in the shifted profile. Similarly, Nassar *et al.* proposed iteratively shifting the storage profile upwards to eliminate negative storage levels. The storage size was determined based on the final profile's highest storage level [158]. Kichou *et al.* suggested a similar method where the difference between the starting storage level and the lowest storage level is used for sizing [159]. Data from the implemented storage system indicated a discrepancy of less than 5% between real and simulated storage sizes. Moreover, the study found that sub-hourly data resolution has minimal impact on storage sizing accuracy compared to hourly resolution.

To the best of the author's knowledge, only a limited number of analytical methods are available for both storage sizing and placement. Boonluk employed an analytical method with meta-heuristic algorithms to size and place storage [160]. The analytical method sized storage according to the difference between the maximum and minimum storage levels, with the objective of minimizing system loss, voltage fluctuation, and peak demand. The study concluded that the particle swarm algorithm yielded superior objective values compared to the genetic algorithm. Gu *et al.* utilized an analytical method with the NSGA-II genetic algorithm to size

and place energy storage [161]. The analytical method determined storage size based on either the maximum charge and discharge energy or the cumulative charge and discharge energy. The genetic algorithm optimized storage placement and energy level, with the objective of minimizing system loss, voltage fluctuation, and storage capacity. The study demonstrated that optimal storage size and placement reduced voltage fluctuation and power loss.

2.8 Research Gap

Among the four main approaches for energy storage design, the enumerative approach is the simplest to implement, relying on trial and error. This approach is also flexible, allowing for the incorporation of complex models, such as non-convex storage models. However, it is calculation-intensive and time-consuming, making it impractical for processing large solution spaces, such as those involving storage sizing and placement. Additionally, it cannot find optimal solutions beyond the defined search range.

In comparison, the meta-heuristic approach is generally faster than the enumerative approach, as it intelligently navigates the solution space, representing a more efficient form of trial and error. This approach is not only simple to implement but also capable of accommodating complex non-convex models. However, meta-heuristic approaches still lag behind mathematical optimization and analytical approaches in terms of speed. Additionally, most meta-heuristic algorithms are unable to guarantee a global optimum due to their stochastic nature, and the inability to locate optimal solutions outside the defined search range is also a notable shortcoming.

In contrast, some mathematical optimization methods are faster than both meta-heuristic and enumerative approaches. Additionally, they can guarantee a global optimum, provided the model is convex. However, they often struggle with non-linear and non-convex models, requiring approximations in such cases. Furthermore, their algorithms are often presented in a black-box manner, making it challenging to explain the results.

On the other hand, the analytical approach offers a balance of strengths. It is faster than meta-heuristic and enumerative approaches and can handle non-convex models. When applied to convex models, the analytical approach converges to the global optimal solution, while with non-convex models, it can converge to a near-optimal solution. Most importantly, the analytical approach is explainable, as storage is sized according to the largest cumulative charge or discharge it can experience. This contrasts with other approaches that find solutions through trial and error or rely on complex black-box algorithms. A summarized comparison highlighting the advantages of the analytical approach is presented in Table 2.2.

	Analytical	Mathematical	Meta-heuristic	Enumerative
Fast Speed	✓	✓	X	X
Global Optimal	✓	✓	X	X
Non-Convex Model	✓	X	✓	✓
Explainable	✓	X	X	X

Table 2.2: Analytical approach advantages when compared to other storage sizing methods.

The current landscape of analytical methods for designing energy storage reveals several limitations that hinder their broad applicability. Some of these methods may not work with erratic storage profiles and may fail to produce an optimal solution. Many existing methods are tailored to energy systems with over-generation, making them unsuitable for other types of systems. Additionally, some analytical methods do not account for storage energy leakage, which can affect the accuracy of long-term storage sizing. Furthermore, some methods overlook storage power limits, resulting in designs with unrealistic power requirements. Several analytical methods also do not require equal starting and ending storage levels, compromising the repeatability of the storage profile for future time horizons. As a result, the storage size determined by these methods may only be valid for the current design time horizon, and not for future time horizons.

The next chapter will introduce an analytical storage sizing method that addresses the aforementioned issues. The method can be applied to all types of storage profiles, including increasing, decreasing, and stable profiles that are

neither increasing nor decreasing. It also accounts for storage energy limits, power limits, and energy leakage. Moreover, the sized storage will have equal starting and ending storage levels, ensuring the sizing's validity for future time horizons. The method focuses on the technical aspects of storage sizing. The sizing is not affected by economic variability and will always yield the storage size that maximizes storage utilization while eliminating wasted storage capacity.

3
Storage Sizing

Contents

3.1 Introduction

This chapter presents an analytical method to optimally size energy storage in microgrid systems, with the objective of maximizing storage energy utilization while eliminating unused storage capacity. The method enables fast calculation speeds, calculates the exact optimum, and handles non-linear models. The method first constructs a temporal storage profile of stored energy, based on how the storage is charged and discharged in response to renewable generation and load demand. Storage is sized according to the largest cumulative charge or discharge in the profile. In essence, the storage profile represents how storage is utilized within a given system, and the method sizes optimal storage to maximize that profile, such that storage utilization is maximized and unutilized or wasted storage is eliminated. The proposed method is extended iteratively to account for storage's energy and power limits, as well as energy leakage. Two solar-battery case studies are used to demonstrate the method. The first study shows that optimally sized storage does not have wasted capacity due to over-sizing, nor does it cause energy deficits due to under-sizing. The second case study shows that increasing the storage size reduces the marginal increase in energy provided by storage, indicating diminishing returns. The diminishing return thresholds are defined by the largest daily and annual storage designs. The proposed method can be used as a decision support tool for energy analysts to determine required storage capacity when coupled with known renewable generation and load demand.

This chapter is structured as follows. Section 3.2 introduces the storage sizing method and expands it iteratively to account for storage lifespan models. The Monte Carlo simulation is also introduced to account for uncertainties in generation and demand. Section 3.3 benchmarks the proposed method against mathematical, meta-heuristic, and enumerative optimizations. Section 3.4 presents a case study on a theoretical solar-battery system with an overall surplus of solar generation to demonstrate the sizing method. Section 3.5 introduces a second case study on a real solar-battery home with excess demand. This case study illustrates that increasing

storage size has a diminishing return on the additional storage energy provided to the system. Section 3.6 summarizes the key contributions and findings from the chapter.

3.2 Method

The proposed method sizes storage with the objective of maximizing storage energy utilization while eliminating unused storage capacity. Sizing is conducted within the physical constraints of storage energy level dynamics, energy limits, and power limits. The method begins by constructing storage energy level profiles. The differences between critical points in the profile determine the cumulative charge or discharge. A matrix is proposed to calculate these differences. Based on the trend in the storage profile, the storage is sized according to the largest cumulative charge or discharge extracted from the matrix. An iterative method is then applied to account for the storage's energy and power limits, as well as energy leakage. Finally, the sizing algorithm is combined with a Monte Carlo simulation to account for uncertainties in generation and demand. This chapter aims to demonstrate the sizing method using a microgrid setup, a conventional operational control strategy, and a simplified storage model.

3.2.1 Storage Profile

The independent microgrid has three main components: renewable generation, electricity demand, and energy storage, as shown in Fig. 3.1. The system uses a conventional operation control strategy to maximize renewable consumption, where renewable generation is the primary energy supply, and storage is the secondary supply [119]. The precedence means renewable generation is used first to meet the demand. Once the demand is satisfied, surplus generation is charged into energy storage. However, when generation alone cannot meet the demand, storage discharges energy to meet the demand. When storage does not have enough energy to discharge, the demand cannot be met, and an energy deficit occurs.

Fig. 3.1(a) shows the scenario when generation is greater than demand. Part of the generation ($G(t)$) directly supplies the demand ($D(t)$), while the remaining

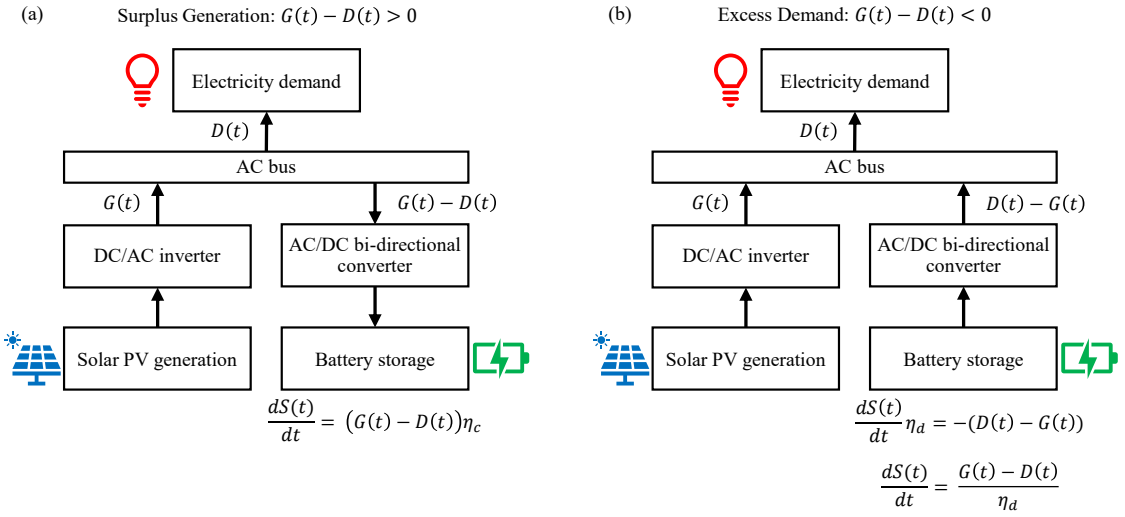

Figure 3.1: Independent microgrid setup and control in scenarios with (a) surplus generation and (b) excess demand. The microgrid is controlled using a conventional operation strategy to maximize renewable consumption. The equations model the change in lithium battery's stored energy in relation to generation, demand, and storage efficiency. The arrows indicate power flow directions.

surplus generation $(G(t) - D(t))$ is charged into storage. The storage energy's $(S(t))$ rate of change due to charging is the product of surplus generation and charge efficiency (η_c). Fig. 3.1(b) shows the scenario when generation cannot meet the demand. Generation directly supplies the demand, and the remaining unmet demand $(D(t) - G(t))$ is supplemented by storage. The product of the storage energy's rate of change due to discharging and the discharge efficiency (η_d), is equal to the power required to supplement the unmet demand. Rearranging the equation shows the change in storage energy is equal to the unmet demand divided by the discharge efficiency.

The storage behaviors from both scenarios in Fig. 3.1 are modelled by Eq. (3.1).

$$\frac{dS(t)}{dt} = (G(t) - D(t))\,\eta(t), \tag{3.1}$$

$$\text{where: } \eta(t) = \begin{cases} \eta_c, & \text{if } G(t) - D(t) > 0, \\ \frac{1}{\eta_d}, & \text{if } G(t) - D(t) < 0, \end{cases}$$

$$\int_t^{t+\Delta t} \frac{dS(t)}{dt}\,dt = \int_t^{t+\Delta t} (G(t) - D(t))\,\eta(t)\,dt,$$

$$S(t + \Delta t) - S(t) = (G(t) - D(t))\,\eta(t)\,\Delta t,$$

$$S(t + \Delta t) = S(t) + (G(t) - D(t))\,\eta(t)\,\Delta t, \tag{3.2}$$

Where $S(t)$ is the storage energy level, $G(t)$ is generation, $D(t)$ is demand, and $\eta(t)$ is storage efficiency. The storage efficiency is the charge efficiency (η_c) when generation is greater than demand, and one over the discharge efficiency (η_d) when demand is greater than generation. Eq. (3.1) is integrated from the current time step (t) to a future time step ($t + \Delta t$) to calculate the change in storage level. The integration is calculated via linear approximation by assuming the time interval is small, such that dt is approximated using Δt. The approximation means demand, generation, and storage efficiency are constant during each small time interval. The integration yields Eq. (3.2), which is time-discrete. The equation says the storage energy level at a future time step ($S(t + \Delta t)$) is equal to the current storage level ($S(t)$) plus the change in storage level. The change in storage level is equal to the difference between generation and demand, multiplied by storage efficiency and the time interval (Δt). Eq. (3.2) models storage behaviors, and is used to construct the storage profile.

For short-term storage sizing, Eq. (3.2) is sufficient. Note that the time frame for short-term storage depends on the storage device. For example, a lithium battery loses 2% of its energy per month due to self-discharge [162], while a flywheel energy storage can lose more than 20% of its kinetic energy per hour due to friction [163]. Note that battery storage self-discharge can be caused by various factors, such as self-discharge from internal chemical reactions, damage and defects that cause internal short circuits, and loads from storage monitoring systems [164]. Eq. (3.2) is modified to account for energy loss from storage leakage, forming Eq. (3.3).

$$\begin{aligned} S(t + \Delta t) &= S(t)\,(1 - \sigma) + (G(t) - D(t))\,\eta(t)\,\Delta t, \\ \text{where: } \eta(t) &= \begin{cases} \eta_c, & \text{if } G(t) - D(t) > 0, \\ \frac{1}{\eta_d}, & \text{if } G(t) - D(t) < 0, \end{cases} \\ \text{and } \sigma &= 0, \text{ if } S(t) < 0, \end{aligned} \tag{3.3}$$

Where σ is the storage energy leakage rate. Note that the energy leakage rate is expressed as a percentage per unit time interval. This equation is used to construct the storage profile. During the construction, the leakage rate is set to zero if the

storage level falls below zero. The model can be applied to most energy storage devices controlled using a conventional operation strategy.

3.2.2 Critical Storage Level

The method sizes storage based on the largest increase or decrease in the storage profile, equivalent to the largest cumulative charge or discharge that the storage can experience over the design time horizon. The increases and decreases are calculated via the difference between critical points in the storage profile. Eq. (3.4) calculates the critical points by setting the storage profile's derivative equal to zero and finding the roots.

$$\begin{gathered} \text{Solve } \frac{dS(t)}{dt} = 0 \text{ for all } t, \\ \text{such that critical points are: } t_1,\, t_2,\, \cdots,\, t_n, \\ \text{and critical storage levels are: } S(t_1),\ S(t_2),\, \cdots,\, S(t_n), \end{gathered} \tag{3.4}$$

Moreover, computational functions, such as SciPy's argrelextrema, find critical points by comparing each point with their preceding and following points [165]. If a point's storage level is higher or lower than those of its neighboring points, then it is a critical point. In rare cases, if both the starting and ending storage levels are higher or lower than their neighboring storage levels, then they are also critical points.

3.2.3 Difference Matrix

The critical points' storage levels are used by the difference matrix $\mathbf{D}$ in Eq. (3.5) to capture the storage level differences essential for storage sizing.

$$\begin{aligned} \mathbf{D} &= \mathbf{L} + \mathbf{C} - \mathbf{C}^T, \\ \text{where : } \mathbf{L} &= \begin{cases} l_{j,k} = 0, & \text{if } j \le k, \\ l_{j,k} = S(T) - S(0), & \text{if } j > k, \end{cases} \\ \mathbf{C} &= \mathbf{1}_n^T\, \mathbf{C}_n, \\ \mathbf{C}_n &= [S(t_1),\, S(t_2),\, \cdots,\, S(t_n)], \\ \text{and } \mathbf{1}_n &= [1,\, 1,\, \cdots,\, 1], \end{aligned} \tag{3.5}$$

The resulting matrix $\mathbf{D}$:

$$\begin{bmatrix} 0 & S(t_2)-S(t_1) & \cdots & S(t_n)-S(t_1) \\ (S(T)-S(0))+S(t_1)-S(t_2) & 0 & \cdots & S(t_n)-S(t_2) \\ \vdots & \vdots & \ddots & \vdots \\ (S(T)-S(0))+S(t_1)-S(t_n) & (S(T)-S(0))+S(t_2)-S(t_n) & \cdots & 0 \end{bmatrix},$$

In essence, matrix $\mathbf{D}$ pairs critical storage levels and calculates the difference between them. $\mathbf{L}+\mathbf{C}$ produce the first half of the pairs, and $\mathbf{C}^T$ produce the second half. Matrix $\mathbf{C}$ is created via the dot product of the transposed horizontal vector of all-ones ($\mathbf{1}_n^T$) and the horizontal vector of critical storage level ($\mathbf{C}_n$). Matrix $\mathbf{L}$ is a lower triangular matrix with row index j and column index k, where the lower-left half below the diagonal is filled with the difference value between the starting ($S(0)$) and ending storage levels ($S(T)$). The purpose of matrix $\mathbf{L}$ is to push the lower-left half of matrix $\mathbf{C}$ into the second design time horizon, as storage levels in the second time horizon can also govern the sizing. The maximum and minimum of matrix $\mathbf{D}$ correspond to the largest increase and decrease in the storage profile, which also represents the largest cumulative charge or discharge that the storage can experience. The proposed algorithm sizes storage based on the largest cumulative charge or discharge that the storage can experience

3.2.4 Storage Sizing

Eq. (3.6) states that storage size depends on the difference matrix $\mathbf{D}$ and the overall storage profile trend.

$$E = \begin{cases} |\min(\mathbf{D})|, & \text{if } S(T)-S(0) > 0, \\ \max(\mathbf{D}), & \text{if } S(T)-S(0) < 0, \\ \max|\mathbf{D}|, & \text{if } S(T)-S(0) = 0, \end{cases} \tag{3.6}$$

If the overall storage profile increases, that is, the ending storage level ($S(T)$) is greater than the starting storage level ($S(0)$), then storage size (E) is equal to the absolute value of the difference matrix's minimum ($|\min(\mathbf{D})|$), corresponding to the largest decrease in the storage profile. Conversely, if the overall storage profile decreases ($S(T)-S(0) < 0$), then storage size is equal to the difference matrix's maximum ($\max(\mathbf{D})$), corresponding to the storage profile's largest increase. Lastly, if the overall storage profile neither increases nor decreases ($S(T)-S(0) = 0$), then storage

size is equal to the maximum absolute value of the difference matrix ($\max|\mathbf{D}|$), corresponding to the storage profile's largest absolute increase or decrease. The following three paragraphs explain the theories behind the equation's three scenarios.

When the overall storage profile increases, more energy has been charged into storage than discharged, due to an overall surplus of generation. The surplus indicates total generation is more than enough to support the system. In this scenario, the storage's purpose is to store just enough energy to supplement periods where generation cannot support the system. During these periods, the storage discharges energy, corresponding to decreases in the storage profile. If storage is sized to accommodate the largest cumulative discharge, it can also accommodate any smaller discharges. Thus, when the overall storage profile increases, storage is sized to accommodate the largest cumulative discharge, corresponding to the largest decrease in the storage profile.

When the overall storage profile decreases, storage has discharged more energy than charged due to an overall excess of demand. The excess demand indicates that the total generation is insufficient to support the system. In this scenario, the storage's purpose is to meet as much demand as possible, by storing as much energy as possible. To do this, storage needs to charge as much energy as possible during surplus generation, corresponding to increases in the storage profile. If the storage is sized to accommodate the largest cumulative charge, it can also accommodate any smaller charges, enabling the storage to store as much energy as possible. Thus, when the overall storage profile decreases, storage is sized to accommodate the largest cumulative charge, corresponding to the largest increase in the storage profile.

When the overall storage profile neither increases nor decreases, storage has discharged as much energy as charged, indicating that the total generation is just enough to support the system. In this scenario, the storage's purpose is to charge from surplus generation and discharge to meet the excess demand. Suppose the storage is sized to accommodate the largest cumulative charge or discharge. In that case, storage can also accommodate any smaller charges and discharges, enabling it to store surplus generation to meet the excess demand. Thus, when the overall

storage profile neither increases nor decreases, storage is sized to accommodate the largest cumulative charge or discharge, corresponding to the largest absolute increase or decrease in the storage profile.

In essence, when storage has charged more energy than discharged, size for the limiting factor that is the largest cumulative discharge. Conversely, when storage has discharged more than charged, size for the largest cumulative charge.

3.2.5 Proof for the Difference Matrix

The method sizes storage based on the largest cumulative charge or discharge that the storage can experience. The largest cumulative charge or discharge is represented by the largest increase or decrease in the storage profile, which is calculated using the storage level differences between critical points in the storage profile. The following proof aims to show that all critical point differences essential for storage sizing are captured by the difference matrix in Eq. (3.5).

The proof begins by presenting an example storage profile and lists equations that calculate all critical point differences in the profile, including those that represent the largest increase or decrease in the storage profile. Then, through contradiction and duplication, the proof demonstrates that less than half of the listed equations are needed to capture the largest increase or decrease in the storage profile. Thus, the proof not only confirms that the difference matrix captures the largest increase or decrease in the storage profile used for storage sizing, but also shows that less than half of all difference equations need to be considered by the matrix, thereby reducing calculation time.

Fig. 3.2(a) shows an example storage profile with critical points identified. The storage profile is extended to two design time horizons (years) because critical points governing the storage size might be in both time horizons. Fig. 3.2(b) lists the differences between critical points' storage levels. The first row contains the differences between the first critical point's storage level and subsequent points'. The second row contains the differences between the second critical point's storage level and subsequent points'. It continues in this fashion until the last row. The

differences are divided into sections A, B, C, D, E, and the following proof shows only differences in sections A and B are essential for storage sizing.

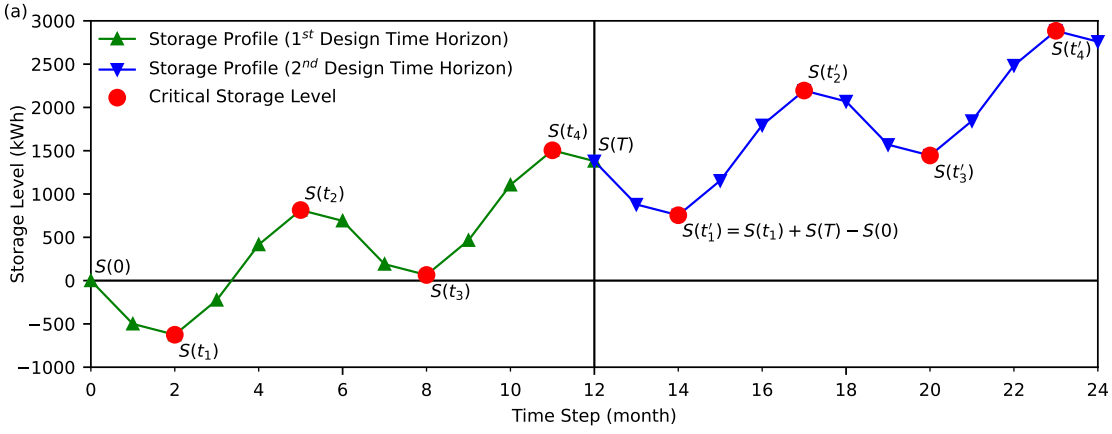

(b)

	Section A			Section D	Section E		
Section A	$S(t_2)-S(t_1)$	$S(t_3)-S(t_1)$	$S(t_4)-S(t_1)$	$S(t_1')-S(t_1)$	$S(t_2')-S(t_1)$	$S(t_3')-S(t_1)$	$S(t_4')-S(t_1)$
	$S(t_3)-S(t_2)$	$S(t_4)-S(t_2)$	$S(t_1')-S(t_2)$	$S(t_2')-S(t_2)$	$S(t_3')-S(t_2)$	$S(t_4')-S(t_2)$	
	$S(t_4)-S(t_3)$	$S(t_1')-S(t_3)$	$S(t_2')-S(t_3)$	$S(t_3')-S(t_3)$	$S(t_4')-S(t_3)$		
Section B	$S(t_1')-S(t_4)$	$S(t_2')-S(t_4)$	$S(t_3')-S(t_4)$	$S(t_4')-S(t_4)$			
Section C	$S(t_2')-S(t_1')$	$S(t_3')-S(t_1')$	$S(t_4')-S(t_1')$				
	$S(t_3')-S(t_2')$	$S(t_4')-S(t_2')$					
	$S(t_4')-S(t_3')$						

Figure 3.2: Example storage profile's (a) position of critical points and their storage levels, (b) all possible differences between critical points' storage levels. The differences are split into five sections, and the proof shows only sections A and B are essential for storage sizing.

Starting with section C, Proof 1 shows the first equation in section C duplicates the first equation in section A. Similar proofs can be made for all equations in section C; therefore, section C is not needed.

Proof 1:

$$\begin{aligned} & S(t_2') - S(t_1') \\ =& (S(t_2) + S(T) - S(0)) - (S(t_1) + S(T) - S(0)) \\ =& S(t_2) - S(t_1), \end{aligned}$$

Moving to section D, Proofs 2.1 to 2.3 show the first equation in section D can never be the storage size in all types of storage profiles (increasing, decreasing, and neither). Similar proofs can be made for all equations in section D; therefore, section D is not needed.

Proof 2.1: If the overall storage profile is increasing, such that: $S(T) - S(0) > 0$, then storage size is equal to the largest decrease in the profile. Let $S(t'_1) - S(t_1)$ be the largest decrease, then:

$$\begin{aligned} S(t'_1) - S(t_1) &< 0, \\ (S(t_1) + S(T) - S(0)) - S(t_1) &< 0, \\ S(T) - S(0) &< 0, \end{aligned}$$

Which contradicts the original assumption: $S(T) - S(0) > 0$.

Proof 2.2: If the overall storage profile is decreasing, such that: $S(T) - S(0) < 0$, then storage size is equal to the largest increase in the profile. Let $S(t'_1) - S(t_1)$ be the largest increase, then:

$$\begin{aligned} S(t'_1) - S(t_1) &> 0, \\ (S(t_1) + S(T) - S(0)) - S(t_1) &> 0, \\ S(T) - S(0) &> 0, \end{aligned}$$

Which contradicts the original assumption: $S(T) - S(0) < 0$.

Proof 2.3: If the overall storage profile is neither increasing nor decreasing, such that: $S(T) - S(0) = 0$, then storage size is equal to the largest change in the profile. Let $S(t'_1) - S(t_1)$ be the largest change, then:

$$\begin{aligned} |S(t'_1) - S(t_1)| &> 0, \\ |(S(t_1) + S(T) - S(0)) - S(t_1)| &> 0, \\ |S(T) - S(0)| &> 0, \end{aligned}$$

Which contradicts the original assumption: $S(T) - S(0) = 0$.

Similarly, Proofs 3.1 to 3.3 show the first equation in section E can never be the storage size in all types of storage profiles (increasing, decreasing, and neither). Similar proofs can be made for all equations in section E; therefore, section E is not needed.

Proof 3.1: If the overall storage profile is increasing, such that: $S(T) - S(0) > 0$, then storage size is equal to the largest decrease in the profile. Let $S(t_2') - S(t_1)$ be the largest decrease, then:

$$\begin{aligned} S(t_2') - S(t_1) &< S(t_2) - S(t_1), \\ (S(t_2) + S(T) - S(0)) - S(t_1) &< S(t_2) - S(t_1), \\ S(T) - S(0) &< 0, \end{aligned}$$

Which contradicts the original assumption: $S(T) - S(0) > 0$.

Proof 3.2: If the overall storage profile is decreasing, such that: $S(T) - S(0) < 0$, then storage size is equal to the largest increase in the profile. Let $S(t_1') - S(t_1)$ be the largest increase, then:

$$\begin{aligned} S(t_2') - S(t_1) &> S(t_2) - S(t_1), \\ (S(t_2) + S(T) - S(0)) - S(t_1) &> S(t_2) - S(t_1), \\ S(T) - S(0) &> 0, \end{aligned}$$

Which contradicts the original assumption: $S(T) - S(0) < 0$.

Proof 3.3: If the overall storage profile is neither increasing nor decreasing, such that: $S(T) - S(0) = 0$, then the first equation in section E is a duplicate of the first equation in section A:

$$\begin{aligned} & S(t_2') - S(t_1) \\ =& (S(t_2) + S(T) - S(0)) - S(t_1) \\ =& (S(t_2) + 0) - S(t_1) \\ =& S(t_2) - S(t_1). \end{aligned}$$

The proofs show that only the critical storage level differences in sections A and B are needed to capture the largest increase or decrease in the storage profile, which represents the largest cumulative charge or discharge that the storage can experience. Moreover, the equations in sections A and B are captured by the difference matrix in Eq. (3.5).

3.2.6 Storage Energy Limit

Battery manufacturers specify cycle life under specific depth of discharge and C-rating to preserve battery health and ensure the intended lifespan of the battery. For example, lithium batteries can have a cycle life of 2,000 cycles, under the conditions that the maximum depth of discharge is 80% of the original battery capacity, and the C-rating is 1C. The maximum depth of discharge limits deep discharge, while C-rating limits high charge and discharge rates; both of which can damage battery health and shorten cycle life [166]. Cycle life is the number of cycles the battery can charge and discharge before the storage capacity degrades to 80% of the original capacity. Thus, limiting the depth of discharge ensures that the battery has enough capacity over its cycle life while accounting for degradation. The battery should be replaced at the end of its cycle life. Eq. (3.7) calculates the storage's total energy capacity when accounting for the depth of discharge.

$$E_{tot} = \frac{E}{DoD_{max} - DoD_{min}}, \tag{3.7}$$

The equation says storage's total energy capacity (E_{tot}) is equal to the storage size (E) divided by the difference between the maximum (DoD_{max}) and minimum depth of discharge (DoD_{min}). In this design method, storage size is the energy capacity in the usable portion of the storage, while the remaining capacity is reserved to compensate for storage degradation.

Storage cannot discharge beyond the maximum depth of discharge, nor charge above the minimum depth of discharge. The storage levels at the maximum and minimum depth of discharge define the storage's energy limits. The upper and lower storage energy limits are defined by Eq. (3.8) and Eq. (3.9).

$$S_{up} = E_{tot}\,(1 - DoD_{min}), \tag{3.8}$$

$$S_{low} = E_{tot}\,(1 - DoD_{max}), \tag{3.9}$$

Where S_{up} and S_{low} are the upper and lower storage limits, E_{tot} is storage's total energy capacity, DoD_{max} and DoD_{min} are the maximum and minimum depth of discharge.

The storage's energy limits are used in Eq. (3.10) when constructing the constrained storage profile.

$$S_{low} \leq S(t) \leq S_{up}, \tag{3.10}$$

The equation says the storage level ($S(t)$) cannot exceed the upper storage limit (S_{up}), nor fall below the lower storage limit (S_{low}). Once the storage level hits the upper limit, energy cannot be charged into storage. Conversely, energy cannot be discharged if the storage level is at the lower limit, preventing deep discharge that can damage battery cycle life.

Eq. (3.10) should hold in the final constrained storage profile. However, it is often too restrictive when used in the iterative storage sizing method, which can cause near-optimal sizing. To solve this issue, Eq. (3.11) relaxes the energy limit constraint by adding a slack term, allowing the storage level to go beyond the upper and lower storage limits.

$$S_{low} - \alpha \left|S(T) - S(0)\right| \leq S(t) \leq S_{up} + \alpha \left|S(T) - S(0)\right|, \tag{3.11}$$
$$\text{and } 0 \leq \alpha < 1,$$

The constraint pushes the storage profile into a sustainable state, while the slack term ensures it does not push too hard to cause near-optimal sizing. The slack is the absolute difference between the last iteration's starting ($S(0)$) and ending storage levels ($S(T)$), scaled by a multiplier (α). The multiplier is a number between zero and one. A large multiplier will cause slow convergence or even non-convergence, while a small multiplier may yield near-optimal sizing instead of the exact optimum. A multiplier of 0.5 should work for most cases. However, a better strategy is to start with a large multiplier, then gradually reduce it at each iteration. As the storage profile converges, the slack term converges to zero, nullifying its effect on the storage energy limits.

3.2.7 Sustainable Starting Storage Level

A constrained storage profile will repeat itself when subject to the same demand and generation patterns in the future. The repeatability ensures the storage size is sustainable, and can support similar demand and generation patterns in the future. Equal starting and ending storage levels characterize sustainability. The sustainable starting and ending storage levels are calculated using Eq. (3.12).

$$\begin{aligned} S(0)_s &= S(T)_s \\ &= \begin{cases} S(T) - \max(S(t)) + S_{up}, \text{ if } S(T) - S(0) \geq 0, \\ S(T) - \min(S(t)) + S_{low}, \text{ if } S(T) - S(0) \leq 0, \end{cases} \end{aligned} \tag{3.12}$$

Where $S(0)_s$ and $S(T)_s$ are the sustainable starting and ending storage levels, $S(0)$ and $S(T)$ are the starting and ending storage levels in the storage profile, $\max(S(t))$ and $\min(S(t))$ are the maximum and minimum storage levels in the storage profile, S_{up} and S_{low} are the upper and lower storage limits. The equation says the sustainable starting storage level is dictated by the difference between the ending and maximum storage levels in an increasing scenario, and by the ending and minimum storage levels in a decreasing scenario. The storage limits are added to re-frame those differences to the usable portion of storage.

3.2.8 Storage Power Limit

High charge and discharge rates can also damage battery health and shorten cycle life [167]. The C-rating relates the battery's energy capacity to power capacity. The maximum charge and discharge rate are calculated based on the C-ratings using Eq. (3.13) and Eq. (3.14), which define the storage's power limits.

$$P_c = E_{tot}\, C_c, \tag{3.13}$$

$$P_d = E_{tot}\, C_d, \tag{3.14}$$

Where P_c and P_d are the maximum charge and discharge rates, E_{tot} is the storage's total energy capacity, C_c and C_d are the storage's charge and discharge C-ratings.

Moreover, the external power structure connected to the storage can also limit charge and discharge rates.

The power limits are used in Eq. (3.15) while constructing the constrained storage profile.

$$-P_d \leq G(t) - D(t) \leq P_c, \tag{3.15}$$

The equation says power charged to or discharged by storage ($G(t) - D(t)$) cannot exceed the maximum charge (P_c) or discharge rates (P_d). The equation limits high charge and discharge rates that can damage battery health. Note that, due to this constraint, the available storage power may sometimes be insufficient to meet excess demand or absorb surplus generation, potentially resulting in unmet demand or curtailed generation. This will be further discussed in the method limitations in Section 3.3.2.

Eq. (3.15) should hold in the final constrained storage profile; however, it is often too restrictive when used in the iterative storage sizing method. In particular, if storage size becomes zero during an iteration, the power limits will also become zero, causing storage size in all subsequent iterations to be zero. Eq. (3.16) relaxes the power limit constraint by adding a slack term, enabling zero storage size to have charge and discharge.

$$-P_d - \alpha\,|S(T) - S(0)| \leq G(t) - D(t) \leq P_c + \alpha\,|S(T) - S(0)|, \tag{3.16}$$
$$\text{and } 0 \leq \alpha < 1,$$

The slack consists of the absolute difference between the last iteration's starting ($S(0)$) and ending storage levels ($S(T)$), scaled by a multiplier (α).

3.2.9 Storage Lifespan

The storage lifespan is calculated using Eq. (3.17).

$$T_{life} = \min(T_{cal},\, \rho\frac{NE}{E_{thru}}) \tag{3.17}$$

Where T_{life} is the battery lifespan in years, T_{cal} is the battery calendar life, ρ is the degradation factor, N is the battery cycle life, E is the storage size, and E_{thru} is

the battery energy throughput over a year. The energy throughput is calculated by summing either the charge or discharge energy in the final constrained storage profile. The manufacturer specifies the battery cycle life and calendar life in terms of number of cycles and number of years, respectively. The degradation factor is a number less than one, which depends on the application of the battery. For example, the degradation factor is smaller with solar-battery systems, as solar intermittency can cause rapid charge and discharge from the battery, damaging the battery and shortening its lifespan.

3.2.10 Iterative Storage Sizing Method

The sizing method is extended iteratively to account for the depth of discharge, maximum charge and discharge rates, and energy leakage. These elements have inter-dependency with the storage size, therefore requiring an iterative approach to solve. The sizing steps are outlined in Fig. 3.3.

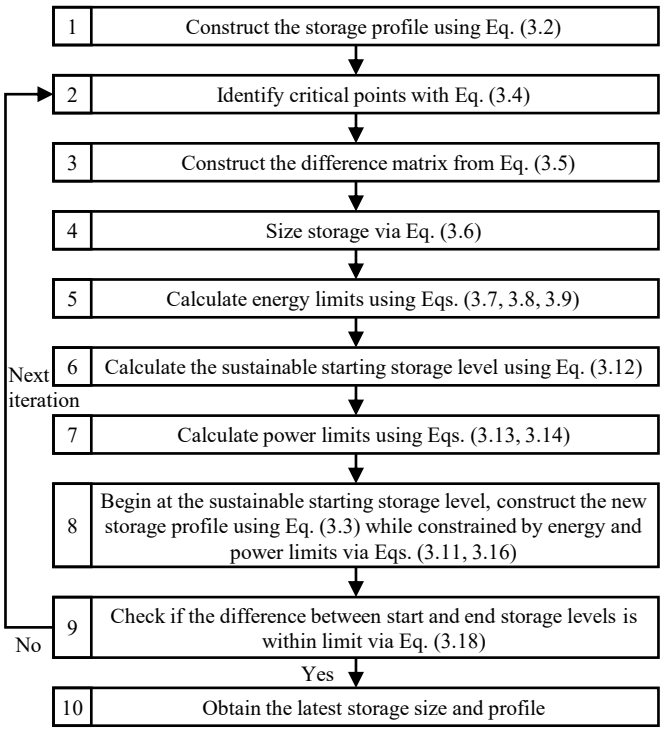

Figure 3.3: The storage sizing steps flowchart. The sizing method uses the equations to calculate the optimal storage size and associated constrained storage profile.

The first step is to construct the unconstrained storage profile. The unconstrained storage profile starts at zero, and storage level at each time step is calculated using Eq. (3.2). Then, critical points are identified in the storage profile using Eq. (3.4) or computer functions. The critical points' storage levels are used in Eq. (3.5) to construct the difference matrix. Then storage size is calculated using the difference matrix via Eq. (3.6), based on the difference between the starting and ending storage levels in the storage profile. The storage size is used in Eqs. (3.7, 3.8, 3.9) to calculate the upper and lower storage limits. The storage limits are used in the sixth step to calculate the sustainable starting storage level via Eq. (3.12). Then, the maximum charge and discharge rates are calculated using Eqs. (3.13, 3.14). The eighth step is to construct the new constrained storage profile. Starting from the sustainable starting storage level, the new profile is constructed using Eq. (3.3) to calculate the storage level at each time step, while constrained by the relaxed storage energy limits via Eq. (3.11), and by the relaxed storage power limits via Eq. (3.16). Note that the starting and ending storage levels used in the relaxed storage energy and power limits come from the previous storage profile. Once the new constrained storage profile is constructed, its starting and ending storage levels are used in the ninth step, to check if the absolute difference between starting and ending storage levels is within the user-defined permissible limit, as stated in Eq. (3.18).

$$|S(T) - S(0)| \leq \epsilon, \tag{3.18}$$

The permissible difference limit (ϵ) dictates the accuracy and significant figures of the resulting storage size. Moreover, it ensures that the starting and ending storage levels are nearly equal, which characterizes a repeatable storage profile. This repeatability ensures that the storage size is sustainable and capable of supporting similar demand and generation patterns in the future. If the difference is beyond the limit, then repeat the process from the second step with the new constrained storage profile. If the difference is within the limit, then the latest storage size and constrained storage profile are the results.

The latest storage size is determined by maximizing storage utilization and eliminating wasted storage capacity. In most scenarios, eliminating wasted storage capacity leads to a smaller storage size, while maximizing storage utilization increases the energy provided by the storage. Thus, in most scenarios, the proposed method also yields the smallest storage size that maximizes the energy provided by the storage to the system.

3.2.11 Monte Carlo Simulation Method

Monte Carlo simulation accounts for the uncertainties in renewable generation and electricity demand. The simulation first generates randomized generation and demand profiles using statistical models. The randomized profiles are fed into the storage sizing algorithm to obtain a distribution of optimal storage sizes. The optimal storage size is then selected based on the distribution. The steps for the Monte Carlo simulation are outlined in Fig. 3.4.

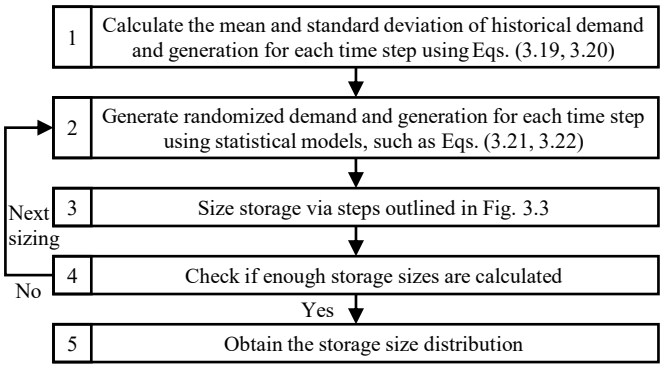

Figure 3.4: Monte Carlo simulation steps flowchart. The simulation enables the sizing algorithm to size storage while accounting for generation and demand uncertainties.

The first step is to calculate the mean and standard deviation of the historical data at each time step. The mean and standard deviation are calculated using Eq. (3.19) and Eq. (3.20), respectively.

$$\bar{x} = \frac{1}{n}\sum_{i=1}^{n} x_i \tag{3.19}$$

$$s = \sqrt{\frac{1}{n-1}\sum_{i=1}^{n}(x_i - \bar{x})^2} \tag{3.20}$$

Where at a particular time step, x is the historical data, n is the number of historical data, $\bar{x}$ is the mean or average value, and s is the standard deviation. For example, historical data from the first hour of the year, for the past ten years, are used to calculate the mean and standard deviation for the first time step.

The second step is to generate randomized demand and generation profiles using probability distribution models. In this study, variations in demand and generation at each time step are assumed to follow the normal distribution [143]. Randomized data following normal distribution are generated using Box-Muller transform via Eqs. (3.21, 3.22).

$$r_{n1} = \sqrt{-2 \ln r_{u1}} \cos(2\pi r_{u2}) s + \bar{x} \tag{3.21}$$

$$r_{n2} = \sqrt{-2 \ln r_{u1}} \sin(2\pi r_{u2}) s + \bar{x} \tag{3.22}$$

Where r_{n1} and r_{n2} are two randomized data following the normal distribution with specified mean ($\bar{x}$) and standard deviation (s). r_{u1} and r_{u2} are two random values between zero and one, generated via uniform distribution. The Box-Muller transform takes two random values between zero and one, and generates two randomized values following the normal distribution. Other statistical models can also model the uncertainties of generation and demand, such as Weibull distribution, Gamma distribution, and AutoRegressive Moving Average model.

The third step is to feed the randomized demand and generation profiles into the storage sizing algorithm outlined in Fig. 3.3, and calculate the storage size. Then, repeat this process from the second step until enough storage sizes are calculated. Finally, gather the results to form a distribution of storage sizes. The distribution gives useful information, such as the mean and standard deviation. The percentile of each storage can also be calculated by ranking the storage sizes from small to large.

3.3 Benchmark

This section benchmarks the proposed method against mathematical, meta-heuristic, and enumerative optimization. A comparison shows that the proposed method has a fast calculation speed, calculates the exact optimum, and can handle non-linear

models. However, three limitations of the proposed method are also identified. These limitations include slower speed with large dataset, inability to maximize energy output in some scenarios, and inaccuracy of the simple storage lifespan model.

3.3.1 Method Advantages

The proposed method was tested on randomly generated scenarios against other sizing methods including: the one-by-one enumerative method for benchmarking, particle swarm meta-heuristic algorithm for locating the global optimum, and Gurobi mathematical programming for speed comparison. The comparison between the methods is shown in Table 3.1.

	Proposed	Mathematical	Meta-heuristic	Enumerative
Fast Speed	✓	✓	X	X
Exact Optimal	✓	✓	X	X
Non-linear Model	✓	X	✓	✓

Table 3.1: Comparison of storage sizing methods.

The proposed method is faster than other methods, calculates the exact optimum, handles non-linear models, and is built on a real-world theory. The fast speed is helpful in applications with repeated sizing, such as the Monte Carlo method or unsupervised machine learning. The ability to calculate the exact optimum yields more precise and accurate answers. The capability to handle non-linear models enables more detailed and accurate storage modelling. Finally, the proposed optimization algorithm is built on a real-world theory that storage should be sized according to the largest cumulative charge or discharge it can experience; the real-world connection enables a deeper understanding of the sizing method.

In most scenarios, the proposed method yielded the same solutions as that from Gurobi mathematical programming and one-by-one enumerative method, while particle swarm algorithm tends to yield near-optimal solutions. However, in some scenarios, the proposed method yield different solutions. These scenarios typically requires storage wastage to maximize storage energy provided to the system, and this will be further discussed in the limitations of the method.

3.3.2 Method Limitations

Three limitations of the proposed method were identified during testing. The first limitation is that while the proposed method is initially faster, other methods can eventually catch up. Each method's calculation speed trendline is shown in Fig. 3.5.

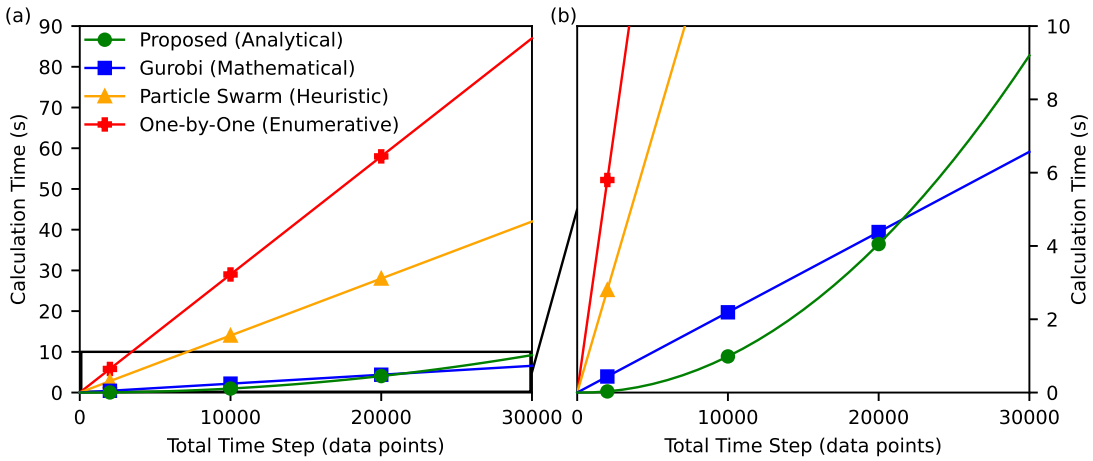

Figure 3.5: Storage sizing methods' speed comparison via (a) calculation time trendlines and (b) zoomed-in window of the trendlines. In the zoomed-in window, the Gurobi mathematical programming method becomes faster than the proposed method at 22,000 data points.

The speed tests are done using an Intel Core i7-9700 processor with randomly generated data. The data size increased at 1,000 data points increments, and tests were repeated 30 times at each increment. The proposed method's calculation time is related to the number of critical points in the storage profile. In contrast, other methods' calculation times are related to the total number of data points in the profile. Since the number of critical points is a fraction of all data points, the proposed method is initially faster. However, the proposed method has a time complexity of $O(n^2)$ due to the matrix used, while other methods have a time complexity of $O(n)$. The time complexity indicates that other methods' calculation times are linearly related to the number of data points. In contrast, the proposed method's calculation time is quadratically related to the number of critical points. Thus, while the proposed method is initially faster, other methods can eventually catch up as the data size increases. However, it is important to

note that, under normal circumstances, such as using hourly data for an entire year, the proposed method remains faster.

The second limitation is that the proposed method's objective is to maximize storage energy utilization while eliminating unused storage capacity. In most scenarios, this objective also maximizes the amount of energy the storage provides to the system. However, in some scenarios, it does not. These scenarios typically involve a high leakage rate of more than 40% per time interval and small charge and discharge rates of less than 0.1C relative to the storage capacity. The small charge and discharge rates mean that the storage power may not be enough to meet the excess demand or absorb the surplus generation, which could result in unmet demand or curtailed generation. To maximize the energy provided, the optimal storage would need a larger energy capacity to increase the charge and discharge rates, ensuring it has sufficient power to meet the large excess demand and surplus generation. However, this larger energy capacity cannot be fully utilized, as the system may lack sufficient surplus generation to fully charge the storage or enough excess demand to fully discharge it. As a result, the storage will operate at lower energy levels to reduce energy leakage, with a portion of the storage remain unused. Therefore, the storage size that maximizes the energy provided will have some wasted capacity in these scenarios. Since the proposed method always eliminates unutilized storage capacity while maximizing storage energy utilization, it yields the storage size that maximizes storage energy provided without wasted capacity, which may not be the size that maximizes storage energy provided in the absolute sense.

The third limitation is that the current battery lifespan model is simple, but can be inaccurate. The current model uses lithium battery manufacturer's recommended depth of discharge and C-rating to preserve battery health, and achieve the specified cycle life. However, studies have shown that renewable intermittency can stress a battery and shorten its lifespan [154]. Lithium battery degradation modelling is an active research area, and many models for calendar and cycle aging have been proposed in recent years [168]. Factors such as usage, time, temperature,

depth of discharge, charge and discharge rates, voltage, and state of charge can all contribute to lithium battery degradation [166].

3.4 Case Study with Surplus Generation

The first case study is on a theoretical solar-battery system with an overall surplus of renewable generation. The case study demonstrates the sizing method, and shows the optimal size does not have wasted storage due to over-sizing, nor cause energy deficits due to under-sizing. Moreover, it shows storage energy leakage can affect long-term storage sizing, as leakage can cause energy deficit to the system.

3.4.1 System Setup

A hypothetical solar PV (photovoltaic) and lithium battery microgrid system is used to demonstrate the storage sizing method. The microgrid setup is shown in Fig. 3.1, and the system is controlled using a conventional operation strategy to maximize renewable consumption [119]. The operation strategy first uses solar generation to meet the demand directly. Once the demand is met, any excess generation is charged into storage. When generation cannot meet the demand, energy is discharged from storage to meet the demand.

3.4.2 Generation, Demand, and Storage Profiles

The solar PV system has an annual generation of 7.2 MWh, and the microgrid's annual electricity demand is 6 MWh. The microgrid system is situated in a northern temperate climate, with warm summers and cold winters. The monthly total generation and demand profiles are shown in Fig. 3.6. The generation profile follows the typical solar generation pattern in the northern temperate zone, with high generation during summer and low generation during winter. Similarly, the demand profile follows the typical electricity demand pattern in the northern temperate zone, with low summer demand and high winter demand.

The lithium battery storage system is assumed to have a charge and a discharge efficiency of 80% [155]. The storage level starts at zero, and storage levels at the end

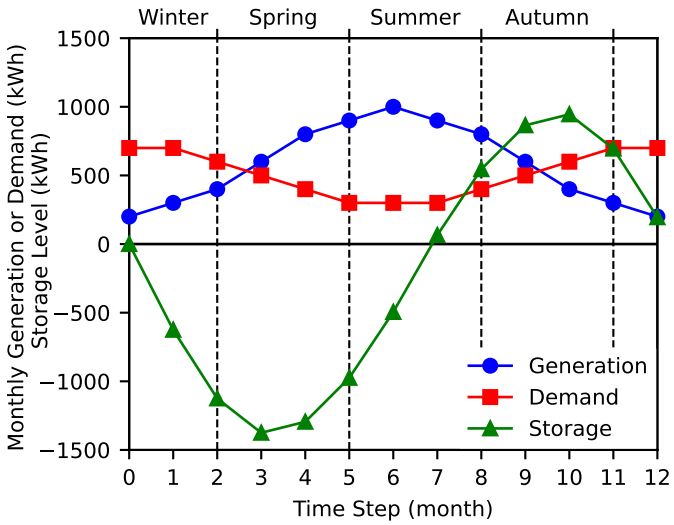

Figure 3.6: Solar-battery microgrid's monthly total solar PV generation, electricity demand, and the lithium battery's unconstrained storage profile. The microgrid is controlled to maximize renewable consumption. In the generation and demand profiles, the nodes represent monthly total energy, and the month begins at the node. In the storage profile, the nodes represent lithium battery's stored energy at each time step. The dashed lines separate the seasons.

of each month are calculated using Eq. (3.2). The resulting unconstrained storage profile is shown in Fig. 3.6. The profile starts in the winter and initially decreases as storage discharges energy to supplement the high winter demand. The decrease stops in early spring, as the rising solar generation balances the falling demand, allowing the generation to satisfy demand directly. Then the profile increases during late spring, summer, and early autumn, as storage charges from the surplus solar generation. The increase stops in late autumn, as the rising demand balances with the falling generation. Finally, the profile decreases again during late autumn and winter due to the excess demand. Overall, the storage profile increased between the start and end of the year, indicating more generation than demand across the year.

3.4.3 Storage Size and Validation

Fig. 3.7(a) shows the unconstrained storage profile extended to two design time horizons (years) with critical points identified. In the first year, the ending storage level ($S(T)$) is greater than the starting storage level ($S(0)$), meaning the overall storage profile increases. In an increasing scenario, storage is sized according to

the profile's largest decrease, corresponding to the largest cumulative discharge the storage can experience. The largest decrease starts from the second critical storage level in the first year ($S(t_2)$), and ends at the first critical storage level in the second year ($S(t_1')$). Correspondingly, the largest cumulative discharge starts in late autumn and ends in early spring, during which excess demand cause the storage to discharge. To size the storage, the difference matrix is constructed using Eq. (3.5). Then, Eq. (3.6) says in an increasing scenario, storage size is equal to the absolute value of the difference matrix's minimum, which is 2125 MWh.

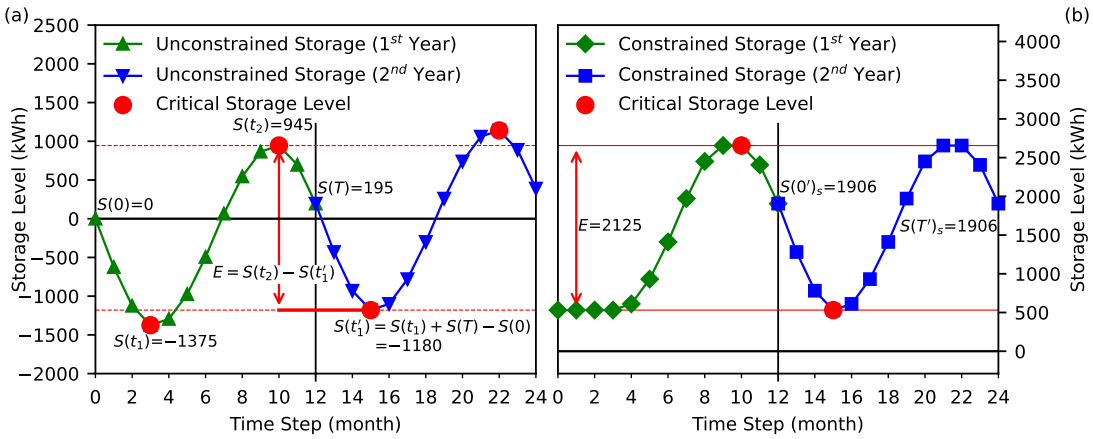

Figure 3.7: Solar-battery microgrid's (a) unconstrained storage profile and (b) constrained storage profile. The unconstrained storage profile shows the critical storage levels used to calculate the storage size (E). The storage size is used to construct the constrained storage profile. In the constrained profile, the red horizontal lines mark the upper and lower storage limits according to 80% depth of discharge. Storage cannot charge beyond the upper limit nor discharge below the lower limit.

Lithium batteries have a recommended depth of discharge of 80% [169], and using Eq. (3.7), the storage energy capacity is calculated to be 2656 kWh. The upper and lower storage limits are calculated using Eqs. (3.8, 3.9) to be 2656 kWh and 531 kWh, respectively. Moreover, lithium batteries typically have charge and discharge C-ratings of 1C [170], which means the maximum charge and discharge rates are 2656 kW according to Eqs. (3.13, 3.14). The constrained storage profile is constructed using Eq. (3.2) while constrained by the storage energy limits via Eq. (3.10) and by the power limits via Eq. (3.15). The constrained storage profile is shown in Fig. 3.7(b). The profile starts during winter, where it stays at the lower

storage limit due to excess winter demand. In early spring, the demand falls while solar generation rises, creating surplus generation to charge the storage, causing the profile to increase. During summer, the profile continues to increase as storage continues to charge. The upper storage limit is reached in early autumn. The storage is sized to store just enough energy to carry through the largest cumulative discharge during late autumn, winter, and early spring. In late autumn, storage begins to discharge due to excess demand, causing the profile to decrease. The storage continues to discharge during winter, and the profile briefly reaches the lower storage limit in early spring. Then, mid-spring begins, and the profile starts to increase as storage charges from the surplus generation again. In the second year of the constrained storage profile in Fig. 3.7(b), the ending storage level is the same as the starting storage level. It shows that the constrained storage profile is sustainable, and can continue indefinitely if generation and demand patterns are repeatable from year to year. The sustainable starting storage level is calculated to be 1906 kWh using Eq. (3.12).

The optimally sized storage is compared with both over-sized and under-sized storage to validate the method. The objective of the method is to maximize storage energy utilization while eliminating unutilized storage capacity. The validation will demonstrate that optimally sized storage neither has unused capacity due to over-sizing nor causes an energy deficit due to under-sizing, thereby maximizing the energy utilization of the storage. Fig. 3.8 shows the constrained storage profiles for optimally sized, oversized, and undersized storage during three design time horizons (years).

For undersized storage, the storage profile starts empty at the lower storage limit during winter. It begins to increase in mid-spring, and reaches the undersized capacity in summer. Then, the profile starts to decrease in late autumn. Due to the undersizing, the storage does not have enough stored energy to carry through the largest cumulative discharge between late autumn and early spring. As a result, the storage empties in winter, and stays empty until mid-spring. The empty storage cannot provide energy to meet the demand, causing energy deficits. In contrast, oversized storage never reaches empty, as it has more than enough capacity to

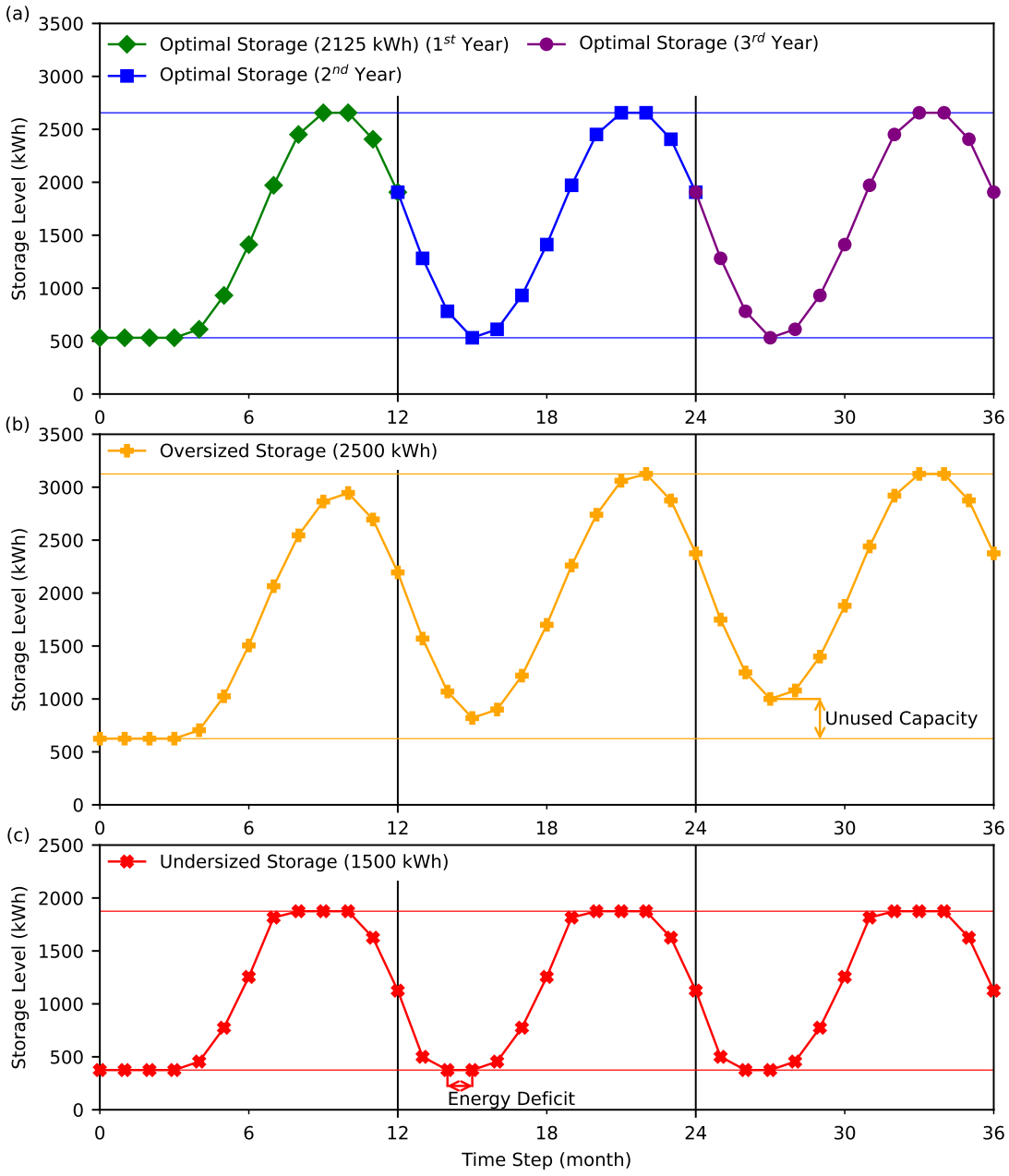

Figure 3.8: Constrained storage profile of (a) optimally sized, (b) oversized, and (c) undersized storage. The profiles encompass three design time horizons (years). The colored horizontal lines mark the upper and lower storage limits according to 80% depth of discharge. Storage cannot charge beyond the upper limit nor discharge below the lower limit, and energy deficits occur when storage cannot discharge to meet the demand. The figure shows optimally sized storage does not have wasted capacity due to over-sizing, nor cause energy deficits due to under-sizing.

carry through the largest cumulative discharge. However, part of the capacity is wasted and never used. Compared to oversized and undersized storage, the optimally sized storage does not have wasted storage capacity nor cause energy deficit due to a lack of storage capacity.

In this study, the energy deficit is minimized within the system by maximizing the storage energy provided to the system, which is achieved by maximizing storage utilization. Thus, the optimal storage size maximizes storage utilization while eliminating unused storage capacity. Note that one may still choose a larger storage size for a greater safety factor, or a smaller size to reduce cost.

3.4.4 Long-term Storage Size

The case study's design time horizon is a year, which is considered long-term for lithium batteries. When sizing for long-term storage, energy leakage can have significant impacts. Lithium batteries are assumed to have a constant energy leakage rate of 2% per month [162]. The iterative sizing method is used to account for leakage. Beginning at the sustainable starting storage level, the storage profile with leakage is constructed via Eq. (3.3) while constrained by Eqs. (3.11, 3.16). Following the steps outlined in Fig. 3.3, the iterative sizing method is conducted using a multiplier of 0.1 and a permissible difference limit of 0.01. The storage size converged at 2115 kWh after seven iterations. Compared to the original sizing, the storage size decreased because leakage reduced the amount of energy in the storage. Fig. 3.9 shows the constrained storage profiles with and without leakage.

When compared, the profile with leakage decreases faster and increases slower, indicating the storage effectively discharges faster and charges slower due to leakage. The profile with leakage also shows that storage size is insufficient to carry through the largest cumulative discharge, and energy deficits will occur in early spring. The energy deficit indicates generation can no longer fully support the demand with the additional loss from storage leakage. Therefore, it is crucial to account for storage leakage when sizing for long-term energy storage.

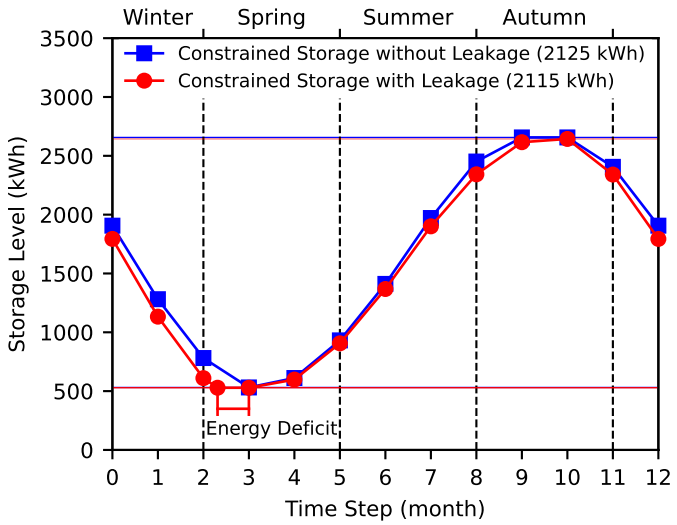

Figure 3.9: Constrained storage profiles with and without accounting for energy leakage. The colored horizontal lines mark the upper and lower storage limits. Storage cannot charge beyond the upper limit nor discharge below the lower limit, and energy deficits occur when storage cannot discharge to meet the demand. The dashed lines separate the seasons.

3.5 Case Study with Excess Demand

The second case study is on a planned solar-battery home near Oxford, the home has an overall excess of electricity demand when compared to its renewable generation. The study shows storage size requirements are high during early summer and early autumn, when both generation and demand are high. Furthermore, the study shows increasing storage size has diminishing returns on storage energy provided to the microgrid, and relates the diminishing return thresholds to the largest daily and annual storage designs.

3.5.1 System Setup

The storage sizing method is applied to a domestic property in Oxfordshire. The owner plans to install roof-top solar PV panels and wants to know what size of lithium battery storage can complement the solar PV. The solar-battery system setup is shown in Fig. 3.10.

The microgrid system consists of a common AC bus that connects all the elements. The grid electricity network connects to the bus, and regulates the

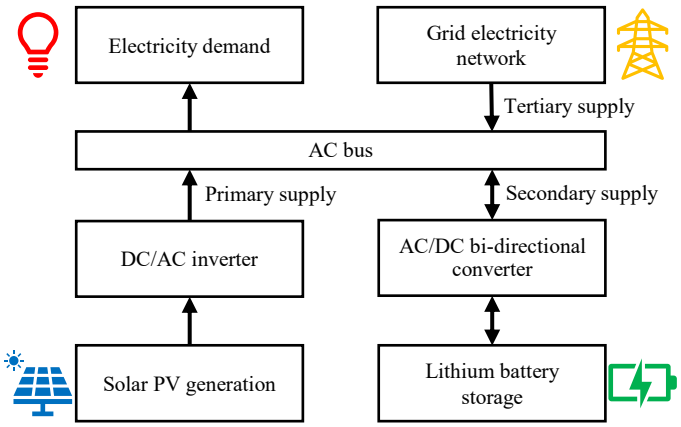

Figure 3.10: The domestic property's solar-battery microgrid setup and operation control strategy. The microgrid uses a conventional operation strategy to maximize renewable consumption and minimize electricity grid reliance. The primary supply is used first when available, then the secondary, and then the tertiary. The arrows indicate power flow directions. Note that power can be charged to or discharged by lithium battery storage, and storage only charges from surplus solar generation.

microgrid's frequency and voltage. The electricity demand directly taps from the bus. The solar PV system connects to the bus via a DC-to-AC inverter, and the lithium battery system connects to the bus via a bi-directional AC/DC converter. The microgrid system is controlled using a conventional operation strategy to maximize renewable consumption [119]. The operation strategy states that solar PV is the primary energy supply, lithium storage is the secondary supply, and grid electricity is the tertiary supply. The precedence means solar generation will be used first to meet the demand. Any excess generation will be charged into lithium storage. When generation cannot meet the demand, energy from storage will be used. When both generation and storage are not enough, grid electricity will be used to meet the demand. The availability of these three supply sources ensures the demand is met at all times.

3.5.2 Solar Generation and Electricity Demand Models

The domestic property's roof faces southwest and pitches at a 50° angle; it can accommodate 7 kW of solar PV panels. The solar PV system has a 10% energy loss, mainly due to the DC-to-AC inverter [79]. The solar generation is simulated

using Pfenninger and Staffell's method via the Renewables.ninja service [79]. The simulation yields hourly solar generation from 2010 to 2019. Then, the data is averaged to produce an hourly solar generation profile for the typical year, shown in Fig. 3.11. Solar generation is lower during winter and higher during summer, due to summer's higher solar insolation and duration. Demand is highest in winter and lowest in summer, with greater variation occurring during the winter months.

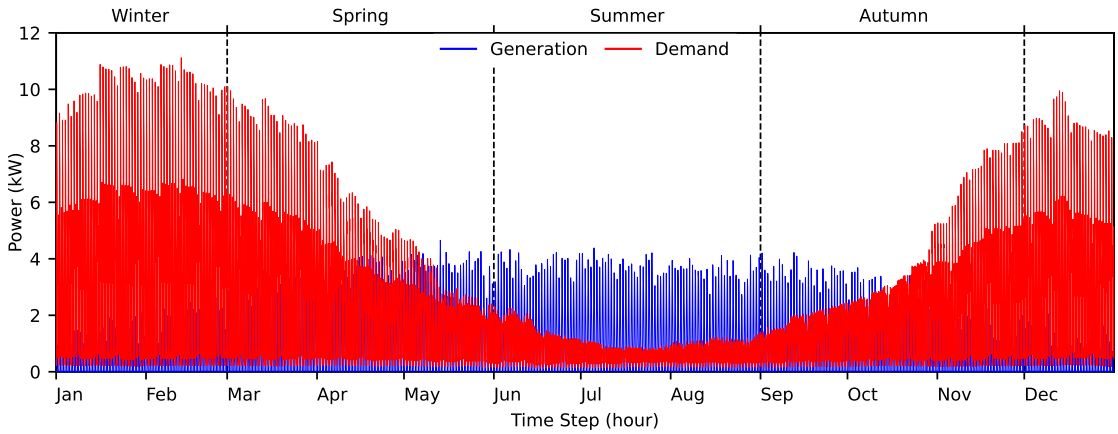

Figure 3.11: Solar-battery microgrid's average hourly solar PV generation and electricity demand in a typical year. The dashed lines separate the seasons.

The house has two electricity meters, one for water and space heating, and one for all other energy usages. The water and space heaters only operates from 4:00 am to 2:00 pm and from 7:00 pm to 11:00 pm. Since 2010, the meter readings have been recorded once every five days. Elexon demand profiles are used to interpolate the hourly demand between readings [86]. Elexon's domestic economy profiles are used to interpolate heating demand, and domestic profiles are used to interpolate all other demand. The domestic economy profiles are zeroed during heaters' non-operational hours. The hourly demand between 2010 and 2019 are modelled, and the data are averaged to produce the hourly electricity demand profile for the typical year, shown in Fig. 3.11. Note that the annual demand is 18 MWh, while the annual generation is 7 MWh.

3.5.3 Annual Storage Size

The lithium battery system is assumed to have a charge and a discharge efficiency of 80% [155]. Based on the demand, generation, and storage efficiencies, the unconstrained storage profile is constructed using Eq. (3.2), as shown in Fig. 3.12.

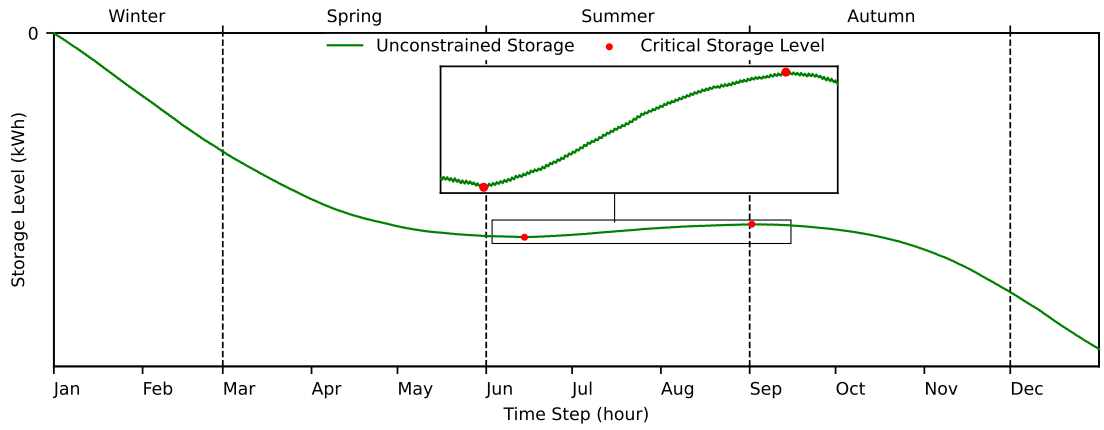

Figure 3.12: Solar-battery microgrid's annual unconstrained storage profile. The overall storage profile decreased between start and end, indicating storage should be sized according to the largest cumulative charge, which is outlined by the critical storage levels in the zoomed-in window.

The overall storage profile decreased between start and end, indicating the total generation is insufficient to support the system. Lithium battery has a recommended depth of discharge of 80% [169], a C-rating of 1C [170], and a leakage rate of 2% per month [162]. Following the steps outlined in Fig. 3.3, the iterative sizing method is conducted using a multiplier of 0.1 and a permissible difference limit of 0.01. The storage size converged at 601 kWh, and the constrained storage profile is shown in Fig. 3.13.

The constrained storage profile has many small peaks and troughs, which outline the daily charge and discharge experienced by storage. These peaks and troughs produce many critical points, but for simplicity, only the two critical points that dictate the storage size are shown in the figure. The difference in their storage levels represents the largest cumulative charge experienced by storage.

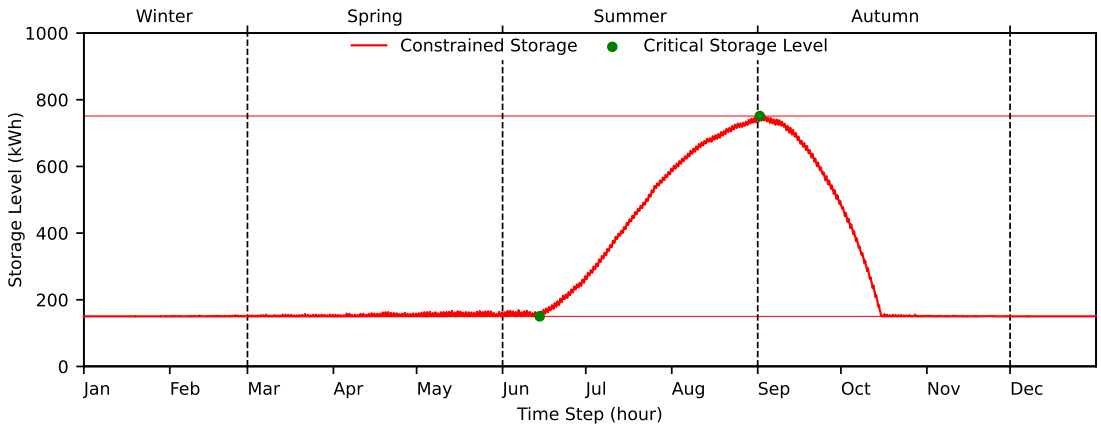

Figure 3.13: Solar-battery microgrid's annual constrained storage profile. The small peaks and troughs in the storage profiles outline the daily charge and discharge experienced by storage. The red horizontal lines mark the upper and lower storage limits, and storage cannot charge beyond the upper limit nor discharge below the lower limit.

3.5.4 Monte Carlo Simulation

The 601 kWh annual storage size is large. To validate this, Monte Carlo simulation is used to see how storage size varies with the uncertainties in demand and generation. Monte Carlo simulation is conducted following the steps outlined in Fig. 3.4, using historical demand and generation data from 2010 to 2019. The resulting storage size distribution after 3000 simulations is shown in Fig. 3.14.

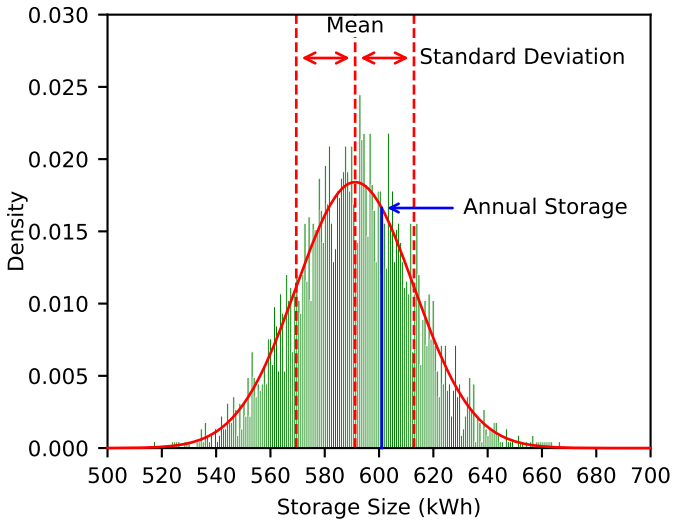

Figure 3.14: Histogram of storage size distribution from Monte Carlo simulation. The annual storage size calculated using typical year demand and generation profiles is within one standard deviation from the mean.

The result shows that 601 kWh storage size is realistic, as it is within one standard deviation from the mean, at the 68^{th} percentile. Note that the storage size makes up the 80% depth of discharge, meaning the total storage capacity is 751 kWh, which is beyond the 100^{th} percentile. This means the total storage capacity can maximize renewable consumption even in the worst-case scenario of the Monte Carlo simulation.

3.5.5 Daily Storage Size

The large storage size is due to the annual design time horizon, which forces the design to account for seasonal storage in addition to daily storage. The storage's seasonal capability is only used once per year; it is charged during summer (June, July, August) and discharged during autumn (September, October), as shown in the constrained storage profile in Fig. 3.13. In contrast, the storage's daily capability is used for everyday of the year: it is charged during the day and discharged at night, as shown by the small peaks and troughs in the figure. The higher charge and discharge frequency means that daily storage provides more energy per unit of storage capacity when compared to seasonal storage.

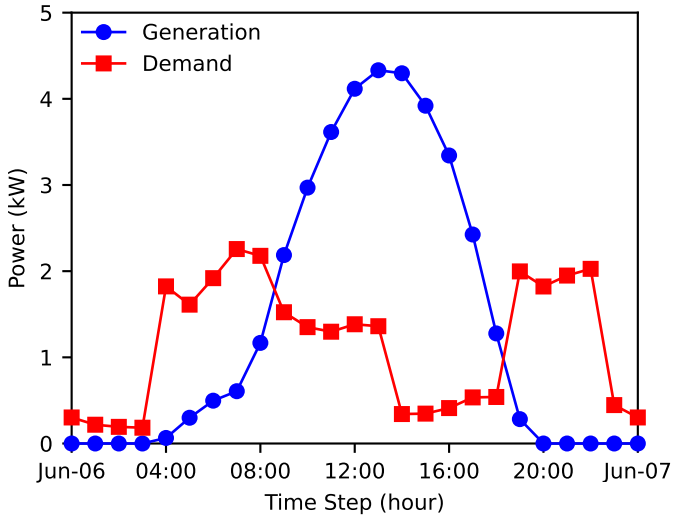

Figure 3.15: Solar-battery microgrid's hourly average solar generation and electricity demand on June 6th. This day requires the largest storage due to high surplus generation during the day and high excess demand at night.

June 6^{th} requires the largest daily storage size, because it has both high surplus generation and excess demand. The largest daily storage size defines the separation between daily and seasonal storage. The day's hourly generation and demand profiles are shown in Fig. 3.15. Solar generation only occurs during daylight hours and peaks at noon. The demand is dominated by the heater, which operates from 4:00 am to 2:00 pm and from 7:00 pm to 11:00 pm. Other demand follows the typical "duck curve" pattern, where demand is lowest at night and then rises in the morning as people wake up. It dips again in the late morning before rising around lunchtime at noon. In the afternoon, it sinks once more before peaking in the evening around dinner time. At night, demand drops to its lowest level.

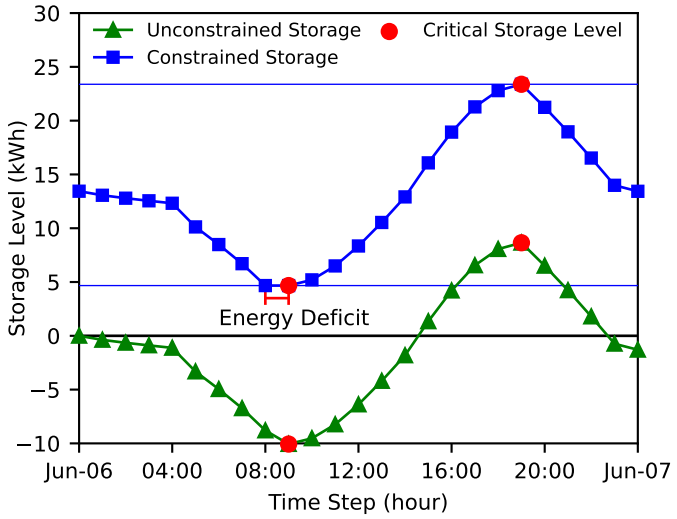

Figure 3.16: Solar-battery microgrid's daily design constrained and unconstrained storage profiles on June 6th. This day requires the largest storage size (19 kWh). The blue horizontal lines mark the upper and lower storage limits. The storage cannot discharge below the lower limits, and energy deficits occur when storage cannot discharge to meet the demand.

The daily design time horizon is considered short-term for lithium batteries; thus, storage leakage is ignored. The constrained and unconstrained profiles are shown in Fig. 3.16, and the resulting storage size is 19 kWh. The unconstrained storage profile is constructed using Eq. (3.2). The profile decreased from start to end, indicating generation is unable to support the system fully, and energy deficits will occur. The constrained profile is obtained following the steps outlined in Fig.

3.2, and energy deficit does occur from 8:00 am to 9:00 am. The constrained profile increases during the day as it charges from surplus solar generation, and decreases at night as it discharges to meet the excess demand.

3.5.6 Storage Size Comparison

Storage has been sized using daily, weekly, and monthly design time horizons to demonstrate the importance of the design time horizon. Storage size for each day, week, and month of the year are calculated; the results are shown in Fig. 3.17.

In Fig. 3.17(a), the monthly storage size is the largest in June at 64 kWh, and is the smallest in December at 0.8 kWh. The monthly design yields storage sizes much smaller than the annual design. This is because the annual design considers seasonal and inter-monthly storage, where generation is stored during high-generation months, and released during low-generation months. From the start of the year, winter months have the smallest storage sizes. The small storage size is due to the low solar generation and high winter demand, which means most generation is directly used to meet the demand, leaving little surplus generation to charge the storage. Since the storage cannot be charged, the resulting storage size is small. During the spring months, generation slowly rises while demand falls, creating more surplus generation to charge the storage, and more excess demand that needs storage to discharge. The storage size increase reflects the increasing storage utilization. The summer begins in June. During this month, solar generation peaks due to the summer solstice, while the demand has been falling, but is still high. The high generation and high demand create large surplus generation and excess demand, resulting in the largest storage size requirement. During peak summer in July and August, solar generation is high while demand is low. Most day-time demand is directly met by solar generation, leaving only nighttime demand that needs storage. Since the summer nightly demand is small, the storage size required to meet that demand is also small. Autumn begins in September. During this month, solar generation remains high while demand is rising. The rising demand creates more excess demand, which requires more storage. Thus, the storage size

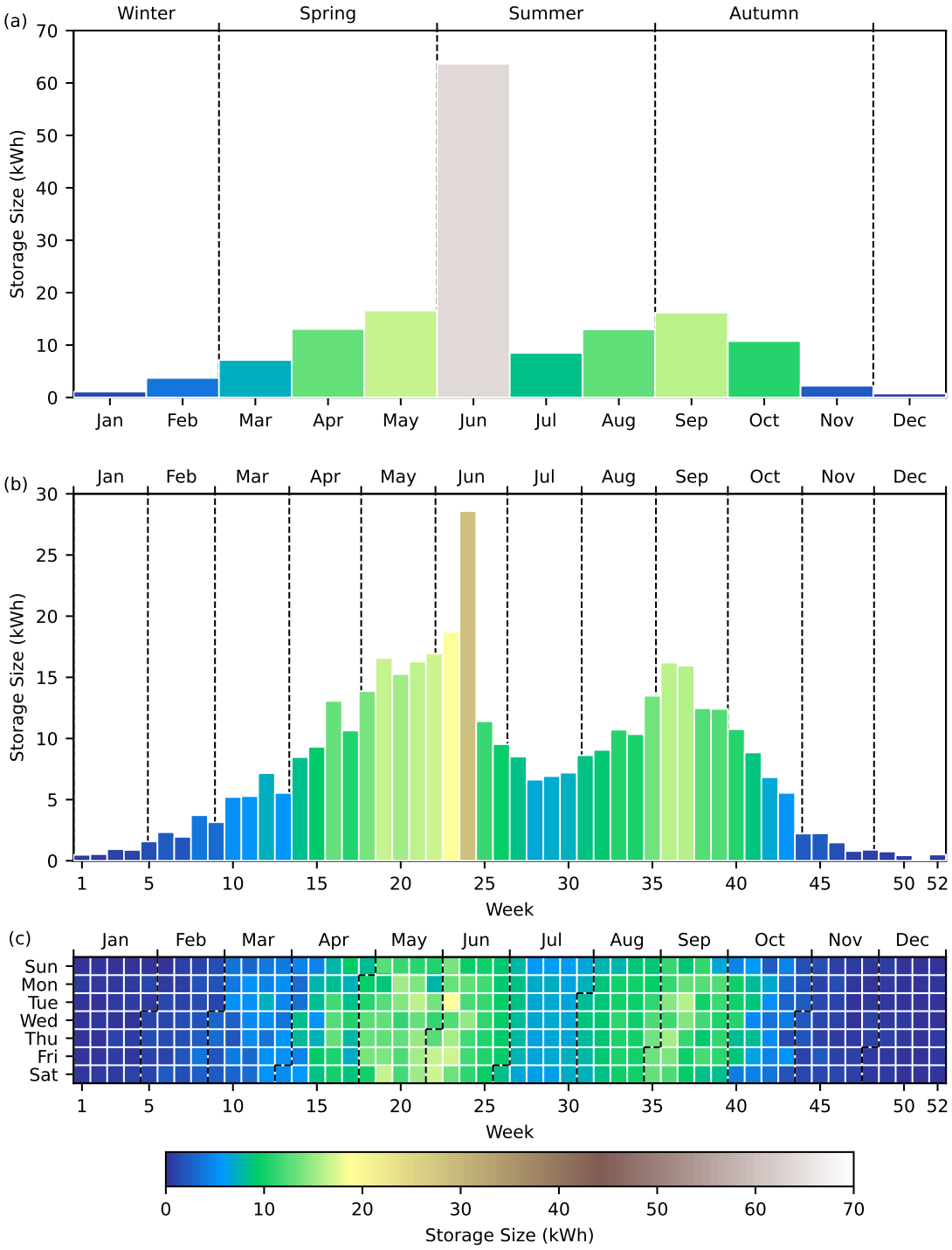

Figure 3.17: Storage size calculated using the (a) monthly, (b) weekly, and (c) daily design time horizon. Storage is sized for each month, week, and day of the year. The dashed lines separate the seasons in (a) and the months in (b) and (c). The largest monthly, weekly, and daily storage sizes are 64 kWh, 29 kWh, and 19 kWh, respectively.

has a small peak during September. In the later autumn months, the rising demand and falling generation mean more generation is directly used to meet the demand, leaving less surplus generation to charge the storage, and causing the storage size to decrease. December has the lowest solar generation due to the winter solstice. The low generation and high demand mean most generation is directly used to meet demand, leaving little surplus generation to charge the storage. Since the storage cannot be charged, the resulting storage size is the smallest in December.

In Fig. 3.17(b), the weekly storage is the largest in the 24^{th} week at 29 kWh, and is the smallest in the 51^{st} week at 0.1 kWh. Storage size for weekly design is smaller than monthly design, because monthly design accounts for inter-weekly storage. The weekly design exhibits similar patterns as the monthly design. The storage size peaks during early summer and early autumn, is smaller during peak summer, and is the smallest during winter. The 51^{st} week contains the winter solstice with the highest demand and lowest generation, which leaves little surplus generation to charge the storage. Since storage cannot be charged, the storage size is the smallest. On the other hand, the 24^{th} week is one week before the summer solstice. During this week, the demand is still high while generation is peaking, creating more surplus generation and excess demand, and causing the storage size to peak. While in the summer solstice week, the generation is higher, but the demand is lower, which means less storage is needed to meet the smaller excess demand.

In Fig. 3.17(c), the daily storage size is the largest on June 6^{th} at 19 kWh, and is the smallest for several days in late December at 0 kWh. The daily design is smaller than the weekly and monthly designs because they account for inter-day storage. Daily design exhibits similar patterns as the weekly and monthly design. The storage size peaks on June 6^{th}, with a smaller peak on September 13^{th} at 16 kWh. Both days have high generation and high demand, creating more surplus generation during the day and excess demand during the night, resulting in larger storage size requirements. On the other hand, storage is not needed for several days in late December. Late December has the highest demand and lowest generation.

All generation are directly used to meet the demand, leaving no surplus generation to charge the storage, resulting in zero storage size.

The pattern exhibited by the daily, weekly, and monthly designs shows storage size is large when generation and demand are high. The high generation and demand create more surplus generation to charge the storage and more excess demand to be met by storage discharge. With low generation and high demand, most generation is directly used to meet the demand, leaving little surplus generation to charge the storage. Since the storage cannot be charged, the resulting storage size is small to avoid wasted storage. On the other hand, with high generation and low demand, most demand is met directly by generation, leaving little excess demand that needs storage; thus, the resulting storage size is also small to avoid wasted storage. For these reasons, peak summer and peak winter require smaller storage, while early summer and early autumn require larger storage.

3.5.7 Storage Size Threshold

To put the daily, weekly, monthly, and annual designs into perspective, constrained storage profiles for storage sizes ranging from 0 to 1000 kWh are constructed via the enumerative method. The total energy discharged by each storage size is calculated from the constrained storage profiles, which is equivalent to the total energy provided by storage to the microgrid. The results are shown in Fig. 3.18.

The figure shows increasing the storage size has a diminishing return on the additional storage energy provided to the system. The largest daily design and the annual designs define the thresholds that separate the figure into three size ranges: daily storage, seasonal storage, and max storage. The daily storage provides the most energy per unit size. Each unit of storage is used for most days during the year; they are charged during the day and discharged at night. Thus, each kilowatt-hour of daily storage capacity can provide a maximum of 365 kWh of energy per year to the microgrid. In comparison, seasonal storage provides much less energy per unit size, because the storage is only used once a year; they are charged during

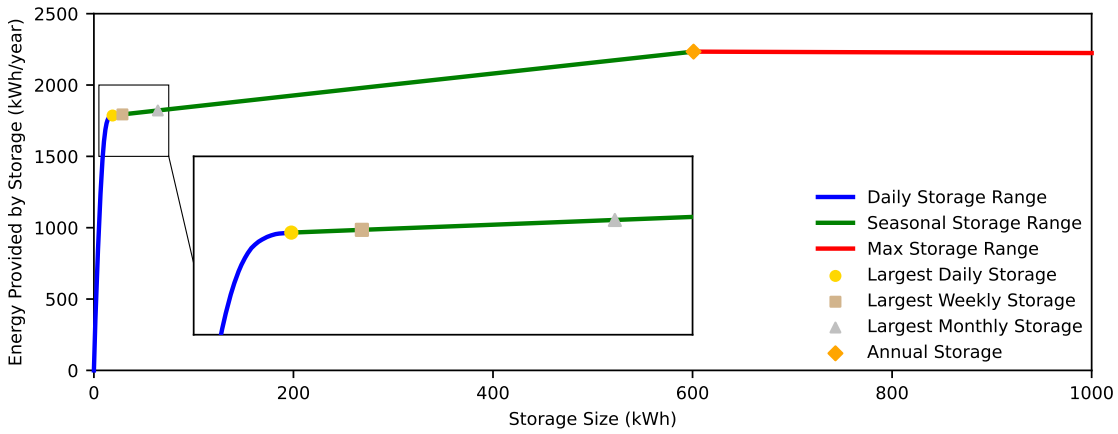

Figure 3.18: Storage size and the associated energy provided to the microgrid. The largest daily storage and the annual storage separate the size ranges of daily, seasonal, and max storage. The zoomed-in window shows the largest daily storage separates the daily and seasonal size ranges. At the annual storage size, all the renewable energy that can be stored is stored, and additional storage does not store nor provide more energy. The largest daily design's storage size (19 kWh) is 3% that of the annual design (601 kWh), but it provides 80% of the energy (1786 kWh/year) supplied by the annual design (2234 kWh/year).

the summer and discharged during autumn. Thus, each kilowatt-hour of seasonal storage capacity can only provide 1 kWh of energy per year.

In this study, the annual design represents the maximum storage size, which is also the smallest size that maximizes the storage energy provided to the system. At maximum storage size, all the available energy that can be stored is stored. Additional storage will not provide more energy, as it neither creates more surplus generation to charge the storage, nor creates more excess demand that needs storage to discharge energy to be met. Moreover, additional storage can actually reduce the energy provided, as extra stored energy induces extra energy leakage. Note that the data used in this design span a year. If the data span a longer design time horizon, the maximum storage size will increase because there will be inter-annual storage, where energy is stored during high-generation years and released during low-generation years.

The annual design requires 601 kWh of storage size to provide 2234 kWh of energy per year, while the daily design requires 19 kWh of storage to provide 1786 kWh of energy per year. Thus, for the presented solar-battery domestic microgrid

system operating on a conventional operation strategy, the largest daily design only requires 3% of the storage size of the annual design, but provides 80% of the energy supplied by the annual design. Since the microgrid application is on a domestic property, the energy not provided by the daily design is easily supplemented by the grid, while cost-saving from the smaller storage size is significant. Thus, the largest daily storage capacity also represents the point where greater diminishing returns begin. Future work should investigate how to efficiently locate the largest daily storage capacity, such as by using Fast Fourier transform to extract the daily storage profile from the annual storage profile.

3.6 Summary

The chapter presents an analytical method to optimally size energy storage. The method first constructs a temporal storage profile of stored energy, based on how storage charges and discharges in response to generation and demand. The storage is sized according to the largest cumulative charge or discharge in the profile. Major contributions made in this chapter are as follows:

- The proposed sizing algorithm is built on a new theory that storage should be sized according to the largest cumulative charge or discharge it can experience.
- The proposed method has a fast calculation speed when applied to a reasonably sized dataset, calculates the exact optimal size that maximizes storage energy utilization, and can handle non-linear models.
- The proposed method yields the optimal storage size that maximizes storage energy utilization while eliminating unutilized storage capacity. When the system operates under a conventional operation strategy, maximizing storage utilization also maximizes renewable consumption in most scenarios.
- The method is extended iteratively to include depth of discharge, maximum charge and discharge rates, and storage leakage. Storage leakage can affect long-term storage sizing, but is often ignored in other analytical methods.

The method is applied to two solar-battery microgrid case studies. The solar-battery microgrids are controlled using a conventional operation strategy, and are physically based in the northern temperate climate zone. Major findings from the case studies are summarized as follows:

- The optimally sized storage does not have wasted storage capacity due to over-sizing, nor cause energy deficits due to under-sizing.
- Energy leakage affects the sizing of long-term storage, and can cause energy deficits in the microgrid system.
- High demand and generation require larger storage, while low demand or low generation requires smaller storage. For these reasons, peak summer and peak winter require smaller storage, while early summer and early autumn require larger storage.
- Increasing storage size has a diminishing return on the additional storage energy provided to the system. The diminishing return thresholds are defined by the largest daily design and the annual design.
- The largest daily design only requires 3% of the storage size of the annual design, but provides 80% of the energy provided by the annual design.

This chapter introduced the proposed storage sizing method. The method is a technical approach that operates without requiring storage costs, which sets it apart from other methods, where errors in storage cost estimates can lead to inaccuracies in storage sizing. Nevertheless, the proposed method can be expanded enumeratively to account for economic variables, including storage cost. The hybridized techno-economic sizing method will be introduced in the next chapter. Moreover, the next chapter will also explore solar PV sizing and its interaction with storage sizing.

The work presented in this chapter has been published in the Journal of Energy Storage as a journal paper. The paper is titled "An analytical method for sizing energy storage in microgrid systems to maximize renewable consumption and minimize unused storage capacity."

4

Storage and Solar Sizing

Contents

4.1 Introduction

This chapter presents a hybridized techno-economic method to optimally size solar photovoltaic and lithium battery storage systems, with the aim of reducing grid electricity reliance. First, the method calculates the maximum solar system size, then systematically iterates between zero and the maximum solar system size. Within each iteration of solar size, the method calculates the maximum storage system size, and then systematically iterates between zero and the maximum storage size. At each iteration, the hybrid renewable system is simulated using demand and generation data, with a simplified system setup and the conventional operation strategy. The method outputs combinations of solar system capacity, storage system capacity, and grid electricity imports. Each combination's levelized cost of electricity is calculated, and the lowest-cost combination is selected as the optimal sizing. The method is applied to a case study based on the city of Oxford. Solar and storage system costs are projected from 2019 to 2100, and the optimal sizing is calculated for each year. The study found that solar photovoltaic is economically competitive, but lithium storage cost is still too high. As solar and storage prices continue to drop, they will make up a greater portion of the energy system. However, there will always be a need for the grid, as it provides flexibility to meet demand that is too costly for solar and storage to meet.

The chapter is structured as follows. Section 4.2 first introduces the equations for the storage and solar sizing method, then it details the steps to conduct the method. The method is divided into three major components. The first component involves determining the maximum storage size. The second component focuses on simulating the hybrid renewable system. The third component deals with the sizing of solar and storage. Section 4.3 presents a case study on a solar-battery microgrid system based on the city of Oxford. The study explores the characteristics of the system design space. It also examines how the system sizing will change according to the cost projection of solar PV and lithium batteries. Section 4.4 summarizes the key contributions and findings from the chapter.

4.2 Methodology

The methodology section will first introduce the equations for solar and storage sizing. Subsequently, step-by-step procedures for conducting solar and storage sizing will be detailed. The following notations in regard to time will be used: the index $t \in \mathcal{T} = \{0, \ldots, T\}$ denotes the time index, and Δt represents the time interval.

4.2.1 Solar PV Size

Solar PV (photovoltaic) sizing is conducted using the capacity factor, calculated with Eq. (4.1).

$$F_t^{PV} = \frac{P_t^{PV}}{E^{PV}}, \tag{4.1}$$

where F_t^{PV} is the solar PV capacity factor, P_t^{PV} is the solar generation power, and E^{PV} is the rated solar PV capacity.

The capacity factor is employed in Eq. (4.2) to calculate the maximum size of solar PV for meeting the demand:

$$E_{max}^{PV} = \max(\frac{P_t^L}{F_t^{PV}}), \text{ if } F_t^{PV} > F_{min}^{PV}, \tag{4.2}$$

Where E_{max}^{PV} is the maximum solar PV size, P_t^L is the load demand power, F_t^{PV} is the solar PV capacity factor, and F_{min}^{PV} is the minimum capacity factor. Essentially, the equation says that for every hour with solar generation, find the solar PV capacity that can meet the demand during that hour, then select the maximum solar PV capacity among all hours. The minimum capacity factor is a user-defined value. It is incorporated to address three scenarios that could lead to excessive solar PV sizing. First, during nighttime, when there is no solar generation, the sizing method would yield an infinite solar size, due to the division by zero. Second, during dusk and dawn, when the duration of sunlight may not cover the full time interval, the small amount of solar generation during these periods could result in excessively large solar sizes. Third, during hours of cloud coverage, solar generation is too low, which would also lead to excessively large solar PV sizes. Therefore, these times are excluded by applying a minimum capacity factor when calculating

the solar PV size. Typically, a minimum capacity factor of 0.01 yields satisfactory solar sizes for use in the proposed method.

4.2.2 Battery Storage Size

The battery storage sizing method is adapted from Sections 3.2.1, 3.2.2, 3.2.3, and 3.2.4. For the reader's convenience, the method's equations are briefly reviewed in this section, as they will be used to outline the steps in the proposed method.

The system is assumed to operate using a conventional operation strategy, such that when solar generation exceeds electricity demand, the surplus generation is charged into the lithium battery storage. When generation is less than demand, the excess demand is met by discharging energy from storage. The storage energy profile is constructed using Eq. (4.3).

$$\begin{aligned} S_{t+\Delta t} &= S_t\,(1-\sigma) + (P_t^{PV} - P_t^L)\,\eta_t\,\Delta t, \\ \text{where: } \eta_t &= \begin{cases} \eta_c, \text{ if } P_t^{PV} - P_t^L \geq 0, \\ \frac{1}{\eta_d}, \text{ if } P_t^{PV} - P_t^L < 0, \end{cases} \\ \text{and } \sigma &= 0, \text{ if } S_t < 0, \end{aligned} \tag{4.3}$$

Where S_t is the storage energy level, σ is the storage energy leakage rate, P_t^{PV} is solar generation, P_t^L is electricity demand, and η_t is the storage efficiency. The storage efficiency is the charge efficiency η_c when generation exceeds demand, and one over the discharge efficiency η_d when demand exceeds generation. The leakage rate is set to zero if the storage level falls below zero.

The storage size is determined using critical points in the storage profile. Eq. (4.4) calculates these critical points by setting the derivative equal to zero and finding the roots. Moreover, computational functions such as SciPy's argrelextrema find critical points by checking whether each point is higher or lower than its neighboring points [165].

$$\begin{gathered} \text{Solve } \frac{dS_t}{dt} = 0 \text{ for all } t, \\ \text{such that critical points are: } t_1,\, t_2,\, \cdots,\, t_n, \\ \text{and critical storage levels are: } S_{t_1},\; S_{t_2},\, \cdots,\, S_{t_n}. \end{gathered} \tag{4.4}$$

The storage level differences used in storage sizing are captured by the difference matrix $\mathbf{D}$ in Eq. (4.5).

$$\begin{aligned} \mathbf{D} &= \mathbf{L} + \mathbf{C} - \mathbf{C}^T, \\ \text{where : } \mathbf{L} &= \begin{cases} l_{j,k} = 0, & \text{if } j \leq k, \\ l_{j,k} = S_T - S_0, & \text{if } j > k, \end{cases} \\ \mathbf{C} &= \mathbf{1}_n^T \, \mathbf{C}_n, \\ \mathbf{C}_n &= [S_{t_1},\, S_{t_2},\, \cdots,\, S_{t_n}], \\ \mathbf{1}_n &= [1,\, 1,\, \cdots,\, 1], \end{aligned} \tag{4.5}$$

The difference matrix $\mathbf{D}$ pairs critical points and calculates the storage level difference between them. The first half of the pairs is generated by $\mathbf{L} + \mathbf{C}$, while the second half is produced by $\mathbf{C}^T$. The critical storage level matrix $\mathbf{C}$ is created through the dot product of the transposed all-ones vector 1_n^T and the critical storage levels vector $\mathbf{C}_n$. The lower-left half of the lower triangular matrix $\mathbf{L}$ is filled with the difference between the ending storage level S_T and the starting storage level S_0. Matrix $\mathbf{L}$ pushes the lower-left half of matrix $\mathbf{D}$ into the second design time horizon, as critical storage levels in the second time horizon can also influence sizing.

The difference matrix is used in Eq. (4.6) to determine the maximum storage size.

$$E_{max}^S = \begin{cases} |\min(\mathbf{D})|, & \text{if } S_T - S_0 > 0, \\ \max(\mathbf{D}), & \text{if } S_T - S_0 < 0, \\ \max|\mathbf{D}|, & \text{if } S_T - S_0 = 0, \end{cases} \tag{4.6}$$

The equation says that maximum storage size E_{max}^S depends on the difference matrix $\mathbf{D}$ and the overall storage profile trend. If the overall storage profile is increasing, such that the ending storage level S_T is greater than the starting storage level S_0, then the storage size is equal to the absolute value of the difference matrix's minimum, corresponding to the storage profile's largest decrease. Conversely, if the overall storage profile is decreasing, then the storage size is equal to the difference matrix's maximum, corresponding to the storage profile's largest increase. Lastly, if the overall storage profile is neither increasing nor decreasing, then the storage size is equal to the maximum absolute value of the difference matrix, corresponding to the largest change in the storage profile.

As demonstrated in Section 3.5.7, the sizing method determines the maximum storage size within a given design time horizon. For instance, the maximum storage size for a design time horizon of a year is the annual storage size. For the reader's convenience, Fig. 3.18 is adapted into Fig. 4.1 to illustrate that at the annual storage size, all available energy that can be stored into the storage is stored, and further storage size expansion will not provide more storage energy.

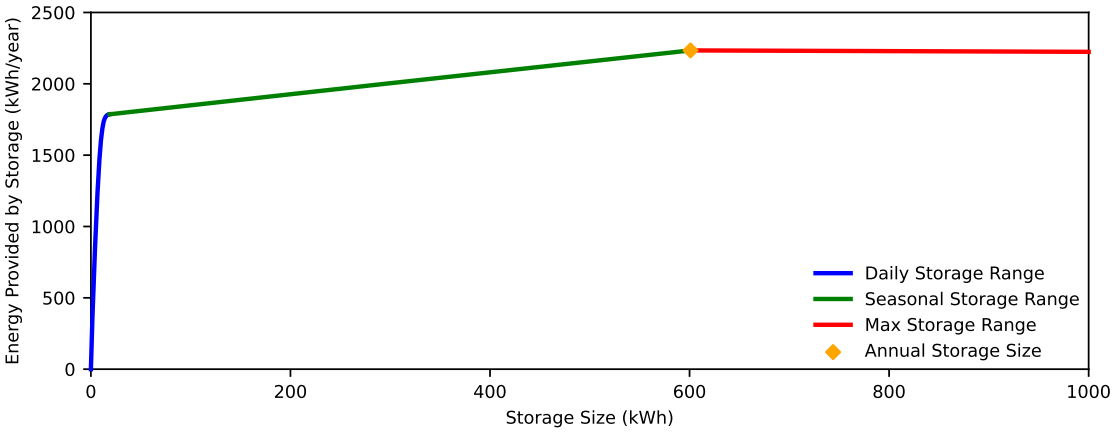

Figure 4.1: Storage size and the associated energy provided to the system. At the annual storage size, all the renewable energy that can be stored is stored, and additional storage does not store nor provide more energy.

4.2.3 Storage Energy and Power Limit

The storage energy and power limit equations are adapted from Sections 3.2.6, 3.2.7, and 3.2.8. For the reader's convenience, the equations are briefly reviewed in this section, as they will be used to outline the steps in the proposed method.

Battery manufacturers specify cycle life under specific depth of discharge, as deep discharge can damage battery health and shorten cycle life [166]. Eq. (4.7) calculates the storage's total energy capacity when accounting for the depth of discharge.

$$E^S_{tot} = \frac{E^S}{DoD_{max} - DoD_{min}}, \tag{4.7}$$

Where E^S_{tot} is the storage's total energy capacity, E^S is the storage size, DoD_{max} and DoD_{min} are the maximum and minimum depth of discharge. In this model, storage size is the energy capacity in the usable portion of the storage, while the remaining capacity is reserved to offset degradation over the storage's cycle life.

The storage levels at the maximum and minimum depth of discharge are defined by storage energy limits in Eqs. (4.8, 4.9).

$$S_{up} = E^S_{tot}\,(1 - DoD_{min}), \tag{4.8}$$

$$S_{low} = E^S_{tot}\,(1 - DoD_{max}), \tag{4.9}$$

Where S_{up} and S_{low} are the upper and lower storage energy limits, E^S_{tot} is storage's total energy capacity, DoD_{max} and DoD_{min} are the maximum and minimum depth of discharge.

The storage energy limits are used in the constraint Eq. (4.10) when constructing the constrained storage profile.

$$S_{low} \leq S_t \leq S_{up}, \tag{4.10}$$

The constraint says the storage level S_t cannot exceed the upper storage limit S_{up}, nor fall below the lower storage limit S_{low}. Once the storage level hits the upper limit, charging stops. On the other hand, discharging stops if the storage level is at the lower limit, preventing deep discharge that can damage battery cycle life.

Eq. (4.10) should hold in the final constrained storage profile. However, it is often too restrictive when used in the iterative storage sizing method, which can cause near-optimal sizing. To solve this issue, Eq. (4.11) relaxes the energy limit constraint by adding a slack term.

$$S_{low} - \alpha\,|S_T - S_0| \leq S_t \leq S_{up} + \alpha\,|S_T - S_0|, \tag{4.11}$$
$$\text{and } 0 \leq \alpha < 1,$$

The slack is the absolute difference between the last iteration's ending storage level S_T and starting storage level S_0, scaled by the multiplier α between zero and one.

A constrained storage profile will repeat itself when subject to the same demand and generation patterns in the future. The repeatability ensures the storage size is sustainable, and can support similar demand and generation patterns in the future. The sustainable starting storage level is calculated using Eq. (4.12).

$$S_{0,s} = \begin{cases} S_T - \max(S_t) + S_{up}, & \text{if } S_T - S_0 \geq 0, \\ S_T - \min(S_t) + S_{low}, & \text{if } S_T - S_0 \leq 0, \end{cases} \tag{4.12}$$

Where $S_{0,s}$ is the sustainable starting storage level, S_t is the storage level, S_0 and S_T are the starting and ending storage levels, S_{up} and S_{low} are the upper and lower storage limits. The equation says the sustainable starting storage level is dictated by the difference between the ending and maximum storage levels in an increasing scenario, and by the ending and minimum storage levels in a decreasing scenario. The storage limits are added to re-frame those differences within the usable portion of storage.

High charge and discharge rates can also damage battery health and shorten cycle life [167]. The C-rating relates the battery's energy capacity to power capacity. The maximum charge and discharge rate are calculated based on C-ratings using Eqs. (4.13, 4.14), which defines the storage power limits.

$$P_c = E^S_{tot}\, C_c, \tag{4.13}$$

$$P_d = E^S_{tot}\, C_d, \tag{4.14}$$

Where P_c and P_d are the maximum charge and discharge rates, E^S_{tot} is the storage's total energy capacity, C_c and C_d are the storage's charge and discharge C-ratings.

The power limits are used in constraint Eq. (4.15) when constructing the constrained storage profile.

$$-P_d \leq P^{PV}_t - P^L_t \leq P_c, \tag{4.15}$$

Under the conventional operation strategy, the difference between solar generation P^{PV}_t and electricity demand P^L_t is the power charged to or discharged by storage. The constraint says storage power cannot exceed the maximum charge P_c or discharge rates P_d.

Eq. (4.15) should hold in the final constrained storage profile; however, it is often too restrictive when used in the iterative storage sizing method, and can cause storage size to converge to zero. Eq. (4.16) relaxes the power limit constraint by adding a slack term, enabling zero storage size to have charge and discharge.

$$-P_d - \alpha\,|S_T - S_0| \leq P^{PV}_t - P^L_t \leq P_c + \alpha\,|S_T - S_0|, \tag{4.16}$$
$$\text{and } 0 \leq \alpha < 1,$$

The slack consists of the absolute difference between the last iteration's ending storage level S_T and starting storage levels S_0, scaled by the multiplier α.

4.2.4 Grid Electricity

According to the conventional operation strategy, when neither generation nor storage can meet the demand, grid electricity is imported to meet the demand. Grid electricity imports are necessary in two scenarios. The first scenario is when the excess demand's power requirement exceeds the maximum discharge rate of the storage. The second scenario is when the excess demand's energy requirement exceeds the stored energy within the storage.

In the first scenario, when the storage's maximum discharge rate cannot meet the excess demand's power requirement, and the grid electricity import needed to supplement the demand is calculated using Eq. (4.17).

$$E_{P,t}^{GR} = (P_t^L - P_t^{PV} - P_d)\Delta t, \text{ if } P_t^L - P_t^{PV} > P_d, \tag{4.17}$$

Where $E_{P,t}^{GR}$ is the grid electricity import due to storage power limit, P_t^L is electricity demand, P_t^{PV} is solar generation, P_d is the storage's maximum discharge rate, and Δt is the time interval.

In the second scenario, when the excess demand's energy requirement exceeds the stored energy within the storage, the grid electricity import needed to supplement the demand is calculated using Eq. (4.18).

$$E_{S,t}^{GR} = (S_{low} - S_{t+\Delta t})\eta_d, \text{ if } S_{t+\Delta t} < S_{low}, \tag{4.18}$$

Where $E_{S,t}^{GR}$ is the grid electricity import due to storage energy limit, S_{low} is the lower storage limit, $S_{t+\Delta t}$ is the storage level in the next time step, and η_d is the storage discharge efficiency. Note that the storage level in the next time step is constrained by the power limits from Eq. (4.16), but not constrained by the energy limit from Eq (4.11). The equation states that in the next time step, if the storage level will fall below the lower storage limit, then the amount of grid electricity import is equal to the difference between the lower storage limit and the storage level in the next time step, multiplied by the discharge efficiency.

The total grid electricity import due to both scenarios is calculated using Eq. (4.19).

$$E_t^{GR} = E_{P,t}^{GR} + E_{S,t}^{GR}, \tag{4.19}$$

Where E_t^{GR} is the total grid electricity import during a time step, $E_{P,t}^{GR}$ and $E_{S,t}^{GR}$ are the grid electricity import caused by the storage power limit and storage energy limit, respectively.

4.2.5 Levelized Cost of Electricity

The cost of the hybrid renewable system is evaluated using LCOE (Levelized Cost of Electricity) from Eq. (4.20).

$$LCOE = \frac{C^{PV} + C^{ST} + C^{GR}}{D_{tot}}, \tag{4.20}$$

Where $LCOE$ is the levelized cost of electricity, C^{PV} is the annualized solar PV cost, C^{ST} is the annualized battery storage cost, C^{GR} is the annual grid electricity import cost, and D_{tot} is the annual electricity demand. In the context of a microgrid system, the annual electricity demand is equivalent to the combined electricity supplied by solar PV, battery storage, and the electricity grid.

The annualized solar PV cost is calculated using Eq. (4.21).

$$C^{PV} = E^{PV}(O^{PV} + I^{PV}\frac{r(1+r)^{n^{PV}}}{(1+r)^{n^{PV}}+1}), \tag{4.21}$$

Where C^{PV} is the annualized solar PV cost, E^{PV} is the solar PV capacity, O^{PV} is the solar PV system O&M (Operation and Maintenance) cost, and I^{PV} is the solar PV system's installed cost. The installed cost, typically a one-time up-front expense, is annualized using the capital recovery factor equation, which consists of the discount rate r and the solar PV system's lifespan n^{PV}.

Similarly, the annualized battery storage system cost is calculated using Eq. (4.22).

$$C^{ST} = E_{tot}^{S}(O^{S} + I^{S}\frac{r(1+r)^{n^{S}}}{(1+r)^{n^{S}}+1}), \tag{4.22}$$

Where C^{ST} is the annualized battery storage system cost, E^{S}_{tot} is the battery's total storage capacity, O^{S} is the O&M cost of the battery storage system, I^{S} is the installed cost of the battery storage system, and n^{S} is the lifespan of the battery storage system.

The annual cost of electricity import is calculated using Eq. (4.23).

$$C^{GR} = \sum_{t=0}^{T} E^{GR}_{t} K^{GR}_{t}, \tag{4.23}$$

Where C^{GR} is the annual cost of electricity import, E^{GR}_{t} is the grid electricity import, and K^{GR}_{t} is the electricity price. The equation calculates the total annual cost by summing the product of grid electricity import and the corresponding electricity price over the entire design time horizon.

The annual demand is calculated using Eq. (4.24).

$$D_{tot} = \sum_{t=0}^{T} P^{L}_{t} \Delta t, \tag{4.24}$$

Where D_{tot} is the annual total demand, P^{L}_{t} is the electricity demand, and Δt is the time interval. The total demand is calculated by summing the product of the demand at each time step and the corresponding time interval over the design time horizon.

4.2.6 Proposed Method

The storage and solar sizing method consists of three major components. The first component is to size for the maximum storage capacity based on solar generation and electricity demand. The second component is to simulate the system and calculate the grid electricity import. The third component utilizes the previous components to conduct storage and solar sizing.

4.2.6.1 Maximum Storage Size

The maximum storage size is determined using steps outlined in Fig. 4.2. The maximum storage size is used to set the storage size search range.

The first step is to construct the unconstrained storage profile using Eq. (4.3). Then, identify critical points in the storage profile using Eq. (4.4) or computer

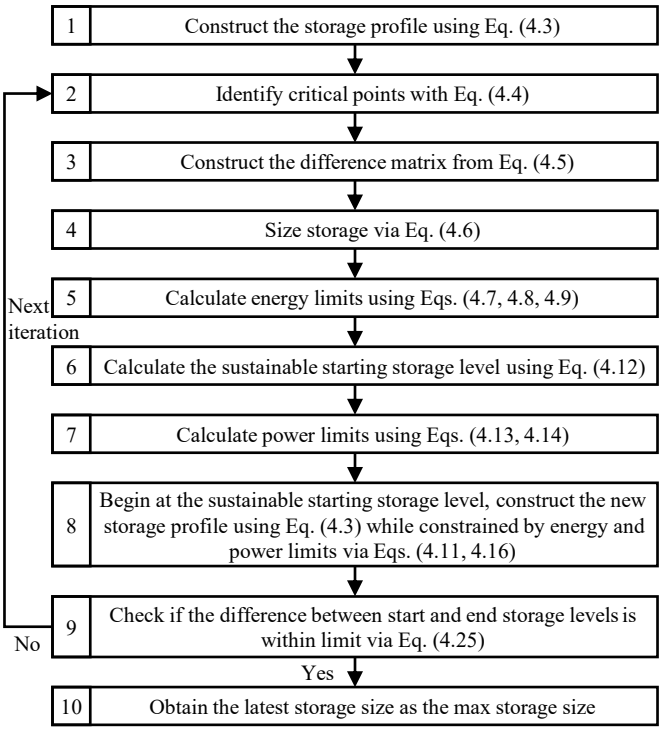

Figure 4.2: The maximum storage sizing steps flowchart.

functions. The critical points' storage levels are used in Eq. (4.5) to construct the difference matrix, and the storage size is calculated using the difference matrix via Eq. (4.6). Subsequently, the storage size is employed in Eqs. (4.7, 4.8, 4.9) to calculate the upper and lower storage limits. These storage limits are then utilized in Eq. (4.12) to determine the sustainable starting storage level. Following this, the maximum charge and discharge rates are calculated using Eqs. (4.13, 4.14). In the eighth step, a new storage profile is constructed. Starting from the sustainable starting storage level, the new profile is created using Eq. (4.3), constrained by the relaxed storage energy limits via Eq. (4.11), and by the relaxed storage power limits via Eq. (4.16). The new constrained storage profile is used in the ninth step to check if the absolute difference between starting and ending storage levels is within the user-defined permissible limit ϵ, as stated in Eq. (4.25).

$$|S_T - S_0| \leq \epsilon, \tag{4.25}$$

If the difference exceeds the limit, repeat the process from the second step with

the new constrained storage profile. If the difference falls within the limit, then the latest storage size is the maximum storage size.

4.2.6.2 System Simulation

The system simulation is conducted using steps outlined in Fig. 4.3. The simulation is used to obtain the grid electricity import profile based on renewable generation and electricity demand.

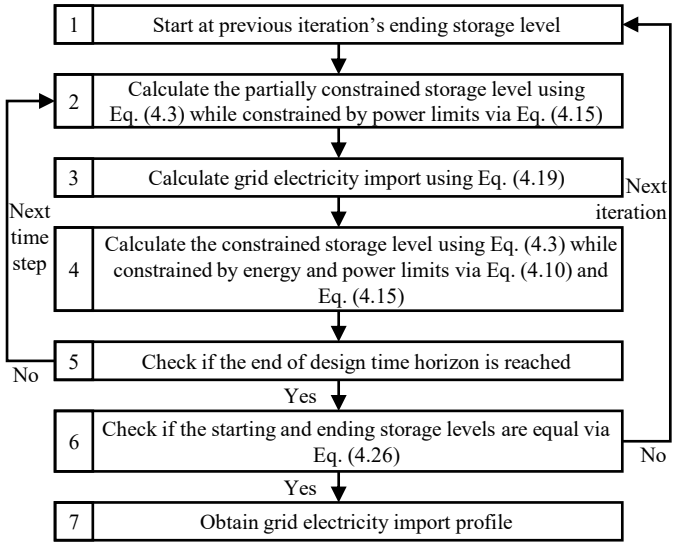

Figure 4.3: The system simulation steps flowchart.

The first step is to select the starting storage level. For the first iteration, the starting storage level is set as the lower storage limit. For subsequent iterations, the starting storage level is set as the ending storage level from the previous iteration. The second step involves calculating the partially constrained storage level in the next time step using Eq. (4.3), while constrained by the power limits from Eq. (4.15). Based on the discharge scheme and the new storage level, the amount of grid electricity import due to storage power limit and storage energy limit are calculated using Eq. (4.17) and Eq. (4.18). The imports are added together in Eq. (4.19) to yield the total grid electricity import. The fourth step is to calculate the constrained storage level in the next time step using Eq. (4.3), constrained by the storage energy limits in Eq. (4.10), and by the storage power limits in Eq. (4.15).

The fifth step involves checking if the end of the design time horizon has been reached. If it has not been reached, proceed to the next time step from the second step. If it has been reached, proceed to the sixth step, which involves checking if the starting and ending storage levels are equal according to Eq. (4.26).

$$S_T = S_0, \tag{4.26}$$

Where S_T and S_0 represent the ending and starting storage levels in the current iteration. Equal starting and ending storage levels characterize the repeatability of the storage profile, implying that the storage profile can repeat itself indefinitely when subjected to the same demand and generation conditions in the future. This repeatability ensures the future sustainability of the storage size. If the storage levels are not equal, proceed to the next iteration by repeating the process from the first step. If the storage levels are equal, obtain the latest iteration's grid electricity import profile.

4.2.6.3 Storage and Solar Sizing

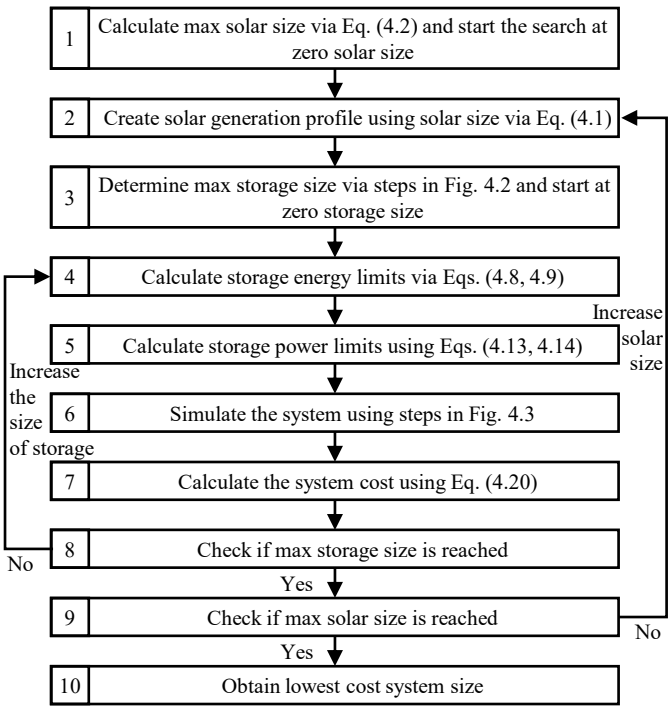

Figure 4.4: The storage and solar sizing steps flowchart.

The storage and solar sizing is conducted via the steps outlined in Fig. 4.4. The first step is to calculate the maximum solar PV size using Eq. (4.2). The maximum solar PV size sets the size search range, and the method begins the search at size zero. The second step is to create the solar generation profile, which consists of solar capacity factor profile scaled by the solar PV capacity, as stated in Eq. (4.1). The third step is to determine the maximum storage size based on the steps outlined in Fig. 4.2. The maximum storage size sets the storage size search range, and the method begins the search at size zero. The fourth step is to calculate the upper and lower storage limits using Eq. (4.8) and Eq. (4.9). The fifth step is to calculate the maximum charge and discharge rates using Eq. (4.13) and Eq. (4.14). The sixth step is to simulate the system and obtain the grid electricity import profile via steps outlined in Fig. 4.3. The seventh step is to calculate the system's levelized cost of electricity using Eq. (4.20), where the annualized solar and storage costs are calculated using Eq. (4.21) and Eq. (4.22), the annual electricity import cost is calculated using Eq. (4.23), and the annual demand is calculated using Eq. (4.24). The eighth step is to check if the maximum storage size has been reached. If not, then incrementally increase the storage size and repeat the process from the fourth step. If it has been reached, then proceed to the ninth step, which is to check if the maximum solar size has been reached. If it has not been reached, then incrementally increase the solar size and repeat the process from the second step. If it has been reached, obtain the lowest-cost system size as the final system sizing.

4.3 Case Study

A hybrid renewable energy system with solar photovoltaic and lithium battery storage is proposed to reduce Oxford's reliance on the grid. The renewable system is modelled using a simplified system setup with the conventional operation strategy.

4.3.1 System Setup

The renewable system setup and operation strategy are shown in Fig. 4.5. The simplified setup features a common AC bus regulated by the electricity grid, with

demand directly connected. Solar PV generation is converted from DC to AC via an inverter, and lithium battery storage, operating in DC, requires a bi-directional AC/DC converter to connect to the bus. The conventional operation strategy states that solar generation will first be used to meet the demand. Any excess generation will be stored in lithium battery storage. When generation cannot meet the demand, storage energy will be used. When both generation and storage are not enough, electricity will be imported from the grid to meet the demand. The availability of these three supply sources ensures that the demand is met at all times.

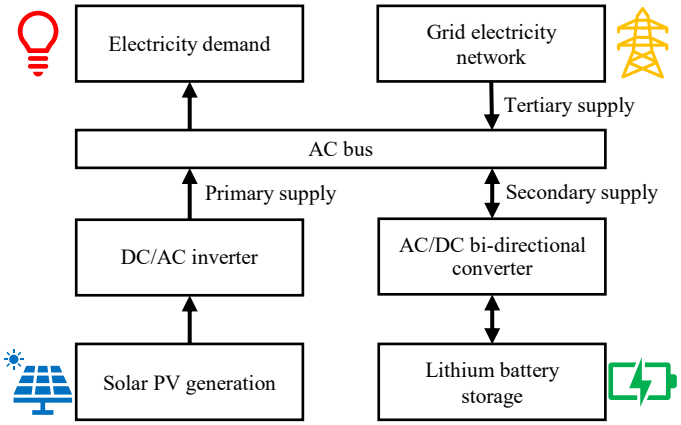

Figure 4.5: The solar-battery microgrid setup and operation control strategy for the city of Oxford. The microgrid uses a conventional operation strategy to maximize renewable consumption and minimize electricity grid reliance. The primary supply is used first when available, then the secondary, and then the tertiary. The arrows indicate power flow directions.

The lithium battery system is assumed to have a charge and a discharge efficiency of 90%, a recommended depth of discharge of 80%, a C-rating of 1C, and a leakage rate of 2% per month [118].

4.3.2 Electricity Demand Profile

Oxford's building electricity demand is modelled using Elexon electricity settlement profiles. The profiles were constructed using half-hourly demand data sampled from Great Britain [86]. There are 120 Elexon profiles, divided into eight classes of domestic and commercial consumers [171]. Within each class, the profiles are further divided into five seasons: winter, spring, summer, high summer, and autumn.

Additionally, within each season, the profiles are categorized into three types of days: Weekday, Saturday, and Sunday. For each of the eight Elexon profile classes, the profiles are compiled into an hourly demand profile spanning a year based on the day of the week and the season.

The BEIS (UK's Department of Business, Energy and Industrial Strategy) provides statistics on the number of meters in each district [172]. The number of domestic meters for Class 1 and 2 is provided individually. Elexon profiles for Class 1 and 2 are then scaled according to the number of meters in the city of Oxford.

The number of non-domestic meters in Classes 3 to 8 is reported collectively. Since these classes represent non-domestic consumers with increasing demand levels, the analysis assumes demand correlates with company size by employees. For instance, Class 3 models small companies, while Class 8 models large ones. The ONS (UK's Office of National Statistics) provides statistics on the number of companies in each district and their sizes [173]. Elexon profiles for Class 3 to 8 are then scaled according to the number and size of the companies in the city of Oxford.

Elexon profiles were originally developed in 1997 [86]. Since then, both domestic and non-domestic electricity demands have changed [174]. To account for these changes, correction factors are calculated using linear regression [175]. First, demand profiles are assembled for all districts in the UK, and annual demand is calculated from these profiles. Then, the calculated demand and actual demand are fed through linear regression to obtain the correction factors, as shown in Table 4.1. The normal distribution of company sizes in each district causes high collinearity in company size data. To work around this collinearity, the annual demands from Classes 3 to 8 are combined and processed through linear regression, yielding a single correction factor. These correction factors reduced the discrepancy between actual and calculated annual demands by more than 90%, as indicated by the R-squared values. The P-Values are less than 0.05, indicating significant correlations between calculated and actual demands. Lower and Upper 95% values define the lower and upper bounds of the 95% confidence interval, within which correction factors reside.

Class	Correction Factor	R-Square	P-Value	Lower 95%	Upper 95%
1	0.84	0.99	0	0.83	0.85
2	0.72	0.96	0	0.70	0.73
3 to 8	2.65	0.90	0	2.56	2.73

Table 4.1: Correction factor for the Elexon demand profiles obtained using linear regression.

These correction factors are applied to the previously determined scaling for each class. The scaled profiles from each class are then added together to form Oxford's demand profile, as shown in Fig. 4.6.

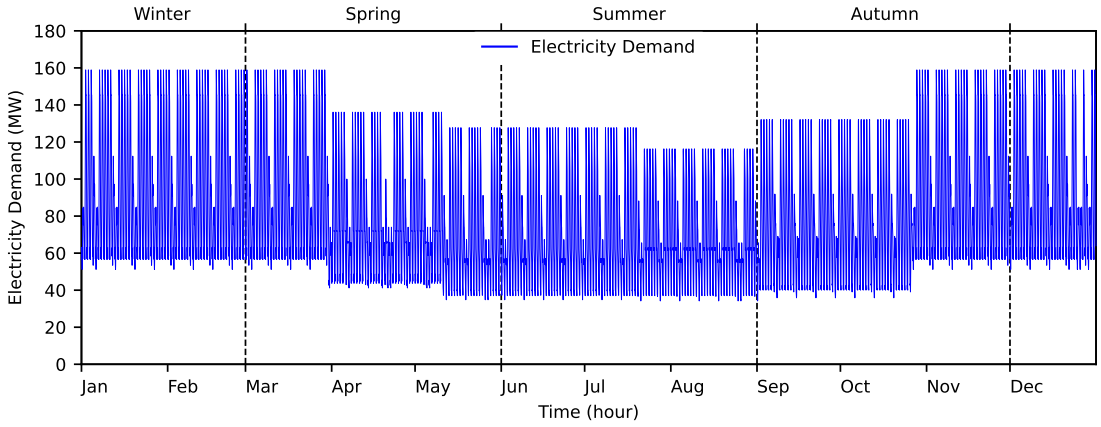

Figure 4.6: Average hourly electricity demand in a typical year. The dashed lines separate the seasons.

The demand profile exhibits slight peaks at night from Economy meters that have cheaper nightly electricity price. Demand then rises in the morning, peaks at noon, and drops in the afternoon. It peaks again at 5 pm when working hours end, then decreases in the evening. Demand is highest during weekdays and lowest on Sundays because non-domestic demand dominate in Oxford. Furthermore, demand is highest during winter and lowest during high summer, with demand variation also greater during winter.

The present approach is benchmarked against a top-down approach. The top-down approach first imports real-time hourly electricity demand for Great Britain, then scales it down according to the ratio between the district's population and Great Britain's total population. For comparison, the hourly demand is summed

into the total annual demand for each district and compared with the actual annual demand [172]. When compared, the present approach's annual total demand is 9% closer to the actual value than the benchmark approach.

4.3.3 Solar Generation Model

The solar capacity factor is calculated using Pfenninger and Staffell's method [79]. The simulation location is set in Oxford, with a system efficiency loss of 10%, mainly due to the DC-to-AC inverter. The panel orientation is set at a 30-degree tilt facing south, which is suitable for European countries [176].

The simulation first obtains solar irradiance and temperature data from NASA's MERRA database. The temperature data is then fed into Huld's temperature-dependent efficiency curve to determine solar panel efficiency [80]. The irradiance data is processed into direct and diffused irradiance using the Boland-Ridley-Lauret model [81]. Direct and diffused irradiance are then scaled according to the solar panel tilt. The capacity factors are calculated using system efficiency, panel efficiency, direct irradiance, and diffused irradiance. The simulation is conducted for five years between 2015 and 2019, and hourly capacity factors are averaged over the five years to reduce anomalies. Fig. 4.7 shows the solar PV generation capacity factor profile.

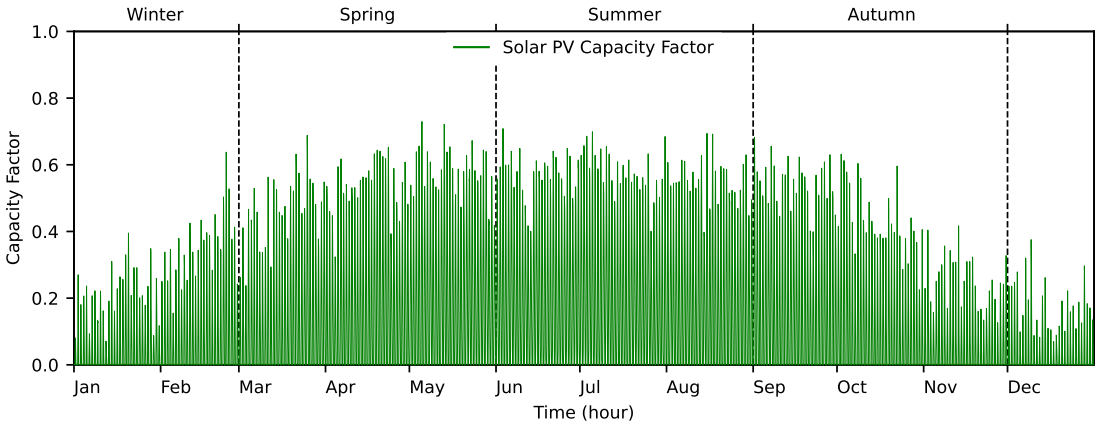

Figure 4.7: Average hourly solar PV generation capacity factor in a typical year. The dashed lines separate the seasons.

The capacity factors are non-zero during sunlight hours, as solar panels only generate electricity in sunlight. Furthermore, the capacity factor peaks at noon due

to high solar intensity and is higher during summer due to increased direct irradiance.

4.3.4 Design Space

The proposed method is implemented following the steps outlined in Fig. 4.4. The method yields combinations of solar PV system capacity, storage system capacity, and grid electricity import that can meet the demand. These combinations form a three-dimensional design space, as shown in Fig. 4.8.

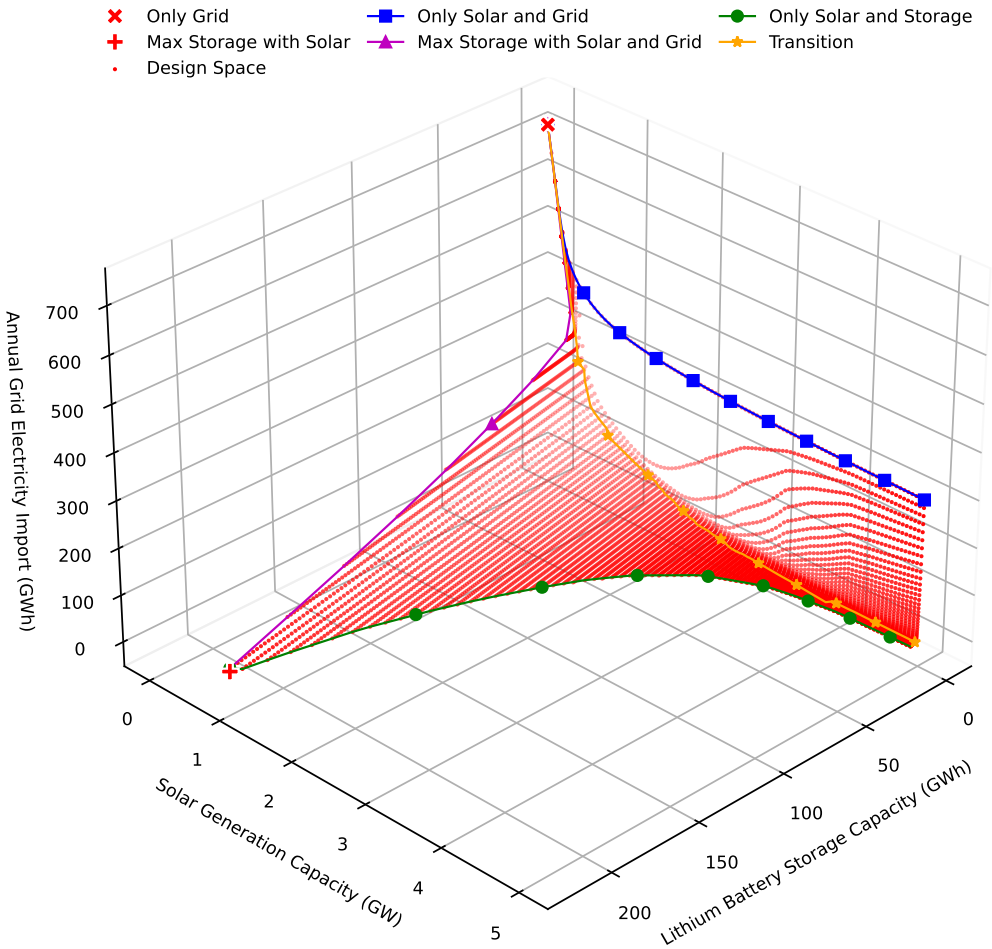

Figure 4.8: Design space for the combinations of solar capacity, storage capacity, and annual grid electricity import that are able to meet the annual electricity demand.

At the top of Fig. 4.8, the data point "Only Grid" indicates that with no solar or storage, the demand relies solely on the grid, resulting in the highest grid electricity import.

At the back-right of the Fig. 4.8, with another perspective shown in Fig. 4.9, the data curve "Only Solar and Grid" demonstrates that without storage, increasing solar system capacity can reduce grid electricity requirements to a certain extent. Beyond a certain point, increasing solar capacity no longer reduces grid electricity import. This is because solar generation is absent at night, and without storage, nightly demand needs to rely on the grid.

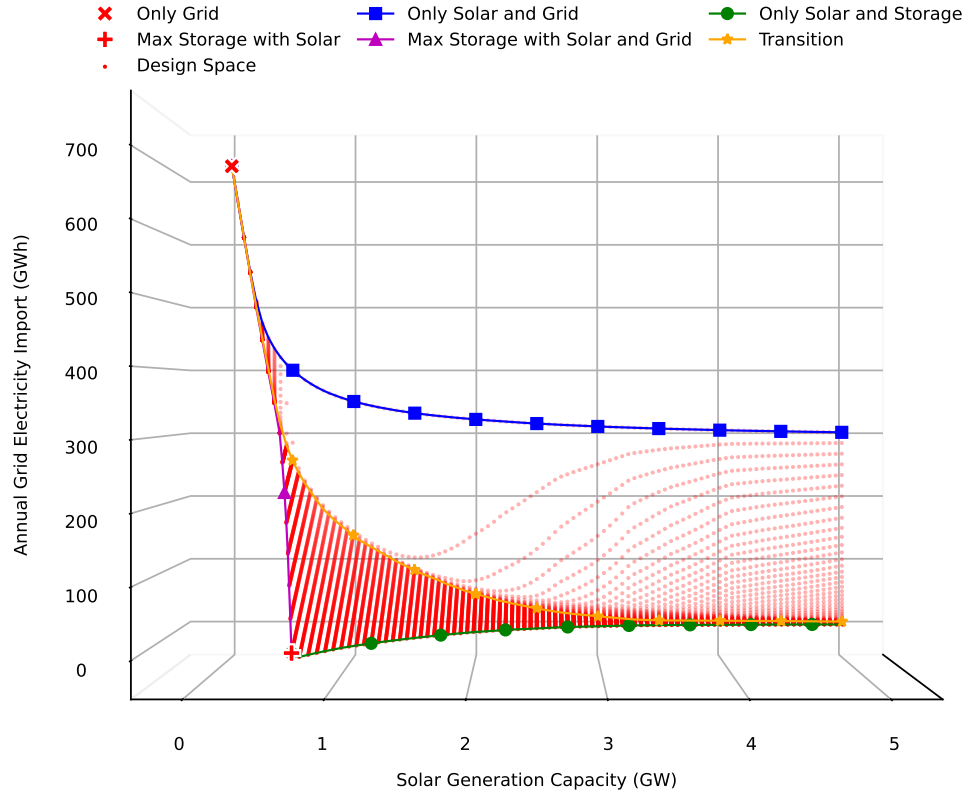

Figure 4.9: Design space view from the left side.

In the middle of Fig. 4.8, the data curve "Transition" defines a transition region, with another perspective from the right side shown in Fig. 4.10. To the right of the transition, increasing storage capacity can significantly reduce grid electricity import. This is because each storage capacity is utilized for most days during the year; they are charged during the day and discharged at night. The high utilization provides more energy to meet demand, reducing the need for grid electricity. After the transition, increasing storage capacity reduces electricity

import at a much slower pace. This is because the additional capacity is only utilized once a year; they are charged during the summer and discharged during fall and winter. The lower utilization provides less energy for demand, resulting in a slower reduction in electricity import [177].

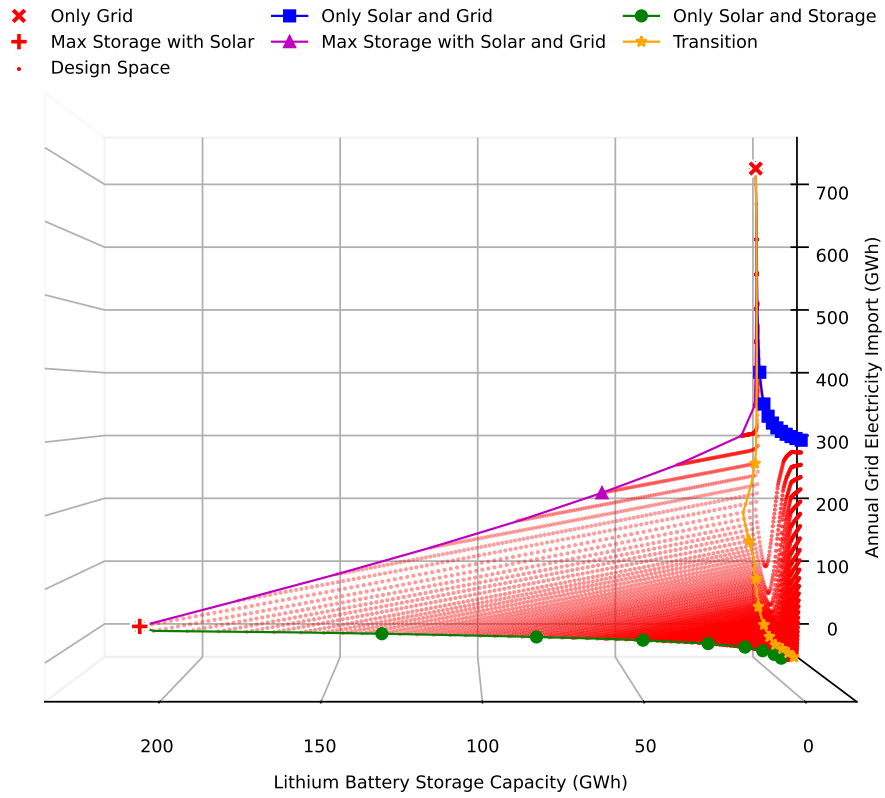

Figure 4.10: Design space view from the right side.

At the back-left of Fig. 4.8, with a better perspective shown in Fig. 4.10, the data curve "Max Storage with Solar and Grid" illustrates that maximum storage capacity increases as solar capacity increases. This is because a larger solar capacity creates more surplus generation that can be stored, thus increasing the maximum storage capacity.

On the left of Fig. 4.8, which is also shown in Fig. 4.10, the data point "Max Storage with Solar" represents the first solar and storage capacity that can meet the demand without relying on grid electricity. In this scenario, the total solar generation is just enough to meet the total demand. With no over-generation,

less demand is directly met by solar, and more demand needs storage, resulting in a higher storage capacity requirement.

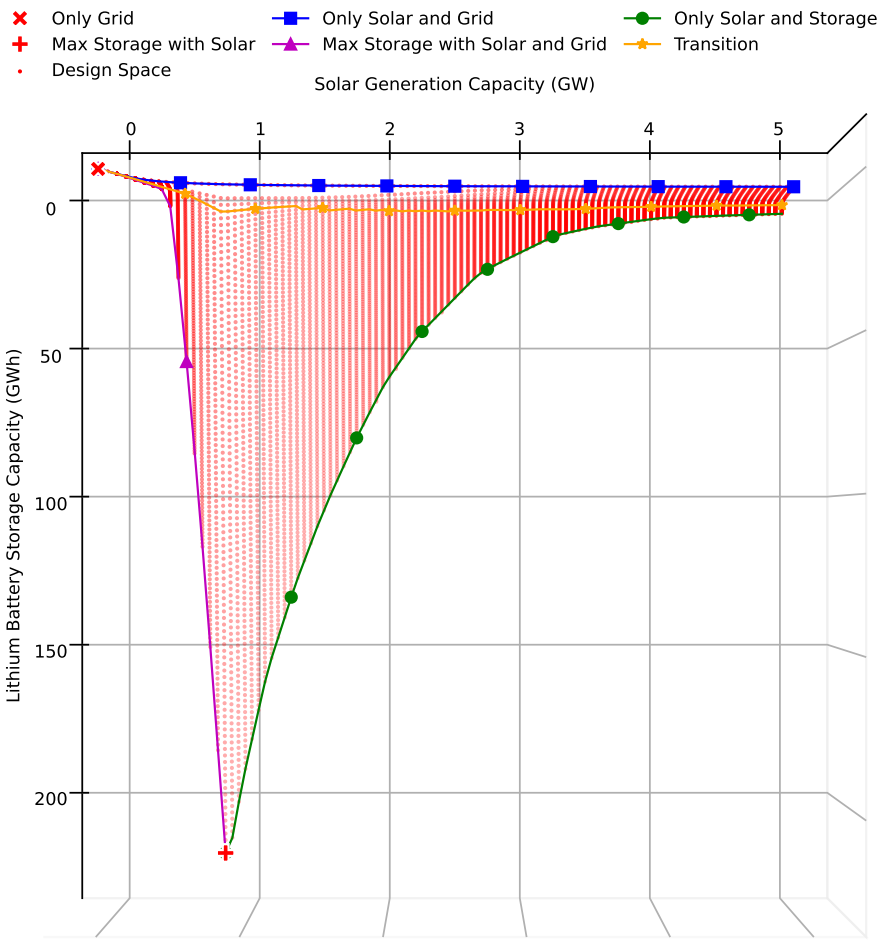

Figure 4.11: Design space view from the top.

At the bottom of 4.8, which is better shown from the top view in 4.11, the data curve "Only Solar and Storage" depicts the solar and storage capacities required to meet demand without grid electricity import. As solar capacity increases, the storage capacity requirement decreases. This is because more demand is directly met via solar generation, and less are met through storage, resulting in a reduction of the storage requirement. However, the reduction in storage requirement has a limit, as solar does not generate energy at night, and without grid electricity, storage is required to meet nighttime demand.

4.3.5 Future Cost Projection

The lifespan of a solar PV system is 30 years, while a lithium storage system is 15 years [178]. The discount rate is 3%, consisting of a 2.5% annual inflation rate and a 0.5% base interest rate. In 2019, solar and storage's installed and O&M (Operation and Maintenance) costs are assumed to be 758 GBP/kW, 7.45 GBP/kW, 330 GBP/kWh, and 8.25 GBP/kWh, respectively [51]. These costs are projected to 2050 by NREL via an aggregation of multiple published projections [178]. The projection predicts that by 2030, solar's installed and O&M costs will decrease to 56% and 73% of the 2019 level, respectively, and storage costs will decrease to 42%. By 2050, solar's installed and O&M costs will decrease to 46% and 65%, respectively, and storage costs will decrease to 32%. The analysis requires costs projected to 2100, so the cost reduction rate between 2050 and 2100 is assumed to be the same as that between 2030 and 2050. By 2100, solar's installed and O&M costs will reduce to 21% and 48%, respectively, and storage costs will reduce to 5%. The cost projections are presented in Fig. 4.12.

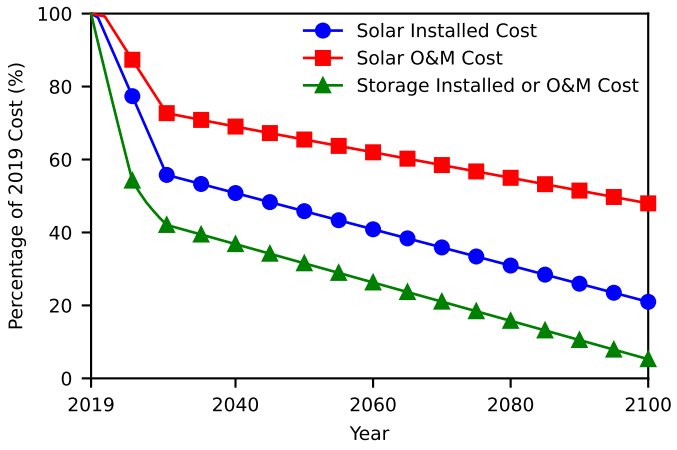

Figure 4.12: Cost projection of solar PV system's installed and O&M costs and lithium battery storage's installed and O&M costs.

4.3.6 Electricity Price

Great Britain's hourly wholesale electricity prices are sourced from the Open Power System Data platform [179]. The price at each hour is calculated from a

five-year average between 2015 and 2019 to reduce anomalies. Fig. 4.13 shows the hourly electricity price profile. Electricity prices are generally higher during winter, and the price variation is also greater. The average electricity wholesale price over the year is 45 GBP/MWh.

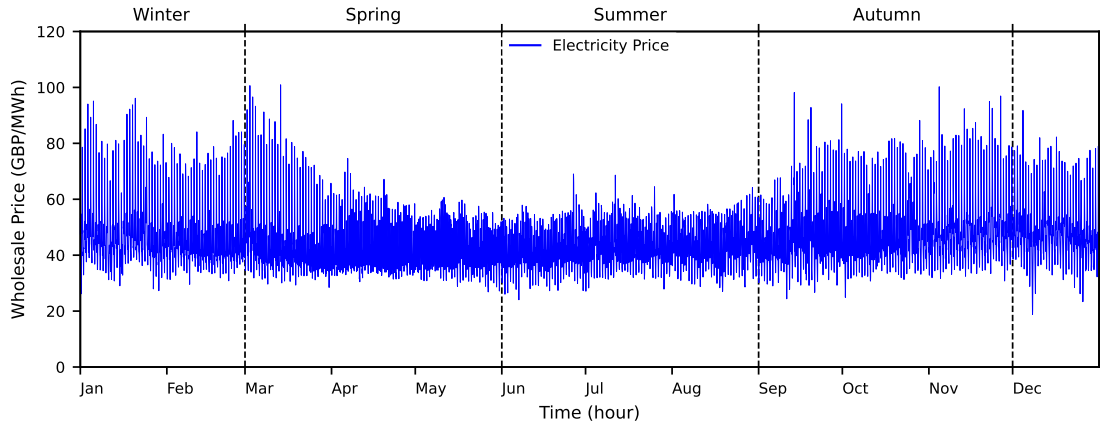

Figure 4.13: Great Britain's hourly wholesale electricity price in a typically year. The dashed lines separate the seasons.

4.3.7 Future System Size

Based on the design space, the LCOE is calculated for each combination, and the combination with the lowest LCOE is selected as the optimal. This process is repeated for each year between 2019 and 2100, and the results are presented in Fig. 4.14.

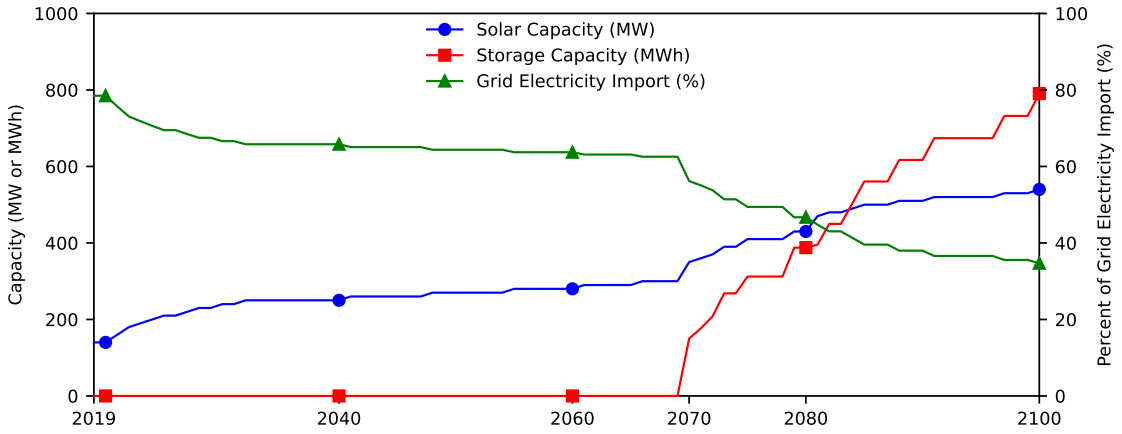

Figure 4.14: The lowest LCOE (Levelized Cost of Electricity) system sizing of the grid-connected solar-battery system for each year between 2019 and 2100.

The optimal system in 2019 consists of 140 MW of solar generation with no storage, and the grid supplies 78% of the energy. The result shows that while solar PV has become economically competitive, lithium storage remains too expensive. As time passes, solar and storage system prices will continue to drop, and they will make up a greater portion of the hybrid renewable system. In 2050, the optimal solar capacity doubles to 270 MW, and grid electricity import reduces to 64%.

Lithium battery storage becomes part of the optimal system in 2070. By then, projected battery system costs have reduced to 21% of the 2019 level, and the solar PV system's installed and O&M costs have reduced to 36% and 58%, respectively. The optimal system consists of 350 MW of solar PV and 150 MWh of lithium storage, reducing grid electricity import to 44%. After storage becomes part of the optimal system, optimal solar and storage capacity begin to increase rapidly. By 2100, the optimal system consists of 540 MW of solar and 790 MWh of storage, reducing electricity import by 33%. Between 2019 and 2100, the optimal system's grid electricity reliance is reduced by 45%, and the LCOE is reduced from 45 GBP/MWh to 28 GBP/MWh.

Solar and storage will make up a greater portion of the hybrid renewable system as their costs decline. However, the increase in solar and storage capacity will eventually slow down, as some demand becomes too costly to meet with solar and storage alone. For instance, meeting the nightly winter demand would require either large storage to store surplus summer generation or large solar capacity to generate sufficient energy in winter. Therefore, there will always be a need for grid electricity, which provides flexibility at a competitive price.

Note that the results rely on major assumptions, such as a consistent decrease in solar and storage prices, and consistent electricity demand, solar generation, and electricity price profiles. Furthermore, the system operates under a conventional operation strategy that only allows electricity import, not export. Different operation strategies, price projections, and generation and demand profiles can all influence the results. Therefore, future research should test alternative operation strategies

and account for uncertainties in prices, demand, and generation. These uncertainties can be addressed using probabilistic methods like Monte Carlo simulation.

Additionally, the approach used in this chapter involves an enumerative method, which is an exhaustive search approach. Other search methods, such as meta-heuristic algorithms like particle swarm optimization or genetic algorithms, could be employed to explore the size search space more efficiently and may converge on an optimal solution more quickly.

4.4 Summary

The chapter presents a hybridized techno-economic method to size solar PV and lithium storage systems with the aim of reducing grid reliance in buildings. The method utilizes analytical methods to determine the maximum solar and storage sizes, which are used to set the boundary for the solution search space. The bounded search space guarantees optimality while reducing the enumerative method's calculation time. Then, the enumerative method systematically iterates through the search space. At each iteration, the hybrid renewable system is simulated, and the cost of the system is calculated. The optimal system size is selected based on the lowest cost. The contributions of this chapter are summarized as follows:

- Novel analytical methods calculate maximum solar and storage system sizes, which are used to define the size search space boundary. The bounded search space guarantees optimal sizing while reducing the number of iterations.

- The design space explores the relationship between solar capacity, storage capacity, and the amount of grid electricity import required to support the demand.

- Most studies do not take into account the future trend of solar PV and lithium battery composition in the energy system. This chapter analyzes the future trend with solar and battery system cost projections.

The method is applied to a solar-battery case study on the city of Oxford. The system is controlled using a conventional operation strategy. Major findings from the case study are summarized as follows:

- For an independent solar-battery system, increasing solar capacity can reduce storage requirement to a certain extent. After which, further increases in solar capacity no longer reduces storage requirement. This is because solar energy generation is absent at night, necessitating storage to meet nighttime demand.
- For a solar-grid system without storage, increasing solar capacity can reduce grid electricity import to a certain extent. After which, increasing solar capacity no longer reduces grid electricity import. This is because solar does not generate energy at night, which means nighttime demand needs to be met by grid electricity import.
- Solar and storage will make up a greater portion of the hybrid renewable system as their costs decrease. However, grid electricity is always needed, as it provides flexibility at a competitive price.
- The solar and storage capacity increase will eventually slow down, as some demand, such as nighttime winter demand, are too expensive to be met by solar and storage alone.

This chapter explored a hybridized techno-economic method for sizing solar and storage in a microgrid setting. The method did not account for the effects of the electricity network, such as line and transformer capacities. In the next chapter, the electricity network system will be incorporated using optimal power flow. Additionally, the next chapter will delve into storage sizing and placement in hybrid renewable systems with both solar and wind generation.

The work presented in this chapter has been published in the ECEEE (European Council for Energy Efficient Economy) 2022 Summer Study Conference as a conference paper. The paper is titled "Optimal sizing of solar photovoltaic and lithium battery storage to reduce grid electricity reliance in buildings."

5

Storage Sizing and Placement

Contents

5.1 Introduction

This chapter presents a novel analytical method for sizing and placing energy storage in hybrid renewable energy systems, with the objective of maximizing storage utilization while eliminating unutilized storage capacity. The method exhibits fast performance, accommodates non-convex models, and converges effectively to optimal sizing and placement. The method first employs optimal power flow to optimize storage power dispatch. Then, storage profiles are constructed based on the storage dispatch. Subsequently, storage sizing and placement are calculated from these profiles. The proposed method is benchmarked against both meta-heuristic and mathematical optimization methods. The benchmark demonstrates that the proposed method yields the smallest storage size that minimizes generator cost, which is achieved by maximizing storage utilization and eliminating unused storage capacity. Moreover, the benchmark finds that storage tends to be placed on buses with large generation, large demand, or near congested lines with high power flow. The method is applied to a case study on a carbon-neutral village with wind and solar generation. The study finds that the storage requirement is the highest when renewable generation is just enough to support the system. Additional renewable generators can reduce the storage requirement, but only to a certain extent. This is because storage remains necessary to support demand during calm nights with no solar or wind generation. The proposed method serves as a decision support tool for energy system planners, aiding in optimal storage sizing and placement given known generation and demand.

The chapter is structured as follows. Section 5.2 introduces the proposed method for storage sizing and placement. Section 5.3 introduces the proposed mathematical method used during the benchmark. Section 5.4 presents the benchmark of the proposed method against meta-heuristic and mathematical optimization methods. Section 5.5 provides a case study on storage sizing and placement for a carbon-neutral village. Section 5.6 concludes the chapter with a summary of key contributions and findings from the benchmark and case study.

5.2 Proposed Method

The objective of the proposed method is to maximize the utilization of storage energy while eliminating unused storage capacity. The sizing is performed within the physical constraints of storage energy level dynamics, storage energy limits, storage power limits, and power system constraints, such as bus power balance, branch current flow limits, and bus voltage limits. In most scenarios, eliminating unused storage capacity results in a smaller storage size, while maximizing storage energy utilization also minimizes generator costs. Therefore, an alternative objective of the proposed method is to optimize for the smallest storage size that minimizes generator costs.

The methodology section will first introduce the equations for storage sizing and placement. Then, the step-by-step procedures for conducting storage sizing and placement will be detailed. The following notations will be used: index $i \in \mathcal{N} = \{1, \ldots, N\}$ denotes the bus index among a total of N buses, index $ij \in \mathcal{L} = \{1, \ldots, L\}$ denotes the branch index from bus i to bus j, index $t \in \mathcal{T} = \{0, \ldots, T\}$ denotes the time index, and Δt is the time interval.

5.2.1 Branch Admittance

In optimal power flow, the electricity line and transformer are considered branch elements. They are modelled using the Generalized PI Branch Model, shown in Fig. 5.1.

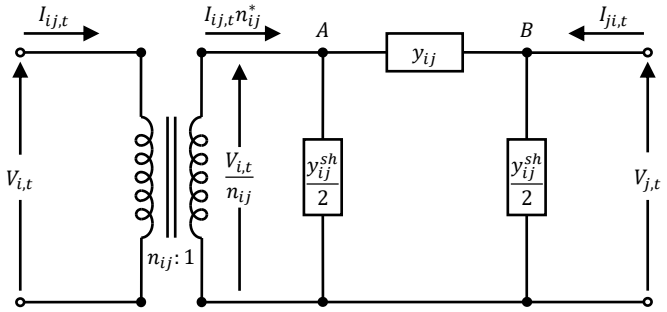

Figure 5.1: The Generalized PI Branch Model for modelling electricity lines and transformers. This model is used to derive the branch current flow equations employed in the calculation of OPF (Optimal Power Flow).

The model uses the turn ratio to account for off-nominal transformers with tap changers and phase shifters. The turn ratio and its complex conjugate are calculated using Eq. (5.1) and Eq. (5.2).

$$n_{ij} = \tau_{ij}\, e^{i\phi_{ij}}, \tag{5.1}$$

$$n^*_{ij} = \tau_{ij}\, e^{-i\phi_{ij}}, \tag{5.2}$$

Where n_{ij} and n^*_{ij} are the transformer turn ratio and its complex conjugate, τ_{ij} is the tap ratio, ϕ_{ij} is the phase shift angle. The turn ratio is equal to one for lines and nominal transformers. The changes in voltage and current due to nominal transformers are accounted for by the per-unit system.

The branch current flow from bus i to bus j is calculated by applying Kirchhoff's current law at point A in the figure, resulting in Eq. (5.3). Similarly, the branch current flow from bus j to bus i is calculated by applying Kirchhoff's current law at point B in the figure, resulting in Eq. (5.4).

$$I_{ij,t} = \frac{1}{n^*_{ij}} \left(\frac{y^{sh}_{ij}}{2} \left(\frac{V_{i,t}}{n_{ij}}\right) + y_{ij} \left(\frac{V_{i,t}}{n_{ij}} - V_{j,t}\right)\right), \tag{5.3}$$

$$I_{ji,t} = \frac{y^{sh}_{ij}}{2} \left(V_{j,t}\right) + y_{ij} \left(V_{j,t} - \frac{V_{i,t}}{n_{ij}}\right), \tag{5.4}$$

Where $I_{ij,t}$ is the branch current flow from bus i to bus j, $I_{ji,t}$ is the branch current flow from bus j to bus i, y^{sh}_{ij} and y_{ij} are the branch's shunt and series admittance, n_{ij} and n^*_{ij} are the transformer turn ratio and its complex conjugate, $V_{i,t}$ and $V_{j,t}$ are the voltage magnitudes at bus i to bus j.

The branch current flow equations from Eq. (5.3) and Eq. (5.4) are jointly represented in Eq. (5.5) using the branch admittance matrix $\mathbf{Y}_{br}$.

$$\begin{bmatrix} I_{ij,t} \\ I_{ji,t} \end{bmatrix} = \begin{bmatrix} \frac{1}{n_{ij} n^*_{ij}} \left(y_{ij} + \frac{y^{sh}_{ij}}{2}\right) & -\frac{y_{ij}}{n^*_{ij}} \\ -\frac{y_{ij}}{n_{ij}} & y_{ij} + \frac{y^{sh}_{ij}}{2} \end{bmatrix} \begin{bmatrix} V_{i,t} \\ V_{j,t} \end{bmatrix} = \mathbf{Y}_{br} \begin{bmatrix} V_{i,t} \\ V_{j,t} \end{bmatrix}. \tag{5.5}$$

5.2.2 Bus Admittance

The branch admittance matrix is expanded into the bus admittance matrix to account for power injection from multiple branches connecting to the same bus. The bus admittance matrix is constructed using Eq. (5.6).

$$\mathbf{Y}_{bus} = \begin{cases} Y_{ii} = y_i^s + \sum\limits_{ij \in \mathcal{L}} \frac{1}{n_{ij} n_{ij}^*} (y_{ij} + \frac{y_{ij}^{sh}}{2}) + \sum\limits_{ji \in \mathcal{L}} (y_{ji} + \frac{y_{ji}^{sh}}{2}), \\ Y_{ij} = \sum\limits_{ij \in \mathcal{L}} -\frac{y_{ij}}{n_{ij}^*} + \sum\limits_{ji \in \mathcal{L}} -\frac{y_{ij}}{n_{ij}}, \text{ if } i \neq j \end{cases} \tag{5.6}$$

Where $\mathbf{Y}_{bus}$ is the bus admittance matrix, Y_{ii} and Y_{ij} are the diagonal and off-diagonal elements of the bus admittance matrix, y_i^s is the bus shunt admittance, y_{ji}^{sh} and y_{ji} are the branch shunt and series admittance, n_{ij} and n_{ij}^* are the transformer turn ratio and its complex conjugate. In both element equations, the first summation is for admittance from bus i to bus j, and the second summation is for admittance from bus j to bus i. Note that the bus admittance matrix reduces back to the branch admittance matrix when only one branch is considered.

For each element in the bus admittance matrix, its real and imaginary parts are the conductance element G_{ij} and susceptance element B_{ij}, as stated in Eq. (5.7).

$$Y_{ij} = G_{ij} + iB_{ij}. \tag{5.7}$$

The bus admittance matrix is used to calculate the power injection at each bus via Eq. (5.8).

$$\mathbf{S}_{bus,t} = \mathbf{V}_t \circ (\mathbf{I}_{bus,t})^* = \mathbf{V}_t \circ (\mathbf{Y}_{bus} \mathbf{V}_t)^*, \tag{5.8}$$

Where $\mathbf{S}_{bus,t}$ is the bus apparent power injection vector, $\mathbf{V}_t$ is the bus voltage magnitude vector, $\mathbf{I}_{bus,t}$ is the bus current flow vector, and $\mathbf{Y}_{bus}$ is the bus admittance matrix. The equation says the bus apparent power injection is equal to the element-wise multiplication (Hadamard product) of bus voltage and the complex conjugate of bus current. The complex conjugate is used to calculate the phase difference between voltage and current. The bus current flow is the product of the bus admittance matrix and bus voltage magnitude.

Each element within the bus apparent power injection vector is the bus apparent power injection $S_{i,t}$. Its real and imaginary parts are the active power injection $P_{i,t}$ and reactive power injection $Q_{i,t}$, as stated in Eq. (5.9).

$$S_{i,t} = P_{i,t} + iQ_{i,t}. \tag{5.9}$$

The bus active and reactive power injections are calculated using Eq. (5.10) and Eq. (5.11), which are derived from Eq. (5.8).

$$P_{i,t} = V_{i,t} \sum_{j=1}^{N} V_{j,t} \left(G_{ij} \cos(\theta_{i,t} - \theta_{j,t}) + B_{ij} \sin(\theta_{i,t} - \theta_{j,t})\right), \tag{5.10}$$

$$Q_{i,t} = V_{i,t} \sum_{j=1}^{N} V_{j,t} \left(G_{ij} \sin(\theta_{i,t} - \theta_{j,t}) + B_{ij} \cos(\theta_{i,t} - \theta_{j,t})\right), \tag{5.11}$$

Where $P_{i,t}$ and $Q_{i,t}$ are the bus active and reactive power injections, G_{ij} and B_{ij} are the conductance and susceptance elements, $V_{i,t}$ and $\theta_{i,t}$ are the bus voltage magnitude and angle.

5.2.3 AC OPF

The OPF (Optimal Power Flow) problem formulation starts with the objective function. The quadratic objective function for generator cost is stated in Eq. (5.12).

$$\min \sum_{i=1}^{N} \sum_{t=0}^{T} C_i^0 + C_i^1 P_{i,t}^G + C_i^2 (P_{i,t}^G)^2, \tag{5.12}$$

Where C_i^0, C_i^1, C_i^2 are the generator cost coefficients, and $P_{i,t}^G$ is the generator active power. Note that in the OPF, the external grid is modelled as a generator, where positive grid power means import from the external grid, and negative grid power means export to the external grid.

For AC OPF, there are four decision variables: generator active power $P_{i,t}^G$, generator reactive power $Q_{i,t}^G$, voltage magnitude $V_{i,t}$, and voltage angle $\theta_{i,t}$.

The bus active and reactive power balance constraints are stated in Eq. (5.13) and Eq. (5.14).

$$P_{i,t} = P_{i,t}^G - P_{i,t}^L - P_{i,t}^S, \tag{5.13}$$

$$Q_{i,t} = Q^G_{i,t} - Q^L_{i,t} - Q^S_{i,t}, \tag{5.14}$$

Where $P_{i,t}$ and $Q_{i,t}$ are the bus active and reactive power injections, $P^G_{i,t}$ and $Q^G_{i,t}$ are the generator active and reactive power, $P^L_{i,t}$ and $Q^L_{i,t}$ are the load active and reactive power, $P^S_{i,t}$ and $Q^S_{i,t}$ are the storage active and reactive power. For storage, positive power means storage charges using energy from the bus, and negative power means storage discharges energy to the bus.

The external grid maintains the power balance within the system. The bus hosting the external grid connection is called the reference bus. The reference bus is constrained by the reference voltage angle $\theta_{ref,t}$ at zero degrees, and the reference voltage magnitude $V_{ref,t}$ at one per unit. The reference voltage angle and magnitude constraints are stated in Eq. (5.15) and Eq. (5.16).

$$\theta_{ref,t} = 0^\circ, \tag{5.15}$$

$$V_{ref,t} = 1p.u. \tag{5.16}$$

The generator active and reactive power limit constraints are stated in Eq. (5.17) and Eq. (5.18).

$$P^G_{i,min} \leq P^G_{i,t} \leq P^G_{i,max}, \tag{5.17}$$

$$Q^G_{i,min} \leq Q^G_{i,t} \leq Q^G_{i,max}, \tag{5.18}$$

Where $P^G_{i,t}$ is the generator active power, $P^G_{i,max}$ and $P^G_{i,min}$ are the maximum and minimum generator active power limits. $Q^G_{i,t}$ is the generator reactive power, $Q^G_{i,max}$ and $Q^G_{i,min}$ are the maximum and minimum generator reactive power limits.

The bus voltage limit constraint is stated in Eq. (5.19).

$$V_{i,min} \leq V_{i,t} \leq V_{i,max}, \tag{5.19}$$

Where $V_{i,t}$ is the bus voltage magnitude, $V_{i,max}$ and $V_{i,min}$ are the maximum and minimum bus voltage limits.

The branch current flow limit constraint is stated in Eq. (5.20).

$$-I_{ij,max} \leq I_{ij,t} \leq I_{ij,max}, \tag{5.20}$$

Where $I_{ij,t}$ is the branch current flow, and $I_{ij,max}$ is the maximum limit of the branch current flow. The constraint is bounded on both sides because the current flow can be negative if the actual flow direction is opposite to the assumed flow direction.

5.2.4 DC OPF

AC OPF is non-linear and non-convex, which requires slower solvers that cannot guarantee a global optimal solution. DC OPF is a linearized version of AC OPF, enabling the use of faster solvers that guarantee global optimality [180]. DC OPF has the following assumptions:

- Reactive powers are ignored.
- Branches are lossless, and resistances are approximately zero. As a result, the real part of admittance is also zero: $G_{ij} = 0$.
- Differences between adjacent buses voltage angles are small, such that: $\sin(\theta_{i,t} - \theta_{j,t}) \approx \theta_{i,t} - \theta_{j,t}$, and $\cos(\theta_{i,t} - \theta_{j,t}) \approx 1$.
- Bus voltage magnitudes are approximately one per unit: $V_{i,t} \approx 1\, p.u.$

With the aforementioned assumptions, the bus active power injection from Eq. (5.10) simplifies to Eq. (5.21).

$$P_{i,t} = \sum_{j=1}^{N} B_{ij}(\theta_{i,t} - \theta_{j,t}), \tag{5.21}$$

Where $P_{i,t}$ is the bus active power injection, B_{ij} is the susceptance element, $\theta_{i,t}$ and $\theta_{j,t}$ are the bus voltage angles at bus i and bus j.

Moreover, with bus voltages equal to one per unit, the equation for branch current flow $I_{ij,t}$ simplifies to Eq. (5.22).

$$I_{ij,t} = B_{ij}(\theta_{i,t} - \theta_{j,t}). \tag{5.22}$$

5.2.5 Storage Sizing

The battery storage sizing method is adapted from Sections 3.2.1, 3.2.2, 3.2.3, and 3.2.4. For the reader's convenience, the method's equations are briefly reviewed here, as they will be used to outline the steps in the proposed method.

The sizing method starts with constructing the storage profile. The storage profile is constructed using Eq. (5.23) by calculating the storage's stored energy level at each time step.

$$
\begin{aligned}
S_{i,t+\Delta t} &= S_{i,t}\,(1-\sigma) + P^{S}_{i,t}\,\eta_t\,\Delta t, \\
\text{where: } \eta_t &= \begin{cases} \eta_{c,t}, & \text{if } P^{S}_{i,t} \geq 0, \\ \frac{1}{\eta_{d,t}}, & \text{if } P^{S}_{i,t} < 0, \end{cases} \\
\text{and } \sigma &= 0, \text{ if } S_{i,t} < 0,
\end{aligned}
\tag{5.23}
$$

Where $S_{i,t}$ is the storage energy level, σ is the energy leakage rate of storage, $P^{S}_{i,t}$ is the storage power, and η_t is the storage efficiency, and Δt is the time interval. The storage efficiency is the charge efficiency $\eta_{c,t}$ when storage power is positive, meaning storage is charging. And it is the inverse of the discharge efficiency $\eta_{d,t}$ when storage power is negative, meaning storage is discharging. This time-discrete equation is used to construct the storage profile. During the construction, the leakage rate is set to zero if the storage level falls below zero.

The method sizes storage based on the maximum increase or decrease in the storage profile, representing the largest cumulative charge or discharge over the design time horizon. These increases and decreases are calculated via the differences between critical points in the storage profile. Eq. (5.24) calculates the critical points by setting the derivative of the storage profile equal to zero and solving for the roots. Alternatively, computational functions such as SciPy's argrelextrema identify critical points by checking if a point's storage level is higher or lower than its neighboring storage levels [165].

$$\begin{gathered}\text{Solve } \frac{dS_{i,t}}{dt} = 0 \text{ for all } t, \\ \text{such that critical points are: } t_1,\ t_2,\ \cdots,\ t_n, \\ \text{and critical storage levels are: } S_{i,t_1},\ S_{i,t_2},\ \cdots,\ S_{i,t_n},\end{gathered} \tag{5.24}$$

The critical storage levels are used by the difference matrix in Eq. (5.25), which pairs critical points and calculates the storage level difference between them. These storage level differences are essential for storage sizing.

$$\begin{aligned}\mathbf{D}_i &= \mathbf{L}_i + \mathbf{C}_i - (\mathbf{C}_i)^T, \\ \text{where : } \mathbf{L}_i &= \begin{cases} L_{i,jk} = 0, & \text{if } j \le k, \\ L_{i,jk} = S_{i,T} - S_{i,0}, & \text{if } j > k, \end{cases} \\ \mathbf{C}_i &= (\mathbf{1}_i)^T \mathbf{S}_i, \\ \mathbf{S}_i &= [S_{i,t_1},\ S_{i,t_2},\ \cdots,\ S_{i,t_n}], \\ \mathbf{1}_i &= [1,\ 1,\ \cdots,\ 1],\end{aligned} \tag{5.25}$$

Where $\mathbf{D}_i$ is the difference matrix, $\mathbf{L}_i$ is the lower triangular matrix, and $\mathbf{C}_i$ is the critical storage level matrix. $L_{i,jk}$ is the element of lower triangular matrix at row j and column k. $S_{i,0}$ and $S_{i,T}$ are the starting and ending storage levels. $\mathbf{S}_i$ is the critical storage level vector, and $\mathbf{1}_i$ is the all-ones vector with the same dimensions.

The difference matrix is used in Eq. (5.26) for storage sizing.

$$E_i = \begin{cases} |\min(\mathbf{D}_i)|, & \text{if } S_{i,T} - S_{i,0} > 0, \\ \max(\mathbf{D}_i), & \text{if } S_{i,T} - S_{i,0} < 0, \\ \max|\mathbf{D}_i|, & \text{if } S_{i,T} - S_{i,0} = 0, \end{cases} \tag{5.26}$$

Where E_i is the storage size, $\mathbf{D}_i$ is the difference matrix, and $S_{i,0}$ and $S_{i,T}$ are the starting and ending storage levels. The equation says that when the overall storage profile increases, meaning the ending storage level is greater than the starting storage level ($S_{i,T} - S_{i,0} > 0$), the storage size E_i is equal to the absolute value of the minimum of the difference matrix ($|\min(\mathbf{D}_i)|$), which corresponds to the largest decrease in the storage profile. Conversely, if the overall storage profile decreases ($S_{i,T} - S_{i,0} < 0$), the storage size is equal to the difference matrix's maximum

$(\max(\mathbf{D}_i))$, corresponding to the largest increase in the storage profile. Lastly, if the overall storage profile neither increases nor decreases ($S_{i,T} - S_{i,0} = 0$), the storage size is equal to the maximum absolute value of the difference matrix ($\max|\mathbf{D}_i|$), corresponding to the largest absolute increase or decrease in the storage profile.

5.2.6 Storage Energy and Power Limit

The storage energy and power limit models are adapted from Sections 3.2.6, 3.2.7, and 3.2.8. For the reader's convenience, the equations are briefly reviewed in this section, as they will be used to calculate the allowable charge and discharge power.

Battery manufacturers specify cycle life under specific depth of discharge and C-rating to preserve battery health, and ensure the intended lifespan of the battery [166]. Eq. (5.27) calculates the storage's total energy capacity when accounting for the depth of discharge.

$$E_{i,tot} = \frac{E_i}{DoD_{max} - DoD_{min}}, \tag{5.27}$$

Where $E_{i,tot}$ is the storage's total energy capacity, E_i is the storage size, DoD_{max} and DoD_{min} are the maximum and minimum depth of discharge. In this design method, storage size is the energy capacity in the usable portion of the storage, while the remaining capacity is reserved to compensate for storage degradation.

Storage cannot discharge below the maximum depth of discharge, nor charge above the minimum depth of discharge. The storage levels at the maximum and minimum depth of discharge define the storage energy limits. The maximum and minimum storage energy limits are defined by Eq. (5.28) and Eq. (5.29).

$$S_{i,up} = E_{i,tot}\,(1 - DoD_{min}), \tag{5.28}$$

$$S_{i,low} = E_{i,tot}\,(1 - DoD_{max}), \tag{5.29}$$

Where $S_{i,up}$ and $S_{i,low}$ are the upper and lower storage energy limits, E_i is the storage size, DoD_{max} and DoD_{min} are the maximum and minimum depth of discharge.

The storage energy limit constraint is defined by Eq. (5.30).

$$S_{i,low} \leq S_{i,t} \leq S_{i,up}, \tag{5.30}$$

The constraint says the storage level $S_{i,t}$ cannot exceed the upper storage energy limit nor fall below the lower storage energy limit. Once the storage level hits the upper limit, energy cannot be charged into storage. Conversely, energy cannot be discharged from the storage if the storage level is at the lower limit.

In practice, the upper and lower storage limits are often too restrictive when used in the iterative storage sizing method, which can cause near-optimal sizing. A slack term is added to address this issue, as shown in Eq. (5.31) and Eq. (5.32).

$$S_{i,max} = S_{i,up} + \alpha \left| S_{i,T} - S_{i,0} \right|, \tag{5.31}$$

$$S_{i,min} = S_{i,low} - \alpha \left| S_{i,T} - S_{i,0} \right|, \tag{5.32}$$

Where $S_{i,max}$ and $S_{i,min}$ are the maximum and minimum storage energy limits, $S_{i,0}$ and $S_{i,T}$ are the starting and ending storage levels of the previous iteration, and α is a multiplier between zero and one. A large multiplier will cause slow convergence or even non-convergence, while a small multiplier may yield near-optimal sizing instead of the exact optimum. A multiplier of 0.5 is suitable for most scenarios.

A constrained storage profile will repeat itself when subject to the same demand and generation patterns in the future. The repeatability ensures the storage size is sustainable and can support similar demand and generation in the future. Equal starting and ending storage levels characterize sustainability. The sustainable starting storage level is calculated using Eq. (5.33).

$$S_{i,0_s} = \begin{cases} S_{i,T} - \max(S_{i,t}) + S_{i,up}, \text{ if } S_{i,T} - S_{i,0} \geq 0, \\ S_{i,T} - \min(S_{i,t}) + S_{i,low}, \text{ if } S_{i,T} - S_{i,0} \leq 0, \end{cases} \tag{5.33}$$

Where $S_{i,0_s}$ is sustainable starting storage level, $S_{i,t}$ is the storage level, $S_{i,up}$ and $S_{i,low}$ are the upper and lower storage limits, $S_{i,0}$ and $S_{i,T}$ are the starting and ending storage levels. The equation says the sustainable starting storage level is dictated by the difference between the ending and maximum storage levels in an increasing storage profile scenario, and by the ending and minimum storage levels in a decreasing storage profile scenario. The storage limits are added to re-frame those differences to the usable portion of storage.

High charge and discharge rates can also shorten the storage lifespan. The maximum charge and discharge rates are calculated using Eq. (5.34) and Eq. (5.35), which use C-ratings to relate the storage's power capacity with its energy capacity.

$$P_{i,c}^{S} = E_{i,tot}\, C_c, \tag{5.34}$$

$$P_{i,d}^{S} = -E_{i,tot}\, C_d, \tag{5.35}$$

Where $P_{i,c}^{S}$ and $P_{i,d}^{S}$ are the maximum charge and discharge rates, $E_{i,tot}$ is the storage's total energy capacity, C_c and C_d are the charge and discharge C-ratings.

The storage power limit constraint is defined by Eq. (5.36).

$$P_{i,d}^{S} \leq P_{i,t}^{S} \leq P_{i,c}^{S}, \tag{5.36}$$

The constraint says the storage power $P_{i,t}^{S}$ cannot exceed the maximum charge rate or the maximum discharge rate.

The maximum charge and discharge rates are often too restrictive when used in the iterative storage sizing method, which can cause storage size to converge to zero. Adding a slack term relaxes the maximum charge and discharge rates, enabling zero storage size to have charge and discharge. The new equations with the slack term are shown in Eq. (5.37) and Eq. (5.38).

$$P_{i,max}^{S} = P_{i,c}^{S} + \alpha\, |S_{i,T} - S_{i,0}|, \tag{5.37}$$

$$P_{i,min}^{S} = P_{i,d}^{S} - \alpha\, |S_{i,T} - S_{i,0}|, \tag{5.38}$$

Where $P_{i,max}^{S}$ and $P_{i,min}^{S}$ are the maximum and minimum storage power limits, $S_{i,0}$ and $S_{i,T}$ are the starting and ending storage levels of the previous iteration, and α is a multiplier between zero and one.

5.2.7 Allowable Storage Power

In practice, storage power is not only limited by the storage power limits, but also by the storage energy limits. The effects of these limits are synthesized into the allowable charge and discharge power, calculated using Eq. (5.39) and Eq. (5.40).

$$P_{i,t,c}^{S} = \min\left(\frac{S_{i,max} - S_{i,t}\,(1-\sigma)}{\eta_{c,t}\,\Delta t},\, P_{i,max}^{S}\right), \tag{5.39}$$

$$P^S_{i,t,d} = \max(\frac{(S_{i,min} - S_{i,t}\,(1-\sigma))\,\eta_{d,t}}{\Delta t},\, P^S_{i,min}), \tag{5.40}$$

Where $P^S_{i,t,c}$ and $P^S_{i,t,d}$ are the allowable charge and discharge power, $S_{i,max}$ and $S_{i,min}$ are the maximum and minimum storage energy limits, $S_{i,t}$ is the storage level, σ is the leakage rate, η_c and η_d are the charge and discharge efficiency, Δt is the time interval, $P^S_{i,max}$ and $P^S_{i,min}$ are the maximum and minimum storage power limits. The allowable charge power equation calculates the maximum charge power that the maximum storage energy limit allows, and compares it to the maximum storage power limit. The smaller of the two is the limiting factor, and is picked as the allowable charge power. Similarly, the allowable discharge equation calculates the maximum discharge power that the minimum storage energy limit allows, and compares it to the minimum storage power limit. The larger of the two is picked as the allowable discharge power due to negative values.

The allowable charge and discharge power are used in constraint Eq. (5.41) when constructing the constrained storage profile.

$$P^S_{i,t,d} \leq P^S_{i,t} \leq P^S_{i,t,c}, \tag{5.41}$$

The constraint says storage power $P^S_{i,t}$ cannot exceed the allowable charge or discharge power. This constraint also ensures the storage energy and power limit constraints are respected.

5.2.8 Non-linear Storage Model

For the linear storage model, constant storage efficiencies are used. In the case of the non-linear and non-convex storage model, the storage efficiency model by Ng *et al.* is employed [181] . The storage efficiency model uses SOC (State Of Charge), calculated using Eq. (5.42).

$$SOC_{i,t} = \frac{S_{i,t} - S_{i,min}}{S_{i,max} - S_{i,min}}, \tag{5.42}$$

Where $SOC_{i,t}$ is the state of charge, $S_{i,t}$ is the storage level, $S_{i,max}$ and $S_{i,min}$ are the maximum and minimum storage limits.

The charge efficiency is modelled by Eq. (5.43), and the discharge efficiency is modelled by Eq. (5.44).

$$\eta_{c,t} = 1 - 0.0197\, SOC_{i,t}, \tag{5.43}$$

$$\eta_{d,t} = 0.9822 + 0.0688\, SOC_{i,t},\ \eta_{d,t} \leq 1, \tag{5.44}$$

Where $\eta_{c,t}$ and $\eta_{d,t}$ are the storage charge and discharge efficiencies. The storage efficiency model leads to the multiplication of storage level and storage power, both of which are decision variables. The multiplication of two decision variables makes the storage model non-linear and non-convex.

5.2.9 Proposed Method Steps

The energy storage placement and sizing method consists of three layers, as shown in Fig. 5.2.

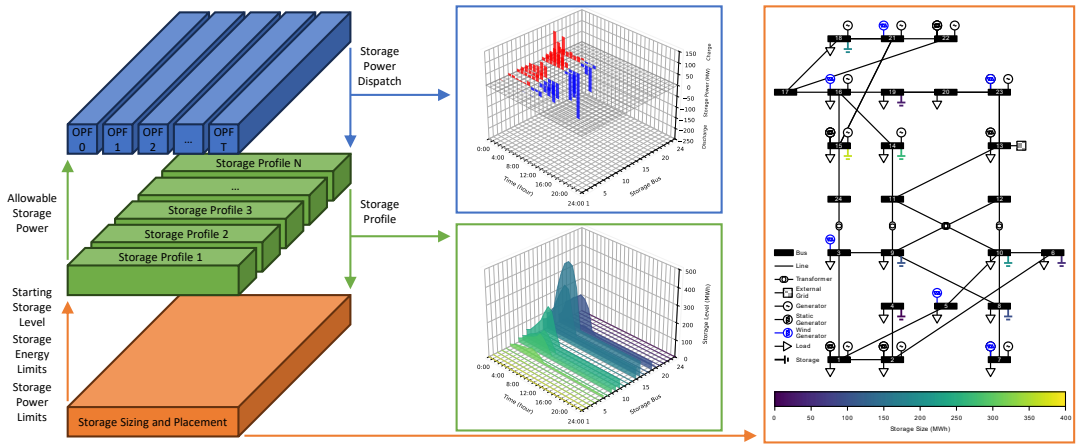

Figure 5.2: Summary of the proposed method. The proposed method has three layers: OPF at each time step (top), storage profile at each bus (middle), storage sizing and placement for the entire system (bottom). The three layers interact with each other during each iteration. The example results in the final iteration are presented for each layer.

At the top layer, the method employs OPF (Optimal Power Flow) to optimize storage power dispatch at each time step. At the middle layer, the method constructs the storage's stored energy profile at each bus, based on the storage power dispatches. At the bottom layer, storage sizing and placement are calculated for the entire system, based on the storage profiles. The layers interact with each other during

each iteration. Three flowcharts will detail the steps for each of the three layers in the proposed method.

5.2.9.1 Optimal Power Flow

The OPF optimizes the storage power dispatch at each time step. It is split into AC OPF and its linearized version, DC OPF. DC OPF can guarantee global optimality, but is less accurate due to the simplifications made during linearization. Both AC OPF and DC OPF are conducted via steps outlined in Fig. 5.3, with AC OPF requiring additional steps.

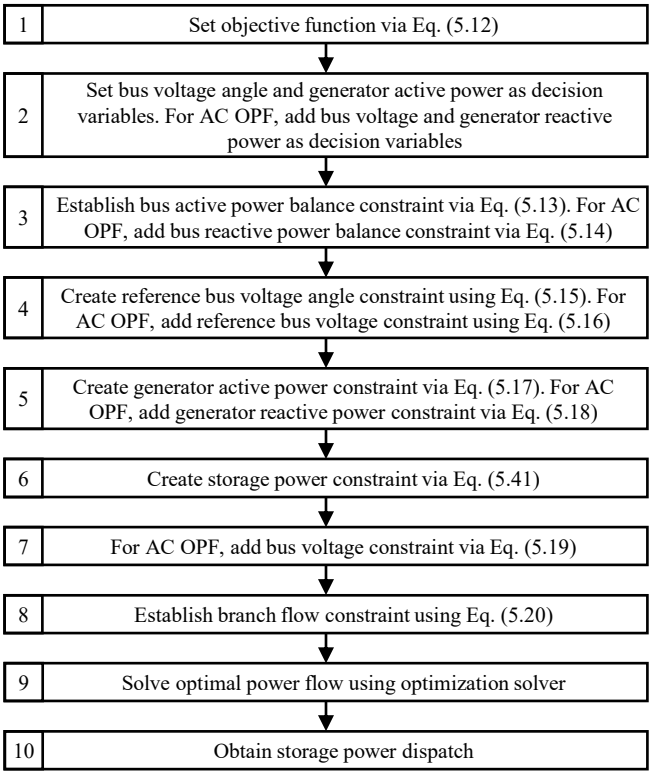

Figure 5.3: The steps flowchart for Optimal Power Flow.

The first step of both OPFs is to set the objective function using Eq. (5.12), which minimizes the generator cost, and encourages renewable consumption. The second step is to set the decision variables as bus voltage angle and generator active power for DC OPF, and add bus voltage magnitude and generator reactive power to the decision variables for AC OPF. The third step is to establish the bus active

power balance constraint via Eq. (5.13) for DC OPF, and add the bus reactive power balance constraint via Eq. (5.14) for AC OPF. For DC OPF, the bus active power injection is calculated using Eq. (5.21), while for AC OPF, the bus active and reactive power injections are calculated using Eq. (5.10) and Eq. (5.11). In the bus power injection equations, the conductance and susceptance elements are obtained from Eq. (5.7), where the admittance elements are from the bus admittance matrix via Eq. (5.6). The renewable generator power is obtained from wind turbine and solar PV models. The load power is obtained from load demand model. The fourth step is to set the reference voltage angle constraint using Eq. (5.15) for DC OPF, and add reference voltage magnitude constraint using Eq. (5.16) for AC OPF. The fifth step is to set the generator active power constraint via Eq. (5.17) for DC OPF, and add the generator reactive power constraint via Eq. (5.18) for AC OPF. The sixth step is to set the storage power constraint via Eq. (5.41). The seventh step is for AC OPF only, and it is to establish the bus voltage constraint using Eq. (5.19). The eighth step is to establish the branch current flow constraint using Eq. (5.20). The branch current flow is calculated via Eq. (5.22) for DC OPF, and is calculated via Eq. (5.3) and Eq. (5.4) for AC OPF. The ninth step is to solve the OPF model using optimization solvers. For DC OPF, a quadratic programming solver is recommended, such as the Gurobi solver. For AC OPF, an interior point solver is recommended, such as the Interior Point OPTimizer. The tenth and final step is to obtain the storage power dispatch from the OPF results.

5.2.9.2 Storage Profile

The storage profile is constructed using the power dispatch from OPF at each time step, which is used to size and place storage. The steps for constructing the storage profile are outlined in Fig. 5.4.

The first step is to start the storage profile at the sustainable starting storage level. Note that in the first iteration, the sustainable starting storage level is set to zero. The second step is for the non-linear storage model only, and it is to calculate the storage charge and discharge efficiency using Eq. (5.43) and Eq. (5.44). The

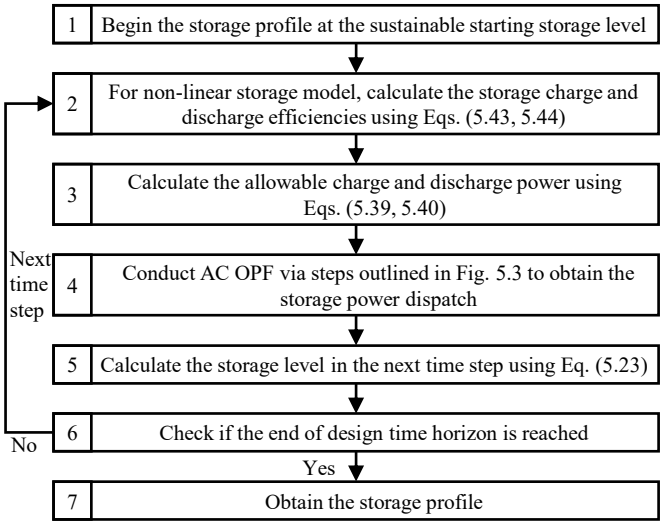

Figure 5.4: The steps flowchart for constructing the storage profile.

SOC (State of Charge) used in the storage efficiency equations is calculated using Eq. (5.42). For the linear storage model, the storage efficiencies are set as constants. Note that in the first iteration, the storage efficiencies are set to one. The third step is to calculate the allowable charge and discharge power for the time step using Eq. (5.39) and Eq. (5.40). Note that in the first iteration, the allowable charge and discharge power are assumed to be infinity. The fourth step is to conduct OPF via the steps outlined in Fig. 5.3 to obtain the optimal storage power dispatch. The fifth step is to calculate the storage level in the next time step using Eq. (5.23). Note that in the first iteration, the leakage rate is assumed to be zero. The sixth step is to check if the end of the design time horizon has been reached. If the end has not been reached, then move to the next time step by repeating from the second step. If the end has been reached, the seventh and final step is to obtain the storage profile for storage sizing and placement.

5.2.9.3 Storage Sizing and Placement

The storage profiles are used to size and place storage. The steps for storage sizing and placement are outlined in Fig. 5.5.

The first step is to construct the first iteration unconstrained storage profile using the steps outlined in Fig. 5.4. The second step is to identify critical points

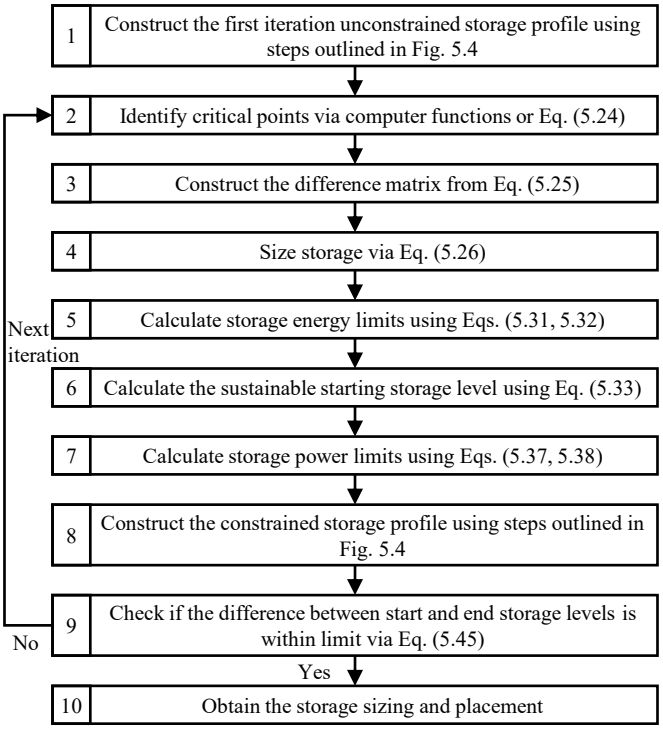

Figure 5.5: The steps flowchart for storage sizing and placement.

in the storage profile using computer functions or Eq. (5.24). The third step is to use the critical points and their storage levels in Eq. (5.25) to construct the difference matrix. The fourth step is to size storage using the difference matrix via Eq. (5.26). The fifth step calculates the maximum and minimum storage energy limits using Eq. (5.31) and Eq. (5.32), where the upper and lower storage energy limits are obtained from Eq. (5.28) and Eq. (5.29). The sixth step is to calculate the sustainable starting storage level using Eq. (5.33). The seventh step calculates the maximum and minimum storage power limits using Eq. (5.37) and Eq. (5.38), where the maximum charge and discharge rates are obtained from Eq. (5.34) and Eq. (5.35). The eighth step is to construct the new constrained storage profile using steps outlined in Fig. 5.4. The new constrained storage profile is used in the ninth step, to check if the absolute difference between starting and ending storage levels is within the user-defined permissible limit, as stated in Eq. (5.45).

$$|S_{i,T} - S_{i,0}| \leq \epsilon, \tag{5.45}$$

Where $S_{i,0}$ and $S_{i,T}$ are the starting and ending storage levels, and ϵ is the permissible difference limit. The permissible difference limit dictates the accuracy and significant figures of the resulting storage size. If the difference is beyond the limit, then repeat the process from the second step with the new constrained storage profile. If the difference falls within the limit, then the tenth and final step is to obtain the latest storage size and their placement as the results. The placement is based on the sizing. At each bus, if the storage size is smaller than the permissible difference limit, then that bus will not have a storage placement.

5.3 Proposed Mathematical Method

For benchmarking purposes, the proposed method is extended using mathematical optimization, creating the proposed mathematical method. The methodology section will first introduce the equations for storage sizing and placement using mathematical optimization. Subsequently, the step-by-step procedures for building the storage profile in the proposed mathematical method will be detailed, along with its utilization for storage sizing and placement.

5.3.1 Mathematical Problem Formulation

The mathematical optimization's problem formulation is categorized as mixed-integer quadratic programming. This section will first introduce the objective function, then the decision variables, followed by the constraints for DC OPF, and finally, the constraints for the mixed-integer linear storage model.

The objective function on generator and storage cost is shown in Eq. (5.46).

$$\min \sum_{i=1}^{N} \sum_{t=0}^{T} C_i^0 + C_i^1 P_{i,t}^G + C_i^2 (P_{i,t}^G)^2 + \sum_{i=1}^{N} C_i^S E_i, \tag{5.46}$$

Where C_i^0, C_i^1, C_i^2 are the generator cost coefficients, $P_{i,t}^G$ is the generator active power, C_i^S is the storage size cost coefficient, and E_i is the storage size.

The decision variables are: bus voltage angle $\theta_{i,t}$, generator active power $P_{i,t}^G$, storage power $P_{i,t}^S$, storage energy level $S_{i,t}$, storage size E_i, and a binary decision variable $b_{i,t}$ for storage dynamics.

The following constraints are for DC OPF. The bus power injection constraint is shown in Eq. (5.47).

$$P_{i,t} = \sum_{j=1}^{N} B_{ij}(\theta_{i,t} - \theta_{j,t}), \tag{5.47}$$

Where $P_{i,t}$ is the bus active power injection, B_{ij} is the susceptance element from the bus admittance matrix, $\theta_{i,t}$ and $\theta_{j,t}$ are the bus voltage angles at bus i and bus j.

The bus active power injection is used in the bus power balance constraint shown in Eq. (5.48).

$$P_{i,t} = P^G_{i,t} - P^L_{i,t} - P^S_{i,t}, \tag{5.48}$$

Where $P_{i,t}$ is the bus active power injections, $P^G_{i,t}$ is the active generator power, $P^L_{i,t}$ is the active load power, $P^S_{i,t}$ is the active storage power.

The reference bus hosting the external grid connection is constrained to a voltage angle of zero degrees, as stated in Eq. (5.49).

$$\theta_{ref,t} = 0^\circ. \tag{5.49}$$

The branch current flow constraint is shown in Eq. (5.50).

$$I_{ij,t} = B_{ij}(\theta_{i,t} - \theta_{j,t}). \tag{5.50}$$

Where $I_{ij,t}$ is the branch current flow, B_{ij} is the susceptance element from the bus admittance matrix, $\theta_{i,t}$ and $\theta_{j,t}$ are the bus voltage angles at bus i and bus j.

The branch current flow is limited by the constraint in Eq. (5.51).

$$-I_{ij,max} \leq I_{ij,t} \leq I_{ij,max}, \tag{5.51}$$

Where $I_{ij,t}$ is the branch current flow, and $I_{ij,max}$ is the maximum limit of the branch current flow. The constraint is bounded on both sides because the current flow can be negative if the actual flow direction is opposite to the assumed flow direction.

The active generator power is limited by the constraint in Eq. (5.52).

$$P^G_{i,min} \leq P^G_{i,t} \leq P^G_{i,max}, \tag{5.52}$$

Where $P^G_{i,t}$ is the active generator power, $P^G_{i,max}$ and $P^G_{i,min}$ are the maximum and minimum active generator power limits.

The following constraints are for the mixed-integer linear storage model. The relationship between storage size and total storage capacity is shown as constraint Eq. (5.53).

$$E_{i,tot} = \frac{E_i}{DoD_{max} - DoD_{min}}, \tag{5.53}$$

Where $E_{i,tot}$ is the storage's total energy capacity, E_i is the storage size, DoD_{max} and DoD_{min} are the maximum and minimum depth of discharge.

The maximum charge and discharge rates are defined by the constraints in Eq. (5.54) and Eq. (5.55).

$$P^S_{i,c} = E_{i,tot}\, C_c, \tag{5.54}$$

$$P^S_{i,d} = -E_{i,tot}\, C_d, \tag{5.55}$$

Where $P^S_{i,c}$ and $P^S_{i,d}$ are the maximum charge and discharge rates, $E_{i,tot}$ is the storage's total energy capacity, C_c and C_d are the charge and discharge C-ratings.

The storage power is limited by the maximum charge and discharge rates, as stated in constraint Eq. (5.56).

$$P^S_{i,d} \leq P^S_{i,t} \leq P^S_{i,c}, \tag{5.56}$$

Where $P^S_{i,d}$ is the storage power, $P^S_{i,c}$ and $P^S_{i,d}$ are the maximum charge and discharge rates.

The maximum and minimum storage energy limits are defined by constraints in Eq. (5.57) and Eq. (5.58).

$$S_{i,up} = E_{i,tot}\,(1 - DoD_{min}), \tag{5.57}$$

$$S_{i,low} = E_{i,tot}\,(1 - DoD_{max}), \tag{5.58}$$

Where $S_{i,up}$ and $S_{i,low}$ are the upper and lower storage energy limits, E_i is the storage size, DoD_{max} and DoD_{min} are the maximum and minimum depth of discharge.

The storage energy limit constraint is shown in Eq. (5.59).

$$S_{i,low} \leq S_{i,t} \leq S_{i,up}, \tag{5.59}$$

Where $S_{i,t}$ is the storage energy level, $S_{i,up}$ and $S_{i,low}$ are the upper and lower storage energy limits

A binary decision variable is used for indicator constraints to model the storage dynamics. The constraint Eq. (5.60) sets the binary variable to one if the storage power is positive, and to zero if the storage power is negative.

$$-M(1 - b_{i,t}) \leq P^S_{i,t} \leq M\, b_{i,t} \tag{5.60}$$

Where $b_{i,t}$ is the binary decision variable, M is a large number, and $P^S_{i,t}$ is the storage power.

The following indicator constraints are employed to model the storage dynamics. When the storage power is positive, the binary decision variable is one, and storage power is charged into the storage. When the storage power is negative, the binary decision variable is zero, and storage power is discharged from the storage. The storage dynamics equations for charging and discharging are Eq. (5.61) and Eq. (5.62).

$$S_{i,t+\Delta t} = S_{i,t}\,(1 - \sigma) + P^S_{i,t}\,\eta_{c,t}\,\Delta t, \text{ if } b_{i,t} = 1, \tag{5.61}$$

$$S_{i,t+\Delta t} = S_{i,t}\,(1 - \sigma) + \frac{P^S_{i,t}\,\Delta t}{\eta_{d,t}}, \text{ if } b_{i,t} = 0, \tag{5.62}$$

Where $S_{i,t}$ is the storage energy level, σ is the energy leakage rate of storage, $P^S_{i,t}$ is the storage power, $\eta_{c,t}$ and $\eta_{d,t}$ are the storage charge and discharge efficiencies, and Δt is the time interval.

5.3.2 Proposed Mathematical Method Steps

The proposed mathematical method differs from the proposed method in that storage profiles are obtained via mathematical optimization. The proposed mathematical method replaces the steps in Fig. 5.3 and Fig. 5.4 with the steps in Fig. 5.6.

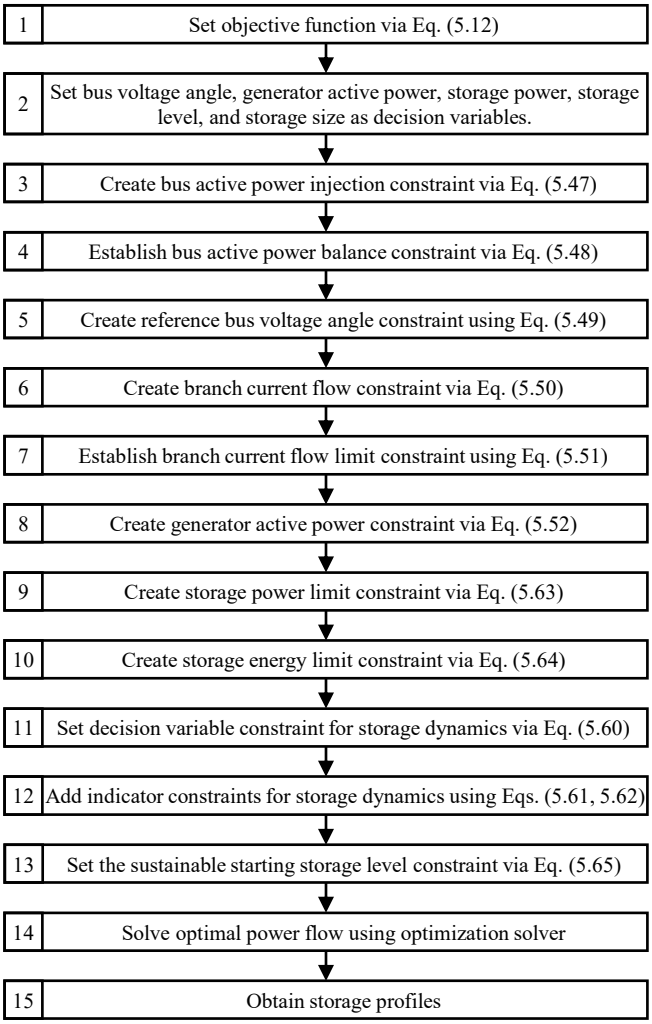

Figure 5.6: The steps flowchart for constructing the storage profile in the proposed mathematical method.

The proposed mathematical method utilizes the relaxed storage power limit constraint defined in Eq. (5.63).

$$P^S_{i,min} \leq P^S_{i,t} \leq P^S_{i,max}, \tag{5.63}$$

The constraint says the storage power $P^S_{i,t}$ cannot exceed the maximum storage power limit $P^S_{i,max}$ nor exceed the minimum storage power limit $P^S_{i,min}$.

The relaxed storage energy limit constraint is defined by Eq. (5.64).

$$S_{i,min} \leq S_{i,t} \leq S_{i,max}, \tag{5.64}$$

The constraint says the storage level $S_{i,t}$ cannot exceed the maximum storage energy limit $S_{i,max}$ nor fall below the minimum storage energy limit $S_{i,min}$.

The sustainable starting storage level constraint is shown in Eq. (5.65).

$$S_{i,0} = S_{i,0_s} \tag{5.65}$$

Where $S_{i,0}$ is the storage level at the first time step, and $S_{i,0_s}$ is the sustainable starting storage level.

For the first iteration, the sustainable starting storage level is assumed to be zero, and the storage energy and power limits are assumed to be infinity. After obtaining the storage profile using the steps outlined in the figure, storage sizing and placement are conducted following the steps outlined in Fig. 5.5.

5.4 Benchmark

This section benchmarks the proposed method against meta-heuristic optimization and mathematical optimization. For meta-heuristic optimization, the elitist genetic algorithm is chosen for its ability to handle many decision variables. For mathematical optimization, the Gurobi solver is selected for its fast speed. The benchmark is conducted on an Intel Core i7-9700 processor.

5.4.1 Test System Setup

The benchmark is conducted on the IEEE 24 Bus Reliability Test System, which has a peak load demand of 2,850 MW and a dispatchable peak generation capacity of 3,405 MW, representing an electrical system spanning a large geographical area [182]. The system has three modifications. First, six 200 MW wind farms are added to the system following the layout suggested by Ordoudis *et al.* [183]. Note that wind generation are varied across locations to represent the system's large geographical spread. Second, the external grid's maximum power limit is extended for both electricity import and export. Third, the external grid's cost function is modified by setting the quadratic cost coefficient to one and all other cost coefficients to zero. This modification ensures equal costs for electricity import and export, which puts the system under a conventional operation strategy to encourage renewable consumption. Specifically, the operation strategy prioritizes wind generation to

meet the demand due its lower cost. The external grid's electricity export cost encourages storage to charge from surplus generation, while the electricity import cost encourages storage to discharge energy when generation is insufficient to meet demand. The cost functions of the other generators remain unchanged from MatPower's IEEE Reliability Test System setup [184].

The original generator cost objective function from Eq. (5.12) will be used in the optimality benchmark, while the generator and storage cost objective function from Eq. (5.46) will be used in the speed benchmark. The speed benchmark employs the elitist genetic algorithm and Gurobi solver, and without putting a cost on storage size, they will yield exceedingly large storage size to minimize generator cost. Thus, for the purpose of comparison, storage size cost is added to the objective function, even though the proposed method does not need storage cost to function, as it will always yield the smallest storage size that maximizes storage utilization, and therefore minimizes generator cost.

5.4.2 Electricity Demand and Wind Generation Models

The test system's load demand and wind generation profiles are shown in Fig. 5.7.

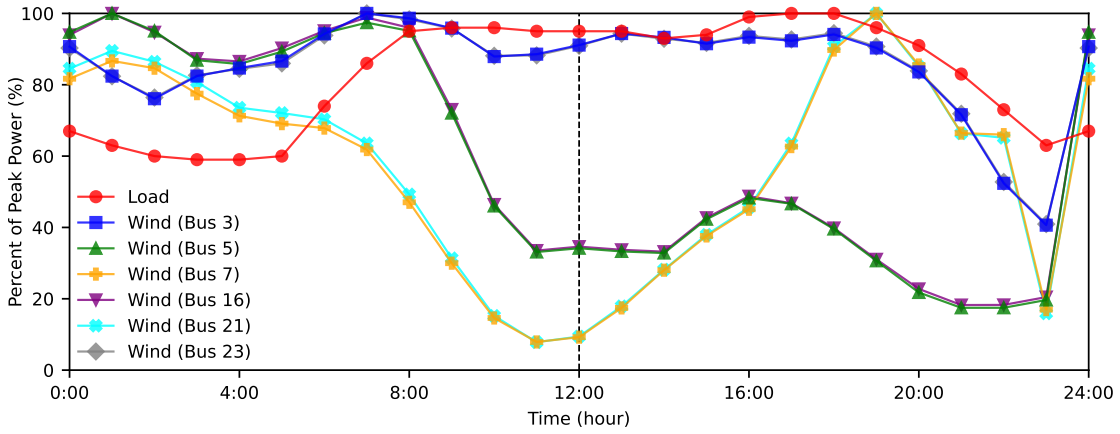

Figure 5.7: Hourly load demand and wind generation profiles for the IEEE Reliability Test System.

The demand profile is based on the peak winter weekday profile from the IEEE Reliability Test System [182]. The profile follows the "duck curve" pattern, in which demand is lowest at night, rises in the morning, dips in the afternoon, peaks in

the evening, and drops off again at night. The demand profiles are scaled by the peak power assigned to each load in the test system. The wind generation profiles are simulated using Staffell and Pfenninger's method [185]. Wind generation is typically lower during mid-day, and higher during morning and evening due to temperature fluctuations. The wind generation profiles are scaled to a peak value of 200 MW, as suggested by Ordoudis *et al.* [183]. The lithium battery system is assumed to have a charge and a discharge efficiency of 90%, a recommended depth of discharge of 80%, a C-rating of 1C, and a leakage rate of 2% per month [118]. The lithium battery storage specifications are in Table 5.1.

Lithium Battery Specification	Value
Charge Efficiency	90%
Discharge Efficiency	90%
Maximum Depth of Discharge	80%
Minimum Depth of Discharge	0%
Charge C-rating	1C
Discharge C-rating	1C
Monthly Leakage Rate	2%

Table 5.1: Lithium battery storage specifications.

5.4.3 Methods Settings

The settings for methods employed in the benchmark and the case study are shown in Table 5.2.

The convergence multiplier controls the speed and accuracy of the proposed method. A large multiplier can cause slow convergence or even non-convergence, while a small multiplier may yield a near-optimal solution instead of the exact optimum. A convergence multiplier of 0.5 is chosen, because it achieves a good balance between speed and accuracy.

The permissible limit controls the precision of the proposed method. The number of decimal places in the permissible limit determines the minimum decimal precision of storage sizes in the solution. A permissible limit of 0.1 is chosen, which means the minimum decimal place of storage sizes in the solution is the tenths place.

Proposed Method	
Convergence Multiplier	0.5
Permissible Limit	0.1
Elitist Genetic Algorithm	
Iteration	100
Population	10
Elite Portion	10%
Parent Portion	50 %
Crossover Rate	50 %
Mutation Rate	10 %
Proposed Mathematical Method	
Convergence Multiplier	0.5
Permissible Limit	0.1
Optimality Gap	0.001 %
Gurobi Mathematical Optimization	
Optimality Gap	0.001 %

Table 5.2: Method Settings for Benchmark and Case Study.

The number of iterations determines how many generations the elitist genetic algorithm will run. More generations allow the algorithm to better explore the solution space, potentially finding a more optimal solution. In the benchmark, 100 iterations are chosen to achieve a similar objective value as the proposed method.

The population size is the number of candidate solutions the elitist genetic algorithm evaluates each generation. A larger population increases diversity, enhancing the potential for finding an optimal solution. However, a population size of 10 is chosen because larger populations have a higher chance of generating invalid solutions, which can cause non-convergence in the OPF.

The elite portion is the portion of the population that will be directly carried over to the next iteration. The portion consists of the best-performing candidate solutions from the current iteration, and they will be carried over to the next iteration without undergoing crossover or mutation. An elite portion of 10% is chosen.

The parent portion is the portion of the top-performing population that will selected as the parents. The parent solutions will undergo crossover and mutation to generate offspring solutions. A parent portion of 50% is chosen.

The crossover rate is the probability that two parent solutions will be combined to form child solutions. The crossover rate is set at 50%.

The mutation rate is the probability that a random change occurs within a candidate solution. Mutation enables the algorithm to explore new regions of the solution space. The mutation rate is set at 10%.

The optimality gap is the percentage difference between the best-known solution and the proven bound in mixed-integer programming. It is calculated as the absolute difference between their objective values, normalized by the proven bound. An optimality gap of 0.001% is chosen to ensure both Gurobi and the proposed mathematical method achieve near-optimal solutions within a reasonable time frame.

5.4.4 Proposed Method Vs. Genetic Algorithm

The proposed method is first benchmarked against the elitist genetic algorithm. The elitist genetic algorithm starts with a randomly generated population. Individuals in the population are evaluated for their objective cost. The top performers are selected as the elites and preserved to the next generation. The top portion of the population is chosen as the parents, and they are used in the cross-over and mutation process to generate offspring. The offspring are added to the old population to form a new population. Then, the process is repeated with the new population. After several iterations, the best solution is selected as the optimal.

5.4.4.1 Speed Benchmark

The speed benchmark against the elitist genetic algorithm is shown in Fig. 5.8. In the speed benchmark, the storage size cost coefficient is set to one, enabling the genetic algorithm to converge to similar solutions as the proposed method. Moreover, DC OPF and a mixed-integer linear storage model were used in the speed benchmark for faster calculation speeds.

The benchmark shows that the proposed method reached the optimal solution in 40 seconds, while the elitist genetic algorithm took 23 minutes to find a near-optimal solution. With larger population sizes, the genetic algorithm frequently

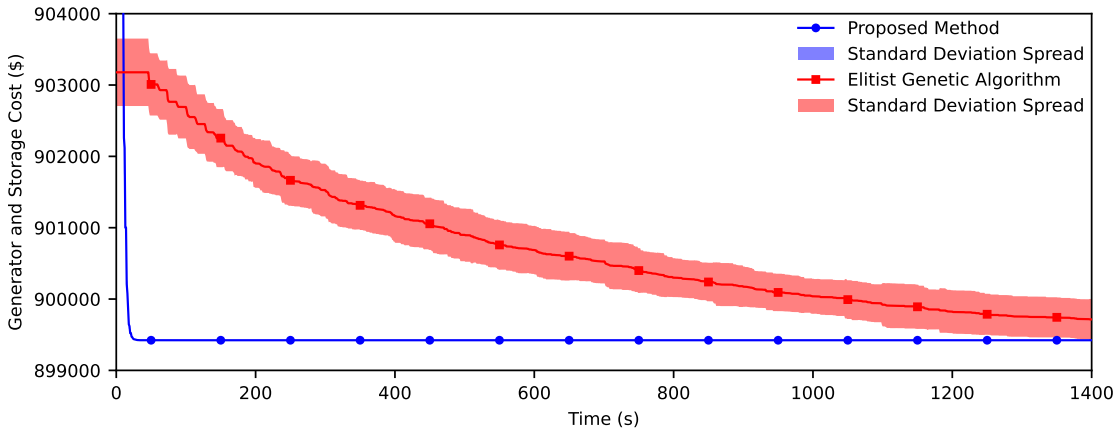

Figure 5.8: The speed benchmark between the proposed method and the elitist genetic algorithm. Solid lines depict the average objective cost over 30 runs, and shaded regions represent the standard deviation spread from the average. The proposed method minimized the objective cost within 40 seconds, while the elitist genetic algorithm achieved a similar objective cost after 23 minutes.

generates invalid storage configurations during crossover and mutation, leading to DC OPF convergence failures. Moreover, with low storage costs, the elitist genetic algorithm produces oversized storage with little utilization, essentially wasting the storage. In comparison, the proposed method optimizes from a technical perspective and consistently yields the smallest, fully utilized storage size that minimizes generator cost.

5.4.4.2 Optimality Benchmark

To demonstrate that the proposed method consistently yields the smallest storage size that minimizes generator costs, its solution is evaluated via offsetting, which is done by systematically adding or removing storage capacity at each bus. The generator cost objective function is used, and the results are shown in Fig. 5.9.

The results show that increasing storage capacity beyond the optimal design does not further reduce generator costs, while reducing it leads to higher costs. The generator cost is minimized using OPF, while the sizing method minimizes storage size by maximizing utilization and eliminating unused capacity. The proposed method maximizes storage utilization based on available generation and demand. Therefore, increasing storage capacity beyond the optimal design does not increase

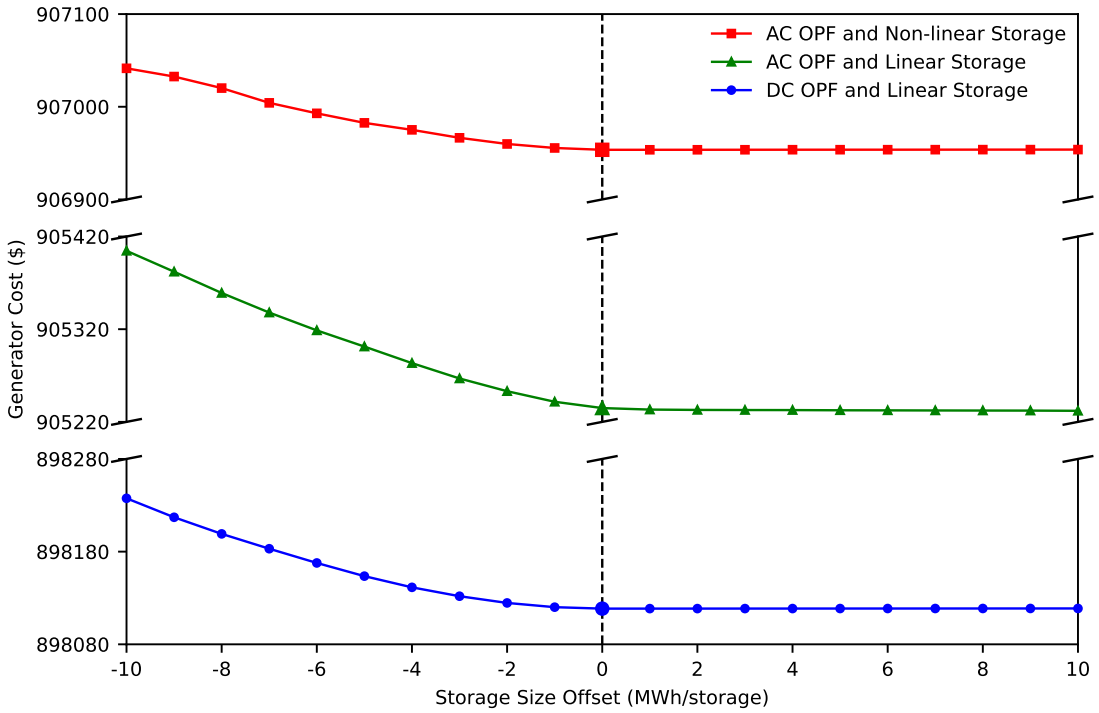

Figure 5.9: Storage size offset from the proposed method's solution. The offset shows that the proposed method's solution is optimal, as adding storage capacity to the solution does not further reduce generator cost, while removing storage capacity from the solution increases generator cost. Moreover, the proposed method can still yield optimal solution when coupled with non-linear and non-convex models.

utilization, as additional storage neither creates more surplus generation for charging, nor excess demand for discharging. Without increased utilization, increasing storage capacity beyond the optimal design does not further reduce generator costs.

The results confirm that the proposed method effectively determines the smallest total storage size that minimizes generator cost. This finding is consistent across all three combinations of models: DC OPF with a mixed-integer linear storage model, AC OPF with a mixed-integer linear storage model, and AC OPF with a mixed-integer non-linear storage model. Note that minimizing generator cost also maximizes renewable consumption when operating under a conventional operation strategy. The results also show that the proposed method achieves good convergence with non-convex models. Since both AC OPF and the storage model are non-convex, global optimality is not guaranteed due to potential local minima in their solution spaces. Nevertheless, AC OPF remains a valuable tool for power system analysis,

offering a more accurate representation of the power system. Similarly, more precise storage models are often non-linear and non-convex. Thus, the method's ability to handle non-convex models is valuable for accurate system modeling.

5.4.4.3 Storage Size and Placement

The storage size and placement determined using the proposed method with DC OPF and a mixed-integer linear storage model are shown in Fig. 5.10. The total storage size is 1303 MWh. The largest storage unit is placed on bus 15, which also hosts the largest load demand. In general, larger storage units are placed on

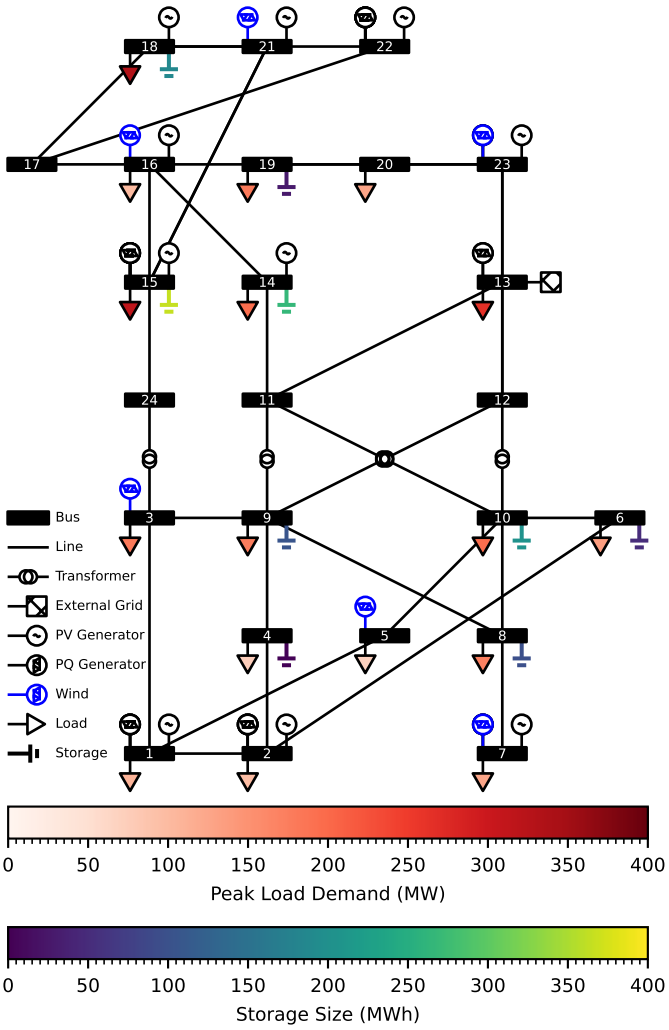

Figure 5.10: Storage size and placement determined using the proposed method with DC OPF and a mixed-integer linear storage model in the IEEE Reliability Test System. Larger storage units are placed on buses with high demand.

buses with larger demand. The only exception is bus 13, which has a large demand but no storage. This is because bus 13 also hosts the external grid, which directly supports the large demand. The relationship between demand and storage size is shown in the figure, where large storage size follows the high demand.

The storage size and placement determined using AC OPF with a mixed-integer linear storage model are shown in Fig. 5.11. The total storage size is 1208 MWh,

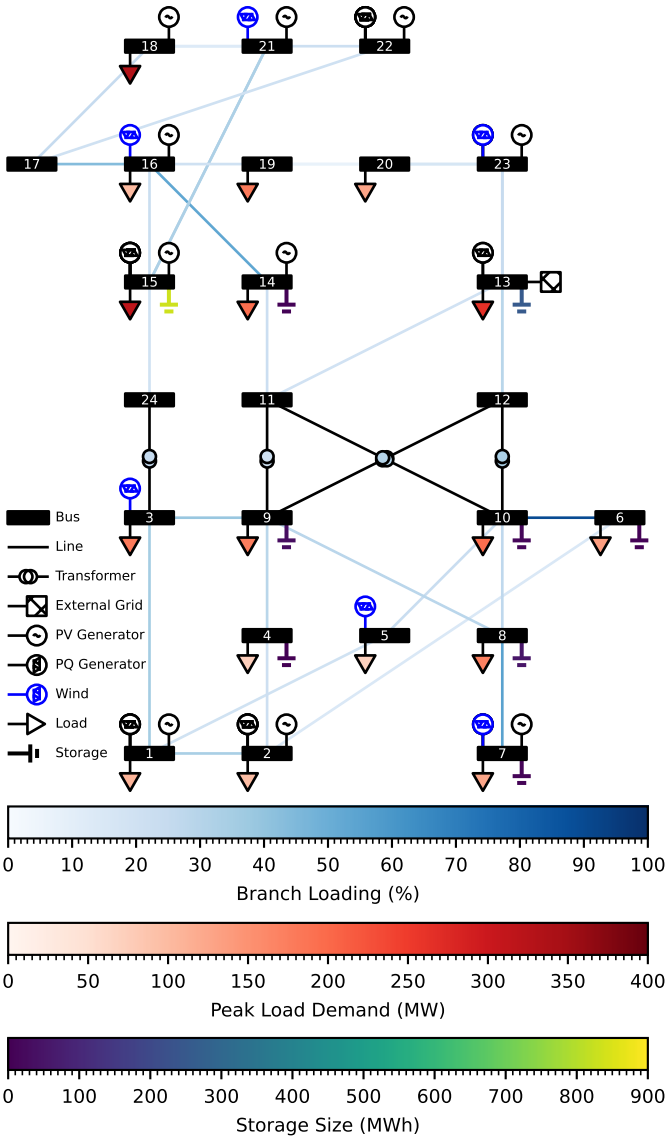

Figure 5.11: Storage size and placement determined using the proposed method with AC OPF and a mixed-integer linear storage model in the IEEE Reliability Test System. Larger storage units are placed on buses with both high generation and demand, while smaller storage units are placed near high-loading lines.

which is smaller than that of the DC OPF. The smaller storage size results from the fact that AC OPF accounts for network losses. Energy is lost when transferred through lines and transformers, which means less energy from generation can get to storage. Since less generation can charge the storage, the storage size requirement is also smaller. The largest storage unit is placed on buses 13 and 15, both of which

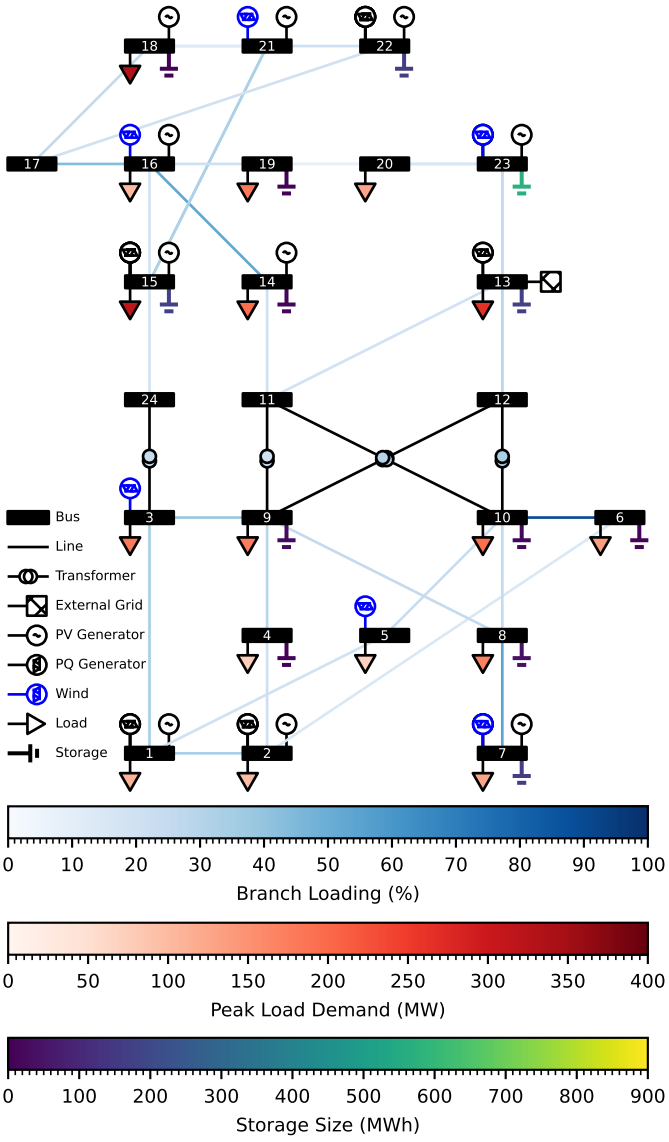

Figure 5.12: Storage size and placement determined using the proposed method with AC OPF and a mixed-integer non-linear storage model in the IEEE Reliability Test System. Larger storage units are placed on buses with high generation. Medium-sized storage units are placed on buses with both high demand and high generation, while smaller storage units are placed near high-loading lines.

have high generation and high demand. Generally, AC OPF places larger storage units to fewer buses when compared to DC OPF. Smaller storage units are placed near congested branches, such as the line between buses 6 and 10, the line between buses 7 and 8, the line connecting to bus 14, and the transformer connecting to bus 9. The relationship between the smaller storage unit placement and line loading is shown in the figure. Regardless of AC or DC OPF, a small storage is consistently placed on bus 4 to balance the demand and generation in that region.

The storage size and placement determined using AC OPF with a mixed-integer non-linear storage model are shown in Fig. 5.12. The total storage size is 1350 MWh, which is larger than that from the AC OPF with a linear storage model. This increase is due to the higher average storage efficiency of the non-linear storage model. Higher efficiency reduces energy losses during charging and discharging, allowing more energy to be stored. Thus, the storage size increases to accommodate the additional energy that can now be charged into the storage. The largest storage unit is placed on bus 23, which hosts the largest generation. This placement leverages the higher storage efficiency, enabling more generation to be charged into storage. Medium-sized storage units are placed on buses with both high demand and high generation, such as buses 13 and 15. Smaller storage units are placed near congested branches.

5.4.5 Proposed Mathematical Method Vs. Gurobi Optimization

The proposed method is benchmarked against Gurobi mathematical optimization. Gurobi currently cannot handle non-linear functions efficiently; therefore, DC OPF and a mixed-integer linear storage model are used. The problem formulation is mixed-integer quadratic programming. Moreover, the problem formulation means Gurobi cannot optimize the OPF and storage model separately. Instead, both OPF and storage model must be optimized together. This also implicitly constrains the optimization to optimize across the entire time horizon, instead of optimizing the OPF at each individual time step, like that of the proposed method. Thus, for the purpose of comparison, the proposed method is modified to use mixed-integer

quadratic programming for constructing the storage profile, while the rest of the method remains the same. This modification creates the proposed mathematical method, enabling it to optimize OPF along the entire time horizon, and making it comparable to Gurobi. Moreover, Gurobi requires storage cost in the objective function, or else it will yield an exceedingly large storage size to minimize generator cost. Thus, the generator and storage cost objective function is used for the speed benchmark, and the storage size cost coefficient is set to 0.01. This objective function enables Gurobi to produce solutions similar to those of the proposed mathematical method. Note that the proposed method does not require storage cost, and will always yield the smallest storage size that can minimize generator cost.

5.4.5.1 Speed Benchmark

The speed benchmark between the proposed mathematical method and Gurobi mathematical optimization is shown in Fig. 5.13. The benchmark shows that the proposed mathematical method achieved a similar objective cost as Gurobi optimization, but Gurobi optimization is faster. Moreover, both Gurobi and the proposed mathematical method achieved lower objective costs than the original proposed method. This is because mixed-integer quadratic programming optimizes

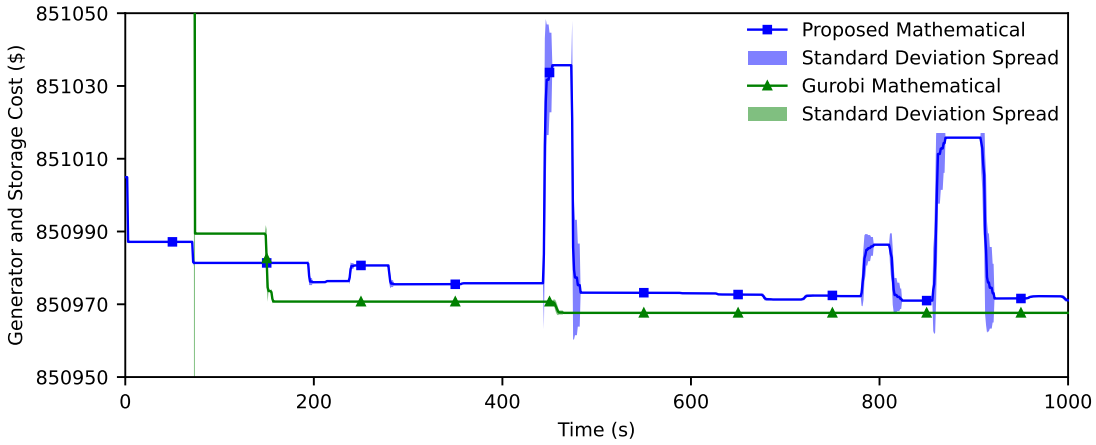

Figure 5.13: The speed benchmark between the proposed mathematical method and Gurobi mathematical optimization. Solid lines depict the average objective cost over 30 runs, and shaded regions represent the standard deviation spread from the average. The proposed mathematical method is slower but can achieve a similar objective cost as Gurobi mathematical optimization.

across the entire time horizon, which also implicitly optimizes the generator scheduling in addition to maximizing the renewable consumption. Generators are scheduled to charge the storage during times of low demand. Then, during times of high demand, storage discharges energy to support the load. The optimized generator scheduling further reduces objective cost, as the benchmark shows. However, mixed-integer programming is non-convex, which means it may yield near-optimal storage sizing and placement. This is evident in the speed benchmark, where the objective cost spikes as the proposed mathematical method attempts to escape a local optimum.

5.4.5.2 Optimality Benchmark

The proposed mathematical method does not need storage cost, as it always yields the smallest storage size that minimizes generator cost. The small storage size is achieved by maximizing storage utilization and eliminating wasted storage. To demonstrate this, the proposed mathematical method's solution is offset by adding or removing storage capacity. The offset storage capacities are fed into Gurobi to calculate the generator cost, and the results are shown in Fig. 5.14.

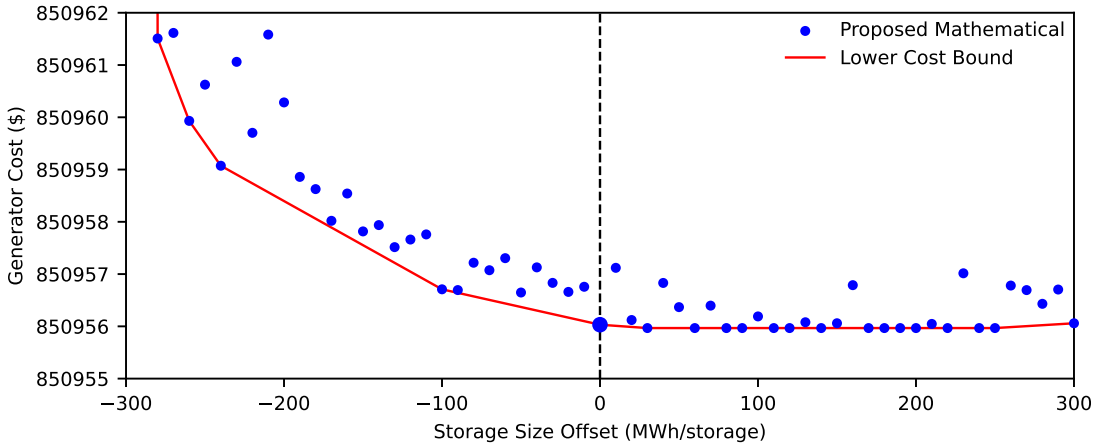

Figure 5.14: Storage size offset from the proposed mathematical method's solution. The offset shows that the proposed mathematical method's solution is near-optimal, as adding a small amount of storage capacity to the solution can reduce the generator cost. However, further additions of storage capacity do not further reduce generator cost, while removing storage capacity from the solution increases generator cost.

The result shows that the proposed mathematical method yields a near-optimal solution. As adding a small amount of storage capacity to the near-optimal solution can further reduce the generator cost. The near-optimality is caused by the mixed-integer programming, which cannot guarantee global optimality. Nevertheless, the trendline shows that adding more storage capacity does not further reduce generator cost, while removing storage capacity increases the generator cost.

5.4.5.3 Storage Size and Placement

The storage size and placement determined using the proposed mathematical method are shown in Fig. 5.15. The total storage size is 10973 MWh, which is much larger than that from the proposed method. The larger size is due to the mixed-integer quadratic programming problem formulation, which optimizes across the entire time horizon. This problem formulation implicitly optimizes generator scheduling in addition to maximizing renewable consumption. The generators are scheduled to charge the storage during low demand, and then the storage discharges that energy to support loads during high demand. The extra energy from generators causes the larger storage size requirement. The storage placement also differs from the proposed method. Larger storage is placed on more buses. This includes buses with cheaper generators, buses with high generation and high demand, and buses connecting to the transformers.

The benchmark demonstrates that the proposed method is faster than the elitist genetic algorithm, and can better handle non-convex models when compared to Gurobi mathematical optimization. The proposed mathematical method incorporates a mixed-integer quadratic programming problem formulation, allowing it to optimize across the entire time horizon and achieve a lower objective cost. In contrast, the proposed method avoids using mixed-integer programming, resulting in faster calculation speed and better convergence to the global optimal solution. Moreover, the proposed method does not require storage cost to optimize, and will always yield the smallest storage size that minimizes generator cost. Under a conventional operation strategy, minimizing generator cost also maximizes renewable

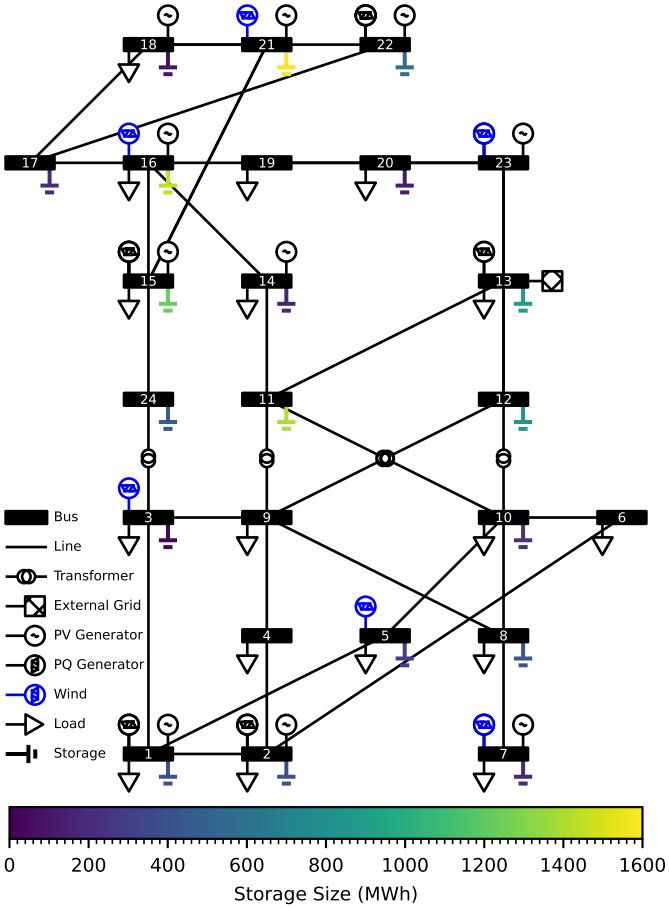

Figure 5.15: Storage size and placement determined using the proposed mathematical method with DC OPF and a mixed-integer linear storage model in the IEEE Reliability Test System. Larger storage units are placed on buses with high generation and demand, cheap generators, and near transformers.

consumption. The versatility of the proposed method extends to incorporating both AC OPF and DC OPF. When using DC OPF, the storage tends to be placed near large demand and large generation. AC OPF exhibits a similar tendency, but also places storage near congested lines or choke points with high power flow.

5.5 Case Study

The Salt Cross Garden Village is a planned carbon-neutral village north of Oxford. At the village's edge is a primary substation, connecting the village to the electricity transmission network. The substation consists of a transformer connecting the external and internal buses, which steps the voltage down from 110 kV to 10 kV.

The external bus connects to the external transmission grid and the wind turbines. The wind turbines are situated at the corner edges of the village. The internal bus connects to 16 distribution feeder lines, which connects the 500 prosumer buildings with roof-top solar PV generation. The village's electricity will be supplied by a mixture of wind, solar, battery, and energy from the external grid.

5.5.1 System Setup

The Garden Village's electricity system is modelled in Pandapower. The distance between the wind turbines and the substation is one kilometer, and the lines connecting them are modelled using "149-AL1/24-ST1A 110.0" lines in Pandapower [186]. The transformer in the substation is modelled using the "63 MVA 110/10 kV" transformer. The feeder lines connecting the substation to the prosumer buildings are modelled using "149-AL1/24-ST1A 10.0" lines. The distance between prosumer buildings along a feeder line is 50 meters, with 31 to 32 buildings on each feeder line. Each building and wind turbine is hosted by an electrical bus. Each bus is also a potential placement site for lithium battery storage. The lithium battery storage specifications are in Table 5.1. The lithium battery system is assumed to have a charge and a discharge efficiency of 90%, a recommended depth of discharge of 80%, a C-rating of 1C, and a leakage rate of 2% per month [118].

The case study's objective is to size and place storage to maximize renewable consumption within the village. The objective is achieved by setting the external grid cost function's quadratic cost coefficient to one, and zeroing other cost coefficients. The cost function puts an equal price on electricity import and export, which puts the village under a conventional operation strategy to encourage renewable consumption. The operation strategy will first use wind and solar generation to meet the demand. Once the demand is met, excess renewable generation is first charged into storage, while any remaining excess is exported to the external grid. When renewable generation is not enough to meet the demand, energy is discharged from storage to meet the demand. When storage does not have enough energy to discharge, the demand is met by electricity imported from the external grid.

5.5.2 Electricity Demand Model

Electricity demand data were obtained from real buildings in England, with 500 unique profiles selected and cleaned. Missing values shorter than one hour were interpolated using adjacent half-hourly averages, while longer gaps were filled with the average of the same hour from the preceding and following days. The half-hourly data were then aggregated to hourly resolution to align with the hourly renewable generation data, which were generated using Pfenninger and Staffell's method. Note that data resolutions below one hour have minimal impact on storage sizing accuracy [159].

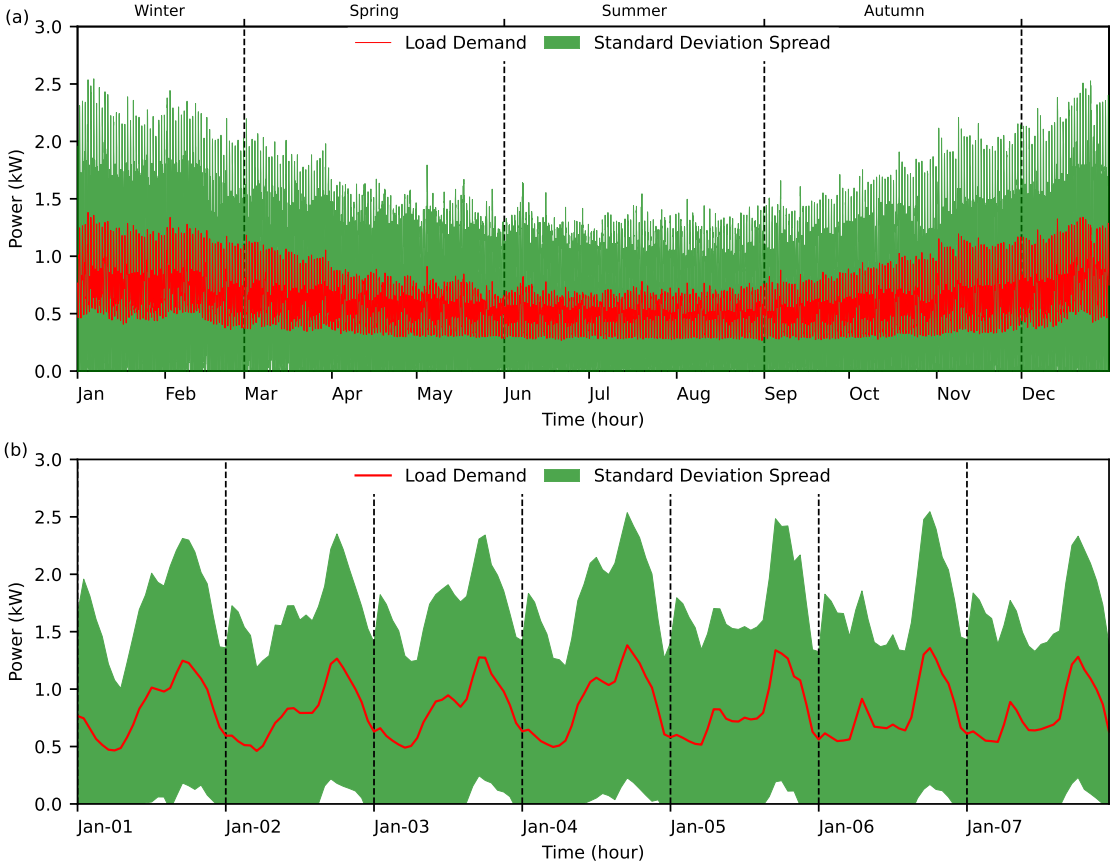

Figure 5.16: Hourly mean and standard deviation of the 500 load demand profiles are presented for (a) the entire year, and (b) the first week of the year. The solid line indicates the average hourly load demand among the 500 prosumer buildings, while the shaded region represents the standard deviation spread around the average.

The hourly mean and standard deviation of the 500 demand profiles are shown in Fig. 5.16. Demand is higher in winter due to heating requirements and lower in

summer due to shorter nighttime hours. Additionally, demand variation is greater during winter. The average annual electricity demand per building is 5.2 MWh.

5.5.3 Solar Generation Model

The rooftop solar PV generation data are modelled using Pfenninger and Staffell's method [79]. The solar PV locations are based on each building's location within the village. Panels are tilted at 60° and oriented between azimuth angles of 90° and 270°, facing east to west. A 10% efficiency loss is assumed due to the DC-to-AC inverter. Pfenninger and Staffell's method uses solar irradiance and temperature data from NASA's MERRA database. Temperature data are applied to Huld's efficiency curve [80], while irradiance is split into direct and diffuse components

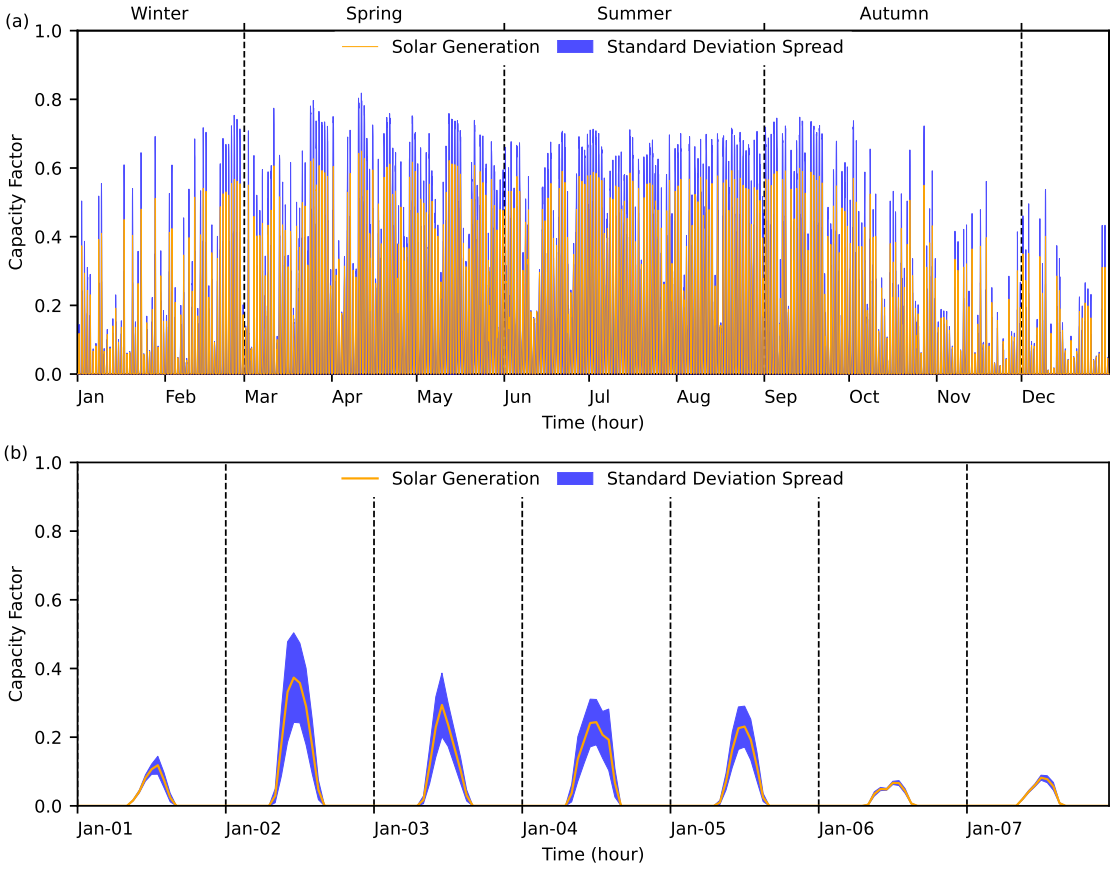

Figure 5.17: Hourly mean and standard deviation of the 500 solar PV generation profiles are presented for (a) the entire year, and (b) the first week of the year. The solid line indicates the average hourly solar generation, while the shaded region represents the standard deviation spread around the average.

using the Boland-Ridley-Lauret model [81]. These irradiance components are then scaled according to the solar panel tilt. Solar generation is calculated using system efficiency, panel efficiency, direct irradiance, and diffused irradiance.

The hourly solar generation capacity factors are shown in Fig. 5.17. Solar generation occurs during daylight hours, peaking at noon, and is higher in summer due to greater solar intensity and longer days. The standard deviation of solar generation is also larger in summer, as clouds and rain can significantly impact output.

5.5.4 Wind Generation Model

Wind generation is modelled using Staffell and Pfenninger's method [185]. The wind turbines, located at the corner edges of the village, are Siemens SWT-1.3-62 models

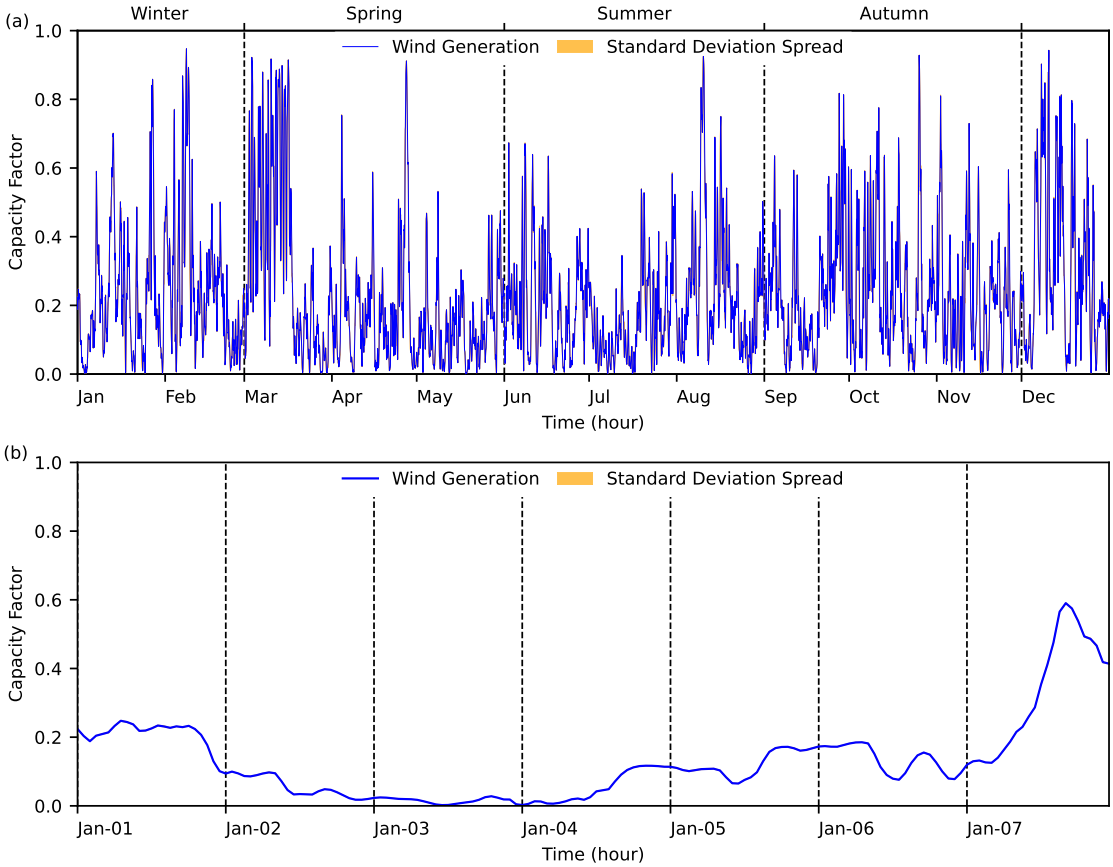

Figure 5.18: Hourly mean and standard deviation of the four wind generation profiles are presented for (a) the entire year, and (b) the first week of the year. The solid line indicates the average hourly wind generation, while the shaded region represents the standard deviation spread around the average.

with a rated capacity of 1.3 MW, a hub height of 49 meters, and a blade length of 30 meters. Wind speeds are sourced from NASA's MERRA database, interpolated to the turbine locations using Locally Weighted Scatterplot Smoothing Regression, and adjusted to the hub height using the logarithmic wind profile. Power generation is calculated from wind speeds using the manufacturer's power curve.

The hourly wind generation capacity factors are shown in Fig. 5.18. Wind generation is typically higher in winter and lower in summer, complementing solar generation. Together, wind and solar provide a more consistent energy supply.

5.5.5 Sensitivity Analysis

A sensitivity analysis is conducted by varying solar and wind generation. The goal is to examine how variations in generation affect total storage requirements and grid energy exchange. DC OPF and a mixed-integer linear storage model were used for the sensitivity analysis, as they have better optimum convergence. AC OPF was tested for the sensitivity analysis, but due to its non-convexity, the results were sub-optimal when the system lacked wind generation. These sub-optimal results did not fully utilize storage and sometimes preferred higher-cost energy from the external grid. The results from the sensitivity analysis are shown in Fig. 5.19.

The sensitivity analysis figure will be discussed from left to right, then top to bottom. The sensitivity analysis shows that without wind and solar generation, storage size is zero, as storage cannot charge due to a lack of renewable generation. Moreover, electricity import from the external grid is also the highest, as demand is met solely by electricity import. Increasing the solar capacity reduces grid electricity import and increases the storage size requirement, as now the storage can charge from surplus solar generation. At 7 kW of solar capacity per building, the generation is enough to support the entire village, and excess solar generation is exported to the external grid. The storage size is also the largest at this solar capacity because excess demand is still larger, which means more storage capacity is required to charge and discharge to meet the large excess demand. With just one wind turbine, the generation is still insufficient to fully support the village.

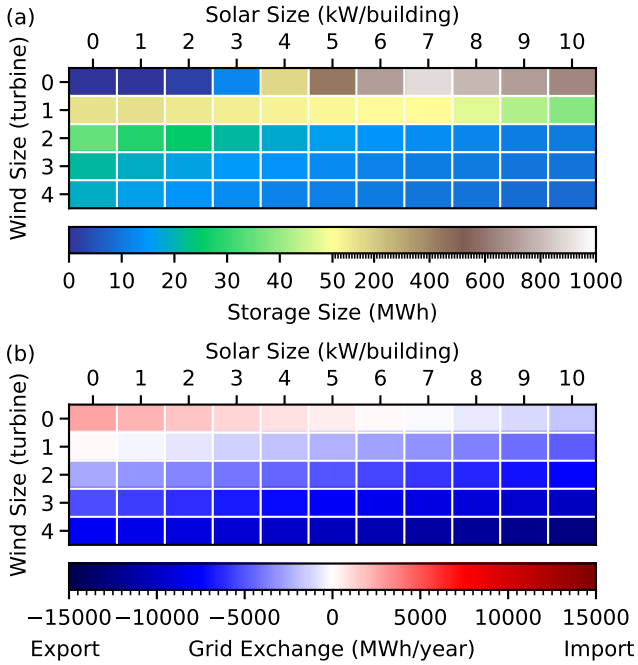

Figure 5.19: Sensitivity analysis using DC OPF with a mixed-integer linear storage model to examine the effects of solar and wind capacity variation on (a) total storage size, and (b) energy exchange with the external grid. The analysis demonstrates that increasing renewable capacity reduces storage size requirements and increases energy exports to the external grid.

Adding 1 kW of solar capacity per building will enable the combined generation to fully support the village and export surplus generation to the external grid. Similarly, when the renewable system is just enough to support the village, the storage requirement is large due to the large excess demand. With the addition of more solar capacity, the storage requirement reduces, as more excess demand is being directly met by renewable generation. Moreover, more renewable generation also means more surplus generation exported to the external grid. With two wind turbines, they can fully support the village. Additional solar capacity will reduce the storage requirement and increase electricity export. Likewise, three or more wind turbines can fully support the village, and each additional wind turbine will reduce storage requirements and increase electricity export. At max solar and wind capacities, the total storage requirement is still 8 MWh. This is because no matter how large the renewables are, there will always be a need for storage, as some calm nights have no wind or solar generation, and demand during those

times requires energy from storage [187].

Note that this case study assumes that the external grid regulates frequency, has no energy exchange limits, and the electrical system has been upgraded to accommodate reverse power flow. As a result, the study allows renewable penetration to exceed 100% of the annual demand. However, in large transmission systems, such as the Texas grid, the maximum feasible renewable penetration with energy storage is typically limited to 80% of the annual demand [188]. This limitation arises due to three key challenges. First, high renewable penetration can compromise grid stability, as solar and wind generation reduce system inertia, making the grid more susceptible to frequency deviations. Second, constraints on grid exchange can restrict the export of excess renewable energy, leading to curtailment of surplus generation. Third, increased renewable penetration can cause grid congestion and induce reverse power flows, necessitating transformer upgrades and additional reactive power support.

5.5.6 Storage Size and Placement Comparison

The renewable setup, consisting of two wind turbines and 4 kW of solar capacity per building, is further analyzed as it achieves a good balance between storage size requirements and the amount of electricity exported. The storage size and placement, determined using DC OPF, are shown in Fig. 5.20. The total storage capacity is 18 MWh, with the largest storage units located at bus 2 and bus 3, which host the wind turbines, each receiving 8 MWh of storage. The remaining 2 MWh of storage is distributed among the 500 prosumer buildings on buses 5 to 504, with individual storage sizes ranging from 2 to 12 kWh. Thus, the DC OPF results prioritize large storage units at the wind turbines and smaller storage units at the prosumer buildings.

DC OPF dispatches only active power, with the majority supplied by the wind turbines. Some of the wind power is delivered through the transformer, while surplus wind power is exported to the external grid. After passing through the transformer, the wind power is distributed via distribution lines to each building.

Figure 5.20: Storage size and placement determined using the proposed method with DC OPF in the carbon-neutral village. Larger storage units are placed on buses hosting wind turbines, while smaller storage units are placed on the 500 prosumer buildings with solar PVs.

At each building, solar generation directly meets a portion of the demand, while any surplus solar generation is either stored in batteries or exported to the external grid.

The storage size and placement determined using AC OPF are shown in Fig. 5.21. The total storage capacity is 21 MWh, which is larger than that from the DC OPF. This increase in size is due to losses in the lines and transformer, which require additional storage capacity to compensate for network losses. It is worth noting that

in the benchmark case, the total storage size decreased from DC OPF to AC OPF due to insufficient renewable generation to meet demand. In such cases, network losses effectively reduce the amount of generation that can be stored, resulting in a smaller storage requirement. In contrast, this case study benefits from a surplus of renewable generation, which not only supports demand but also allows surplus generation to be stored to offset network losses, thereby increasing the storage size.

Figure 5.21: Storage size and placement determined using the proposed method with AC OPF in the carbon-neutral village. Larger storage units are placed on choke point buses before and after the transformer, as well as on buses hosting wind turbines. Smaller storage units are placed on prosumer buildings with a larger difference between generation and demand.

The largest storage unit, with a capacity of 8.4 MWh, is placed at bus 4, which acts as a choke point connecting the village to the substation. The wind turbines at buses 2 and 3 are equipped with storage capacities of 4.4 MWh and 5 MWh, respectively. Bus 1, which hosts the external grid connection and additional wind turbine connections, is assigned 2.7 MWh of storage. Smaller storage units, ranging from 1 to 5 kWh, are distributed among few buses with buildings that exhibit significant differences between solar generation and load demand, requiring storage to maintain balance.

Compared to DC OPF, the results from AC OPF show that larger storage units are placed on fewer buses. This is because AC OPF accounts for network losses, voltage constraints, and reactive power, prioritizing storage sizing and placement to minimize system losses and maintain voltage stability. In contrast, DC OPF simplifies power flow by ignoring reactive power and assuming negligible system losses, leading to the distribution of smaller storage units across more buses to balance active power locally, without considering voltage or loss impacts. This simplification improves computational efficiency and convergence at the cost of model accuracy.

5.5.7 Largest Storage Profiles

The AC OPF dispatches both active and reactive power, with most power coming from wind turbines. As active wind power passes through the line to bus 1, some of it is converted to reactive power due to the line's reactance. At bus 1, most wind power is sent to the transformer, while surplus power is exported to the external grid. From the transformer, both active and reactive wind power are distributed through the distribution lines. Active power is consumed at each building to meet demand, while reactive power is gradually consumed by the distribution lines. At each building, solar generation directly supports some of the demand, while surplus solar generation is charged into storage or exported to the external grid.

The storage profiles of the four largest storage units, along with the total solar PV generation profile, are shown in Fig. 5.22. The storage units are dispatched

in similar patterns, with higher and more frequent charges and discharges during winter. This is due to lower solar generation and higher demand in winter, making the system more susceptible to variability in wind generation and demand. These variabilities necessitate higher and more frequent power dispatch from storage to balance generation and demand. Whereas in the summer, increased solar generation combined with wind generation provides a more consistent output, and the demand is also smaller, which means more demand is being directly met by renewable generation. Thus, storage charge and discharge activities are reduced in summer.

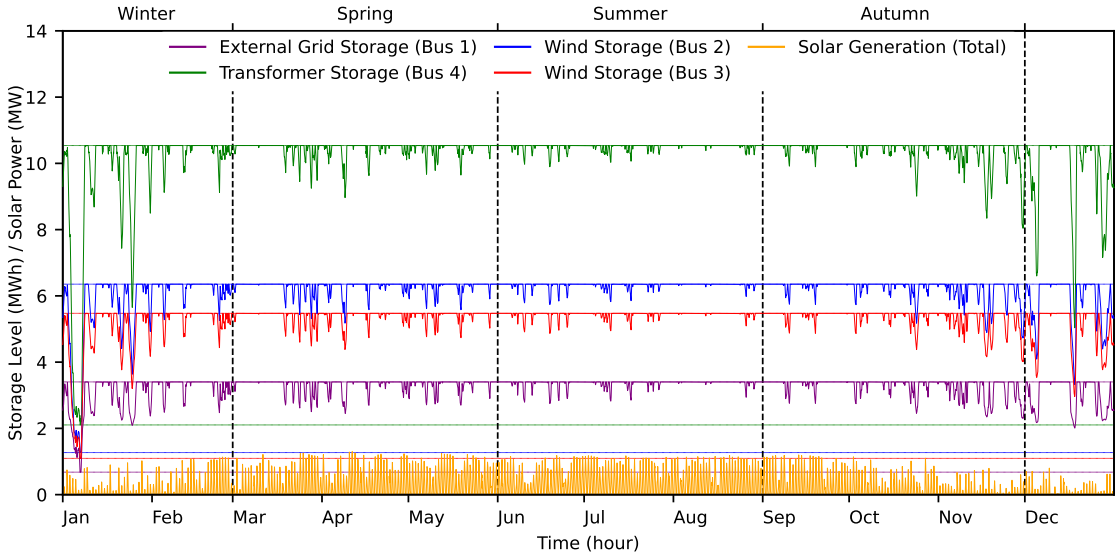

Figure 5.22: Storage profiles for the four largest storage unit, and the total solar PV generation profile. The storage units are dispatched in similar patterns, with larger charges and discharges occurring during winter. This is attributed to lower solar generation and higher load demand during winter, making the system more susceptible to the variability in wind generation and load demand.

The case study shows that when renewable generation is just enough to support the system, the storage size requirement is at its highest. Additional generation can reduce the storage requirement, but only up to a certain extent. This is because storage remains necessary to support demand during calm nights with no solar or wind generation. The storage sizing and placement comparison shows that DC OPF tends to place larger storage units near large generation. AC OPF exhibits a similar tendency, but also places large storage units near choke points with high power flow. Moreover, if the generation can support the system, AC OPF will

have a larger storage requirement than DC OPF, as additional energy is stored to compensate for network loss. Conversely, if the generation cannot support the system, AC OPF will yield a smaller storage requirement than DC OPF. This is because the limited generation is further reduced by network loss, resulting in less energy available to charge the storage. The storage profiles show that large storage units are dispatched in similar patterns. Significant charge and discharge activities occur during winter when solar generation is low, and demand is high, making the system more susceptible to variability in wind generation and load demand.

5.6 Summary

The chapter presents a novel analytical method for storage sizing and placement. The objective of the proposed method is to maximize the utilization of storage energy while eliminating unused storage capacity, and in most scenarios, this objective also yields the smallest storage size that minimizes generator cost. The proposed method is faster than meta-heuristic methods, can better handle non-convex models compared to mathematical optimization methods, and exhibits effective convergence to optimal sizing and placement. The proposed method first employs optimal power flow to optimize storage power dispatch. Then, storage profiles are constructed based on the storage dispatch. Subsequently, storage sizing and placement are calculated from these profiles. The proposed method can be applied to all types of storage profiles, while accounting for storage energy limits, power limits, and energy leakage. Moreover, the sized storage will have equal starting and ending storage levels, ensuring the sizing's validity for future time horizons. Major contributions made in this chapter are the following:

- The proposed method yields the optimal storage size and placement. The optimum is defined as the smallest total storage size that minimizes generator cost. The small storage size is achieved by maximizing storage utilization and eliminating wasted storage.

- The proposed method is faster than meta-heuristic methods, can more effectively handle non-convex models when compared to mathematical optimization methods, and exhibits effective convergence to optimal sizing and placement.
- The proposed method is a technical approach that operates independently of storage costs, which differs from other methods that rely on potentially inaccurate storage cost estimates, thus eliminating a significant source of error in sizing and placement.

The method is benchmarked against meta-heuristic and mathematical optimization methods using a modified IEEE Reliability Test System. Then, the method is applied to a case study on a carbon-neutral village. Major findings from the benchmark and case study are summarized as follows:

- The proposed method yields the smallest storage size that minimizes generator cost. Under a conventional operation strategy, minimizing generator cost also maximizes renewable consumption.
- DC OPF tends to place storage near large demand and generation. AC OPF is similar, but also places storage near congested lines or choke points with high power flow.
- If the generation can support the system, AC OPF requires more storage than DC OPF, as additional energy is stored to compensate for the additional network loss. If generation cannot support the system, AC OPF needs less storage than DC OPF, as the limited generation is further reduced by network losses, limiting the energy available to charge the storage.
- When the generation is just enough to support the system, the storage requirement is the highest due to large excess demand. Additional generation can reduce the storage requirement, but only to a certain extent. This is because storage remains necessary to support demand during calm nights with no solar or wind generation.

- Significant charge and discharge from storage occur during winter, when solar generation is low and demand is high, rendering the system more susceptible to variability in wind generation and load demand.

There are three major areas where the current storage sizing and placement method can be improved and extended for future work. First, the problem formulation of the proposed mathematical method can be convexified to guarantee global optimality and improve calculation speed. Second, the proposed method should be applied to power market case studies, such as sizing and placing storage with the objective of minimizing marginal congestion costs and marginal loss costs. Third, alternative operation strategies should be explored, which could enhance battery lifespan, improve power output, and increase profit margins. The limitations and potential future work will be further discussed in the next chapter.

6 Conclusion

Contents

6.1 Introduction

This chapter summarizes the work presented in the thesis, and explains how they fit together to contribute to the main theme. Moreover, the chapter discusses potential areas for improvement and extension in future work.

6.2 Summary

The main purpose of this study is to gain a better understanding of storage design in the context of hybrid renewable systems. This is achieved by exploring storage sizing, storage and solar sizing, and storage sizing and placement, as shown in Fig. 6.1.

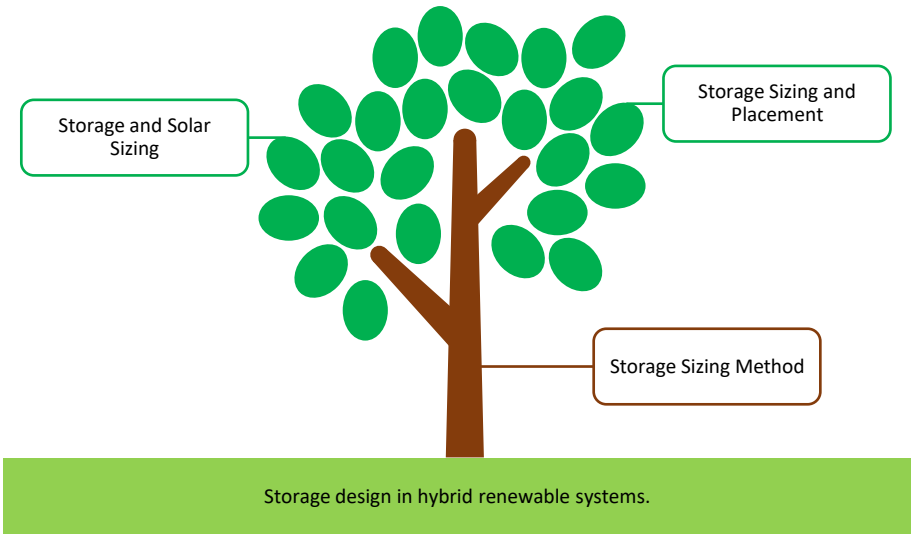

Figure 6.1: Thesis research theme and structure.

The motivation for this research is to gain a better understanding of storage design within the context of hybrid renewable systems. A major component of storage design is sizing, which ensures the proper functioning of energy storage to help mitigate renewable intermittency and non-dispatchability.

In the figure, the tree trunk symbolizes the storage sizing method, serving as the foundation from which subsequent research branches out. This method determines the optimal storage size by considering the largest cumulative charge or discharge that the storage can experience, thereby maximizing storage utilization. A key finding from the research is that increasing storage size results in diminishing returns

in terms of additional energy provided to the system. These diminishing return thresholds are defined by the largest daily storage size and the annual storage size.

A leaf sprouting from the tree represents the storage and solar sizing method. This method utilizes the storage sizing method to define the size search space. It then systematically iterates through the search space to find the optimal storage and solar sizing with the lowest cost. A key finding from the study is that solar and battery storage will make up a greater portion of the energy system as their costs come down. However, there will always be a need for the electricity grid, as it provides flexibility at a competitive cost.

Another leaf represents the storage sizing and placement method. This approach employs optimal power flow to determine power dispatch. Subsequently, the sizing method is used to determine the storage size and placement based on the power dispatch. A key finding from the study is that storage tends to be placed near sites with high generation, high demand, or near lines with high power loading.

6.2.1 Storage Sizing

Chapter 3 introduced a novel analytical method for sizing energy storage. This method draws inspiration from existing methods that size storage based on the storage profile. However, these existing methods have limitations. Some may fail when dealing with erratic storage profiles, while others do not produce optimal sizing. Many analytical methods are tailored exclusively for energy systems with over-generation, making them unsuitable for other systems. Additionally, most methods overlook storage energy leakage, which impacts the accuracy of long-term storage sizing. Some methods do not account for storage power limits, resulting in designs with unrealistic power requirements. Furthermore, some methods do not require equal starting and ending storage levels, rendering the storage profile non-repeatable for future design time horizons. This lack of repeatability implies that the storage size is valid only for the current design time horizon and not for future time horizons. The proposed analytical method for storage sizing addresses these issues.

The method sizes storage based on the theory that when storage charges more than it discharges over the design time horizon, storage should be sized according to the limiting factor, which is the largest cumulative discharge. Conversely, when storage discharges more than it charges over the design time horizon, storage should be sized according to the largest cumulative charge. This method yields the optimal storage size that maximizes storage utilization while eliminating unutilized storage capacity. The optimally sized storage does not have wasted capacity due to over-sizing nor cause energy deficits due to under-sizing.

The method was applied to two solar-battery case studies controlled using a conventional operation strategy and physically located in the northern temperate climate zone. The studies found that when the system operates under a conventional operation strategy, maximizing storage utilization also maximizes renewable consumption. Moreover, high demand and generation require larger storage, while low demand or low generation requires smaller storage. For these reasons, peak summer and peak winter require smaller storage, while early summer and early autumn require larger storage. Increasing storage size exhibits diminishing returns in the additional storage energy provided to the system. The diminishing return thresholds are defined by the largest daily design and the annual design.

6.2.2 Storage and Solar Sizing

Chapter 4 integrated the sizing method with an enumerative approach to conduct techno-economic storage and solar sizing. The new method takes advantage of the diminishing return thresholds of storage to define the search space for the enumerative approach. The storage sizing method determines the maximum storage size within a given design time horizon. For the design time horizon of one year, the maximum storage size is the annual storage size. At this size, all available energy that can be stored within a given year is accommodated by the annual storage size. Further expansion of storage size does not result in the storage providing more energy to the system.

The method employs analytical methods to calculate the maximum solar and storage sizes, defining a bounded search space. This bounded search space guarantees optimal sizing while reducing the number of search iterations. The enumerative approach is then utilized to systematically iterate through the size search space. At each iteration, the system is simulated to determine the system cost. The optimal sizing is selected based on the lowest-cost system.

The method was applied to a grid-connected solar-battery case study operating under a conventional operation strategy. The study explored the design space of system sizes that can meet the demand. The design space has three dimensions: solar size, storage size, and grid electricity import. A transition region, defined by the largest daily storage size, lies in the middle of the design space. On one side of the transition, increasing daily storage size reduces grid electricity import at a high pace. On the other side, increasing seasonal storage size reduces grid electricity import at a much slower pace due to diminishing returns. At the front edge of the design space, increasing solar size also increases maximum storage size, due to more surplus generation that can charge storage. Once solar size is sufficient to support the system without grid electricity import, maximum storage size also peaks due to excess demand. Beyond this point, increasing solar size reduces maximum storage size. This reduction eventually stops, as solar lacks nighttime generation, necessitating storage to support nighttime demand. At the back edge of the design space, grid electricity import is the highest without solar and storage, as the demand entirely relies on the grid. Increasing solar size without storage will reduce grid electricity import. However, the reduction will eventually stop, as solar lacks nighttime generation, necessitating the electricity grid to support nighttime demand.

The lowest-cost system is selected from the design space, and this process is repeated with future cost projections for solar and storage. The study found that solar and storage will make up a greater portion of the hybrid renewable system as their costs come down. However, grid electricity is always needed, as it provides flexibility at a competitive price. The increase in solar and storage size

will eventually slow down, as some demand, such as nighttime winter demand, is too expensive to be met by solar and storage alone.

6.2.3 Storage Sizing and Placement

Chapter 5 integrated the sizing method with optimal power flow to determine the size and placement of storage. The method utilizes optimal power flow to determine the storage power dispatch, after which the sizing method is applied to determine the storage size at each location based on the dispatch.

The proposed method first utilizes optimal power flow to optimize storage power dispatch. Subsequently, storage profiles are constructed based on the storage dispatch. The method then calculates the optimal storage sizing and placement using these profiles. The optimum is defined as the smallest total storage size that minimizes generator cost, achieved by maximizing storage utilization. This proposed method represents a technical approach that operates without requiring storage costs. This is in contrast to other methods, where inaccuracies in storage cost estimates can lead to errors in storage sizing and placement.

The method is benchmarked and applied to a case study on a carbon-neutral village with solar and wind generation. The study compares storage sizing and placement using AC optimal power flow and DC optimal power flow. The findings indicate that DC optimal power flow tends to place storage near areas with high demand and generation, while AC optimal power flow also places storage near congested lines or choke points with high power flow. Moreover, if generation can support the system, AC optimal power flow requires more storage, as additional energy is stored to compensate for increased network loss. However, if generation cannot support the system, AC optimal power flow requires less storage, as the limited generation is further reduced by network losses, limiting the energy available to charge the storage. The study also examined storage power dispatch and found significant charging and discharging occur during winter, when solar generation is low and demand is high. This makes the system more susceptible to variability in wind generation and load demand. The method serves as a decision support

tool for energy system planners, aiding in optimal storage sizing and placement given known generation and demand.

6.3 Discussion

The proposed analytical method sizes energy storage based on the largest cumulative charge or discharge that the storage can experience. The method optimally sizes storage with the objective of maximizing energy utilization while eliminating unused storage capacity. In most scenarios, reducing wasted capacity results in a smaller storage size, while maximizing storage utilization increases the energy output of the storage. Consequently, in most scenarios, the proposed method also yields the smallest storage size that maximizes the storage energy provided to the system. This finding also holds true for sizing and placing storage, where the optimal sizing and placement yield the smallest total storage size that maximizes the storage energy delivered to the system, ultimately minimizing generator costs. Moreover, at the optimal storage size, all available energy that can be stored is utilized, as storage energy utilization is maximized. Adding storage capacity beyond the optimal size does not increase energy output, as it neither generates additional surplus energy to charge the storage nor creates more excess demand that requires energy from storage discharge. Therefore, the optimal storage size can also be considered as the maximum storage size, since any additional capacity beyond this point does not provide more storage energy to the system. Leveraging this property, the proposed method is used to calculate the maximum storage size, which defines the search range for sizing. An enumerative approach is then applied to exhaustively search through this range to identify the lowest-cost system size.

The proposed method addresses several limitations in the current landscape of analytical methods for energy storage design. First, some analytical methods may not work with erratic storage profiles, and many existing methods are tailored to energy systems with over-generation and increasing storage profiles, making them unsuitable for other types of storage profiles. The proposed method resolves this issue, as it can be applied to all types of storage profiles, including increasing,

decreasing, and stable profiles that are neither increasing nor decreasing. The broad applicability of the proposed method stems from its sizing principle, which focuses on the largest cumulative charge or discharge that the storage can experience, represented by the largest increase or decrease in the storage profile. Second, some analytical methods do not account for storage energy leakage, which can affect the accuracy of long-term storage sizing. The proposed method accounts for energy leakage by iteratively extending the original sizing method. When applied to a case study, the method found that energy leakage impacts long-term storage sizing and can lead to energy deficits in the system. Third, some methods do not consider storage power limits, resulting in storage designs with unrealistic power requirements. The proposed method takes power limits into account by relating them to the storage energy capacity through the C-rating. Storage profiles are constructed under these power limit constraints, ensuring that the resulting storage design can operate within realistic power requirements. Lastly, several analytical methods do not require equal starting and ending storage levels, compromising the repeatability of storage profiles for future time horizons. As a result, the storage size determined by these methods may only be valid for the current design time horizon, but not for future time horizons. The proposed method introduces equal starting and ending storage levels as a stopping criterion for the iterative process. Consequently, the constrained storage profile from the proposed method will always have equal starting and ending storage levels, ensuring the sizing's validity for future time horizons.

The proposed method is benchmarked against other methods, including the enumerative method, meta-heuristic methods such as particle swarm and genetic algorithms, and mathematical optimization methods such as linear, quadratic, and mixed-integer programming. The enumerative method is simple to implement, as it relies on an exhaustive search to navigate the solution space and find the optimal solution. It is also flexible, allowing for the incorporation of complex models, such as non-convex storage and cost models. However, compared to the proposed method, the enumerative method is slow and computationally intensive, making it unsuitable for complex solution spaces, such as those encountered in

storage sizing and placement. Additionally, the enumerative method cannot find optimal solutions beyond the defined search range.

Meta-heuristic methods use algorithms to intelligently explore the solution space through a balance of exploration and exploitation, enabling them to explore complex solution spaces in a timely manner. These methods, which rely on trial and error, are flexible and can easily incorporate complex non-convex models. However, the proposed method can converge to a global optimal solution, while most meta-heuristic methods cannot guarantee a global optimum due to their stochastic nature. Moreover, some meta-heuristic methods also cannot locate optimal solutions beyond the defined search range.

In contrast, mathematical optimization methods use solvers to solve a system of objective and constraint equations representing the storage design problem. These methods are fast and can guarantee a global optimal solution, provided the model is convex. However, the proposed method can handle non-linear and non-convex models without requiring approximation, while most mathematical optimization methods cannot achieve this without approximation. Additionally, these optimization algorithms are often presented in a black-box manner, making it difficult to explain the results.

The proposed analytical method offers a balance of strengths. It is faster than both meta-heuristic and enumerative methods and can handle non-convex models without the need for approximation. When applied to convex models, the analytical approach converges to the global optimal solution. With non-convex models, it can converge to a near-optimal solution. Most importantly, the analytical approach is explainable, as the storage is sized based on the largest cumulative charge or discharge that the storage can experience.

6.4 Future Work

This section suggests potential extensions and improvements for each work in this thesis. Recommendations encompass algorithm enhancements, method extensions, and case study expansions.

6.4.1 Storage Sizing

Three limitations were identified during the testing of the storage sizing method, and they can be addressed in future work.

The first limitation is that with a large number of critical points in the storage profile, the difference matrix is also large, which slows down the method [189]. Data pre-processing can reduce the number of critical points. For example, signal processing algorithms that filter noise can effectively reduce the number of critical points in the storage profile, while preserving the necessary points for sizing [190]. Thus, future research should look into data pre-processing techniques to speed up the method.

The second limitation is that in scenarios with large leakage and small C-ratings, the method may not yield the storage size that maximizes renewable consumption, as it requires storage wastage. However, the method will yield the closest storage size without wasted capacity. Thus, a potential strategy is to use the proposed method's result as a starting point. Then, use meta-heuristic algorithms, such as particle swarm, to search the nearby region for the storage size that maximizes renewable consumption [191].

The third limitation is that renewable intermittency can stress the lithium battery, causing the battery's useful life to be shorter than that specified by the manufacturer. Battery degradation is affected by usage, time, temperature, depth of discharge, charge and discharge rates, voltage, and state of charge [192]. The proposed storage sizing algorithm can handle non-linear models. Thus, future research should consider adopting more accurate and complex lithium battery degradation models with the proposed algorithm, and compare the effects of different degradation models on storage sizing [193]. Moreover, the method can also be expanded to incorporate more complex models for storage efficiency, leakage, energy limits, and power limits.

6.4.2 Storage and Solar Sizing

The storage and solar sizing method can be extended in three major areas in future work.

Firstly, the method can be extended to incorporate wind turbine sizing alongside solar PV and battery storage sizing [194]. The extended method could be applied to a grid-connected solar-wind-battery microgrid system to explore the interrelationships between the sizing of the components. Moreover, the study should investigate the design space of independent solar-wind-battery microgrid systems, as well as grid-connected wind-battery and solar-battery systems.

Secondly, the method can be expanded by incorporating probabilistic methods, such as Monte Carlo simulation. This addition would enable the method to account for uncertainties in renewable generation and electricity demand [195]. The study can leverage probabilistic distributions to generate randomized profiles for solar generation, wind generation, and electricity demand. These profiles can then be used to size battery storage and obtain the distribution characteristics for storage size.

Thirdly, the method should be extended to consider future projections of electricity prices. Historical data on electricity prices can be utilized in machine learning methods, such as recurrent neural networks, to predict future electricity prices [196]. The predicted electricity prices can then be incorporated into the method when studying the future composition of the hybrid renewable system.

6.4.3 Storage Sizing and Placement

There are three major areas where the current storage sizing and placement method can be improved and extended in future work.

Firstly, the proposed mathematical method used in the benchmark yields near-optimal solutions due to the mixed-integer problem formulation. The presence of integer decision variables renders the problem formulation non-convex, which results in near-optimal solutions [197]. A convex problem formulation can guarantee a global optimum and has faster solving speed. Future research should explore methods to convexify the storage sizing and placement problem formulation.

Secondly, the case studies showed that optimal storage sizing and placement reduced generator costs, which also reduced system losses. Moreover, storage units are placed near congested lines with high loading to alleviate congestion. Power markets define regional electricity costs as locational marginal pricing, consisting of marginal energy cost, marginal congestion cost, and marginal loss cost [198]. Energy storage helps reduce power shortages, which alleviates congestion and lowers marginal congestion costs near congested lines [199]. Additionally, energy storage can reduce system losses, thereby reducing marginal loss costs. Future research should utilize the proposed method to lower marginal congestion costs and marginal loss costs in the power market.

Thirdly, this chapter has explored system operation using a conventional operation strategy, where renewable energy consumption is prioritized. In the benchmark, the proposed mathematical method demonstrated that alternative operation strategies could lead to a lower objective cost. Other operation strategies are also available to enhance battery lifespan, improve power output, and maximize profit. Future research should further investigate various operation strategies and their impact on storage sizing and placement [200].

References

[1] Valérie Masson-Delmotte et al. "Climate change 2021: the physical science basis". In: *Contribution of working group I to the sixth assessment report of the intergovernmental panel on climate change* 2.1 (2021), p. 2391.

[2] UNFCCC. *Adoption of the Paris Agreement*. Legal Rule or Regulation. 2015. URL: https://unfccc.int/sites/default/files/english_paris_agreement.pdf.

[3] Hannah Ritchie. "Sector by sector: where do global greenhouse gas emissions come from?" In: *Our World in Data* (2020). https://ourworldindata.org/ghg-emissions-by-sector.

[4] Michaja Pehl et al. "Understanding future emissions from low-carbon power systems by integration of life-cycle assessment and integrated energy modelling". In: *Nature Energy* 2.12 (2017), pp. 939–945.

[5] IEA. *World Energy Outlook 2020*. Report. International Energy Agency, 2020.

[6] Wei Feng et al. "A review of microgrid development in the United States–A decade of progress on policies, demonstrations, controls, and software tools". In: *Applied energy* 228 (2018), pp. 1656–1668.

[7] Lori Bird, Michael Milligan, and Debra Lew. *Integrating variable renewable energy: Challenges and solutions*. Tech. rep. National Renewable Energy Lab.(NREL), Golden, CO (United States), 2013.

[8] Mohammed Yekini Suberu, Mohd Wazir Mustafa, and Nouruddeen Bashir. "Energy storage systems for renewable energy power sector integration and mitigation of intermittency". In: *Renewable and Sustainable Energy Reviews* 35 (2014), pp. 499–514.

[9] John P Barton and David G Infield. "Energy storage and its use with intermittent renewable energy". In: *IEEE transactions on energy conversion* 19.2 (2004), pp. 441–448.

[10] Kang Miao Tan et al. "Empowering smart grid: A comprehensive review of energy storage technology and application with renewable energy integration". In: *Journal of Energy Storage* 39 (2021), p. 102591.

[11] Yuqing Yang et al. "Battery energy storage system size determination in renewable energy systems: A review". In: *Renewable and Sustainable Energy Reviews* 91 (2018), pp. 109–125.

[12] M. A. Hannan et al. "Review of optimal methods and algorithms for sizing energy storage systems to achieve decarbonization in microgrid applications". In: *Renewable and Sustainable Energy Reviews* 131 (2020).

[13] Choton K. Das et al. "Overview of energy storage systems in distribution networks: Placement, sizing, operation, and power quality". In: *Renewable and Sustainable Energy Reviews* 91 (2018), pp. 1205–1230.

[14] Bo Yang et al. "Optimal sizing and placement of energy storage system in power grids: A state-of-the-art one-stop handbook". In: *Journal of Energy Storage* 32 (2020), p. 101814.

[15] Han Kun Ren. *Thesis Code*. 2024. URL: `https://github.com/hankunren/thesis.git`.

[16] Edward Hughes et al. *Hughes electrical and electronic technology*. Pearson education, 2008.

[17] Anthony J Pansini. *Electrical distribution engineering*. River Publishers, 2020.

[18] Philip J Heptonstall and Robert JK Gross. "A systematic review of the costs and impacts of integrating variable renewables into power grids". In: *nature energy* 6.1 (2021), pp. 72–83.

[19] Lubna Mariam, Malabika Basu, and Michael F Conlon. "Microgrid: Architecture, policy and future trends". In: *Renewable and Sustainable Energy Reviews* 64 (2016), pp. 477–489.

[20] Samir M Dawoud, Xiangning Lin, and Merfat I Okba. "Hybrid renewable microgrid optimization techniques: A review". In: *Renewable and Sustainable Energy Reviews* 82 (2018), pp. 2039–2052.

[21] A Hina Fathima and K Palanisamy. "Optimization in microgrids with hybrid energy systems–A review". In: *Renewable and Sustainable Energy Reviews* 45 (2015), pp. 431–446.

[22] Kamal Anoune et al. "Sizing methods and optimization techniques for PV-wind based hybrid renewable energy system: A review". In: *Renewable and Sustainable Energy Reviews* 93 (2018), pp. 652–673.

[23] Xuesong Zhou, Tie Guo, and Youjie Ma. "An overview on microgrid technology". In: *2015 IEEE international conference on mechatronics and automation (ICMA)*. IEEE. 2015, pp. 76–81.

[24] KS Rajesh et al. "A review on control of ac microgrid". In: *Renewable and sustainable energy reviews* 71 (2017), pp. 814–819.

[25] Leong Kit Gan, Jonathan KH Shek, and Markus A Mueller. "Hybrid wind–photovoltaic–diesel–battery system sizing tool development using empirical approach, life-cycle cost and performance analysis: A case study in Scotland". In: *Energy Conversion and Management* 106 (2015), pp. 479–494.

[26] Bo Zhao et al. "Optimal sizing, operating strategy and operational experience of a stand-alone microgrid on Dongfushan Island". In: *Applied energy* 113 (2014), pp. 1656–1666.

[27] André Malheiro et al. "Integrated sizing and scheduling of wind/PV/diesel/battery isolated systems". In: *Renewable Energy* 83 (2015), pp. 646–657.

[28] Monaaf DA Al-Falahi, SDG Jayasinghe, and HJEC Enshaei. "A review on recent size optimization methodologies for standalone solar and wind hybrid renewable energy system". In: *Energy conversion and management* 143 (2017), pp. 252–274.

[29] SR Tito, TT Lie, and TN Anderson. "Optimal sizing of a wind-photovoltaic-battery hybrid renewable energy system considering socio-demographic factors". In: *Solar Energy* 136 (2016), pp. 525–532.

[30] Jackson John Justo et al. "AC-microgrids versus DC-microgrids with distributed energy resources: A review". In: *Renewable and sustainable energy reviews* 24 (2013), pp. 387–405.

[31] Hamid Reza Baghaee et al. “Reliability/cost-based multi-objective Pareto optimal design of stand-alone wind/PV/FC generation microgrid system”. In: *Energy* 115 (2016), pp. 1022–1041.

[32] Gang Ma et al. “Multi-objective optimal configuration method for a standalone wind–solar–battery hybrid power system”. In: *IET Renewable Power Generation* 11.1 (2017), pp. 194–202.

[33] Hassan Zahboune et al. “Optimal hybrid renewable energy design in autonomous system using Modified Electric System Cascade Analysis and Homer software”. In: *Energy conversion and management* 126 (2016), pp. 909–922.

[34] MH Nehrir et al. “A review of hybrid renewable/alternative energy systems for electric power generation: Configurations, control, and applications”. In: *IEEE transactions on sustainable energy* 2.4 (2011), pp. 392–403.

[35] Saeedeh Ahmadi and Shirzad Abdi. “Application of the Hybrid Big Bang–Big Crunch algorithm for optimal sizing of a stand-alone hybrid PV/wind/battery system”. In: *Solar Energy* 134 (2016), pp. 366–374.

[36] Ramin Hosseinalizadeh et al. “Economic sizing of a hybrid (PV–WT–FC) renewable energy system (HRES) for stand-alone usages by an optimization-simulation model: Case study of Iran”. In: *Renewable and Sustainable Energy Reviews* 54 (2016), pp. 139–150.

[37] John Twidell. *Renewable energy resources*. Routledge, 2021.

[38] Omar Ellabban, Haitham Abu-Rub, and Frede Blaabjerg. “Renewable energy resources: Current status, future prospects and their enabling technology”. In: *Renewable and sustainable energy reviews* 39 (2014), pp. 748–764.

[39] Miro Zeman. “Introduction to photovoltaic solar energy”. In: *Delft University of Technology* 2.6 (2003).

[40] Yonghong Kuang et al. “A review of renewable energy utilization in islands”. In: *Renewable and Sustainable Energy Reviews* 59 (2016), pp. 504–513.

[41] MS Hossain et al. “Role of smart grid in renewable energy: An overview”. In: *Renewable and Sustainable Energy Reviews* 60 (2016), pp. 1168–1184.

[42] Tze-Zhang Ang et al. “A comprehensive study of renewable energy sources: Classifications, challenges and suggestions”. In: *Energy Strategy Reviews* 43 (2022), p. 100939.

[43] Nathaniel Pearre and Lukas Swan. “Reimagining renewable electricity grid management with dispatchable generation to stabilize energy storage”. In: *Energy* 203 (2020), p. 117917.

[44] Anish Modi et al. “A review of solar energy based heat and power generation systems”. In: *Renewable and Sustainable Energy Reviews* 67 (2017), pp. 1047–1064.

[45] Bhubaneswari Parida, Selvarasan Iniyan, and Ranko Goic. “A review of solar photovoltaic technologies”. In: *Renewable and sustainable energy reviews* 15.3 (2011), pp. 1625–1636.

[46] HL Zhang et al. “Concentrated solar power plants: Review and design methodology”. In: *Renewable and sustainable energy reviews* 22 (2013), pp. 466–481.

[47] Rajmund Przybylak, Robert Sadourny, and Lawrence A Mysak. "The climate of the Arctic". In: (2003).

[48] Eyal Rotenberg and Dan Yakir. "Contribution of semi-arid forests to the climate system". In: *Science* 327.5964 (2010), pp. 451–454.

[49] Trevor Letcher. *Wind energy engineering: A handbook for onshore and offshore wind turbines*. Elsevier, 2023.

[50] Om Prakash Mahela and Abdul Gafoor Shaik. "Comprehensive overview of grid interfaced wind energy generation systems". In: *Renewable and Sustainable Energy Reviews* 57 (2016), pp. 260–281.

[51] International Renewable Energy Agency. *Renewable Power Generation Costs in 2019*. Tech. rep. International Renewable Energy Agency, 2020. URL: `https://www.irena.org/-/media/Files/IRENA/Agency/Publication/2020/Jun/IRENA_Power_Generation_Costs_2019.pdf`.

[52] Rui Xin Huang. *Ocean circulation: wind-driven and thermohaline processes*. Cambridge University Press, 2010.

[53] Antonio F de O Falcao. "Wave energy utilization: A review of the technologies". In: *Renewable and sustainable energy reviews* 14.3 (2010), pp. 899–918.

[54] AM Gorlov et al. "Tidal energy". In: *Elements of physical oceanography* (2001), pp. 103–108.

[55] N d Khan et al. "Review of ocean tidal, wave and thermal energy technologies". In: *Renewable and Sustainable Energy Reviews* 72 (2017), pp. 590–604.

[56] Vineet Kumar Singh and Sunil Kumar Singal. "Operation of hydro power plants-a review". In: *Renewable and Sustainable Energy Reviews* 69 (2017), pp. 610–619.

[57] Ibrahim Yüksel. "Hydropower for sustainable water and energy development". In: *Renewable and Sustainable Energy Reviews* 14.1 (2010), pp. 462–469.

[58] Paul Breeze. *Hydropower*. Academic Press, 2018.

[59] Shafiqur Rehman, Luai M Al-Hadhrami, and Md Mahbub Alam. "Pumped hydro energy storage system: A technological review". In: *Renewable and Sustainable Energy Reviews* 44 (2015), pp. 586–598.

[60] Mingxin Guo, Weiping Song, and Jeremy Buhain. "Bioenergy and biofuels: History, status, and perspective". In: *Renewable and sustainable energy reviews* 42 (2015), pp. 712–725.

[61] Amane Makino and Tadahiko Mae. "Photosynthesis and plant growth at elevated levels of CO2". In: *Plant and Cell Physiology* 40.10 (1999), pp. 999–1006.

[62] Annette Evans, Vladimir Strezov, and Tim J Evans. "Sustainability considerations for electricity generation from biomass". In: *Renewable and sustainable energy reviews* 14.5 (2010), pp. 1419–1427.

[63] Chunlan Mao et al. "Review on research achievements of biogas from anaerobic digestion". In: *Renewable and sustainable energy reviews* 45 (2015), pp. 540–555.

[64] Thushara Kandaramath Hari, Zahira Yaakob, and Narayanan N Binitha. "Aviation biofuel from renewable resources: Routes, opportunities and challenges". In: *Renewable and Sustainable Energy Reviews* 42 (2015), pp. 1234–1244.

[65] David JC MacKay. *Sustainable Energy-without the hot air*. Bloomsbury Publishing, 2016.

[66] Egbert Jolie et al. "Geological controls on geothermal resources for power generation". In: *Nature Reviews Earth & Environment* 2.5 (2021), pp. 324–339.

[67] Diego Moya, Clay Aldás, and Prasad Kaparaju. "Geothermal energy: Power plant technology and direct heat applications". In: *Renewable and Sustainable Energy Reviews* 94 (2018), pp. 889–901.

[68] Austin Anderson and Behnaz Rezaie. "Geothermal technology: Trends and potential role in a sustainable future". In: *Applied Energy* 248 (2019), pp. 18–34.

[69] William Zappa and Machteld Van Den Broek. "Analysing the potential of integrating wind and solar power in Europe using spatial optimisation under various scenarios". In: *Renewable and Sustainable Energy Reviews* 94 (2018), pp. 1192–1216.

[70] Dazhi Yang, Panida Jirutitijaroen, and Wilfred M Walsh. "Hourly solar irradiance time series forecasting using cloud cover index". In: *Solar Energy* 86.12 (2012), pp. 3531–3543.

[71] Graham Sinden. "Characteristics of the UK wind resource: Long-term patterns and relationship to electricity demand". In: *Energy policy* 35.1 (2007), pp. 112–127.

[72] Dominik Heide et al. "Seasonal optimal mix of wind and solar power in a future, highly renewable Europe". In: *Renewable Energy* 35.11 (2010), pp. 2483–2489.

[73] Lucy C Cradden et al. "A 34-year simulation of wind generation potential for Ireland and the impact of large-scale atmospheric pressure patterns". In: *Renewable energy* 106 (2017), pp. 165–176.

[74] Dirk Schindler, Hein Dieter Behr, and Christopher Jung. "On the spatiotemporal variability and potential of complementarity of wind and solar resources". In: *Energy conversion and management* 218 (2020), p. 113016.

[75] Jakub Jurasz et al. "A review on the complementarity of renewable energy sources: Concept, metrics, application and future research directions". In: *Solar Energy* 195 (2020), pp. 703–724.

[76] Tongtong Xu, Kevin A Haas, and Budi Gunawan. "Estimating annual energy production from short tidal current records". In: *Renewable Energy* 207 (2023), pp. 105–115.

[77] Khem Gyanwali, Ryoichi Komiyama, and Yasumasa Fujii. "Representing hydropower in the dynamic power sector model and assessing clean energy deployment in the power generation mix of Nepal". In: *Energy* 202 (2020), p. 117795.

[78] Adil Ahmed and Muhammad Khalid. "A review on the selected applications of forecasting models in renewable power systems". In: *Renewable and Sustainable Energy Reviews* 100 (2019), pp. 9–21.

[79] Stefan Pfenninger and Iain Staffell. "Long-term patterns of European PV output using 30 years of validated hourly reanalysis and satellite data". In: *Energy* 114 (2016), pp. 1251–1265.

[80] Thomas Huld et al. "Mapping the performance of PV modules, effects of module type and data averaging". In: *Solar Energy* 84.2 (2010), pp. 324–338.

[81] Barbara Ridley, John Boland, and Philippe Lauret. "Modelling of diffuse solar fraction with multiple predictors". In: *Renewable Energy* 35.2 (2010), pp. 478–483.

[82] Carsten Croonenbroeck and Georg Stadtmann. "Renewable generation forecast studies–Review and good practice guidance". In: *Renewable and Sustainable Energy Reviews* 108 (2019), pp. 312–322.

[83] Kadir Amasyali and Nora M El-Gohary. "A review of data-driven building energy consumption prediction studies". In: *Renewable and Sustainable Energy Reviews* 81 (2018), pp. 1192–1205.

[84] Amandeep Sharma and Ajay Kakkar. "Forecasting daily global solar irradiance generation using machine learning". In: *Renewable and Sustainable Energy Reviews* 82 (2018), pp. 2254–2269.

[85] U.S. Energy Information Administration. *Annual Energy Outlook 2023*. Report. U.S. Energy Information Administration, 2023.

[86] Elexon. *Load Profiles and their use in Electricity Settlement*. Report. Elexon, 2018.

[87] Ian Richardson et al. "Domestic electricity use: A high-resolution energy demand model". In: *Energy and buildings* 42.10 (2010), pp. 1878–1887.

[88] Aowabin Rahman, Vivek Srikumar, and Amanda D Smith. "Predicting electricity consumption for commercial and residential buildings using deep recurrent neural networks". In: *Applied energy* 212 (2018), pp. 372–385.

[89] Amy Pielow, Ramteen Sioshansi, and Matthew C Roberts. "Modeling short-run electricity demand with long-term growth rates and consumer price elasticity in commercial and industrial sectors". In: *Energy* 46.1 (2012), pp. 533–540.

[90] HyungBin Moon et al. "Forecasting electricity demand of electric vehicles by analyzing consumers' charging patterns". In: *Transportation Research Part D: Transport and Environment* 62 (2018), pp. 64–79.

[91] Ben Anderson and Jacopo Torriti. "Explaining shifts in UK electricity demand using time use data from 1974 to 2014". In: *Energy Policy* 123 (2018), pp. 544–557.

[92] Corentin Kuster, Yacine Rezgui, and Monjur Mourshed. "Electrical load forecasting models: A critical systematic review". In: *Sustainable cities and society* 35 (2017), pp. 257–270.

[93] Jan F Kreider, Peter S Curtiss, and Ari Rabl. *Heating and cooling of buildings: design for efficiency*. CRC Press, 2009.

[94] L Suganthi and Anand A Samuel. "Energy models for demand forecasting—A review". In: *Renewable and sustainable energy reviews* 16.2 (2012), pp. 1223–1240.

[95] Yun Bai et al. "Regression modeling for enterprise electricity consumption: A comparison of recurrent neural network and its variants". In: *International Journal of Electrical Power & Energy Systems* 126 (2021), p. 106612.

[96] Huaizhi Wang et al. "A review of deep learning for renewable energy forecasting". In: *Energy Conversion and Management* 198 (2019), p. 111799.

[97] Hussein Ibrahim, Adrian Ilinca, and Jean Perron. "Energy storage systems—Characteristics and comparisons". In: *Renewable and sustainable energy reviews* 12.5 (2008), pp. 1221–1250.

[98] Seama Koohi-Fayegh and Marc A Rosen. "A review of energy storage types, applications and recent developments". In: *Journal of Energy Storage* 27 (2020), p. 101047.

[99] AG Olabi et al. "Critical review of energy storage systems". In: *Energy* 214 (2021), p. 118987.

[100] Mathew Aneke and Meihong Wang. "Energy storage technologies and real life applications–A state of the art review". In: *Applied Energy* 179 (2016), pp. 350–377.

[101] Matthew L Lazarewicz and Alex Rojas. "Grid frequency regulation by recycling electrical energy in flywheels". In: *IEEE Power Engineering Society General Meeting, 2004.* IEEE. 2004, pp. 2038–2042.

[102] KC Divya and Jacob Østergaard. "Battery energy storage technology for power systems—An overview". In: *Electric power systems research* 79.4 (2009), pp. 511–520.

[103] Sam Koohi-Kamali, NA Rahim, and HJEC Mokhlis. "Smart power management algorithm in microgrid consisting of photovoltaic, diesel, and battery storage plants considering variations in sunlight, temperature, and load". In: *Energy Conversion and Management* 84 (2014), pp. 562–582.

[104] Manuel Götz et al. "Renewable Power-to-Gas: A technological and economic review". In: *Renewable energy* 85 (2016), pp. 1371–1390.

[105] S Ould Amrouche et al. "Overview of energy storage in renewable energy systems". In: *International journal of hydrogen energy* 41.45 (2016), pp. 20914–20927.

[106] AB Gallo et al. "Energy storage in the energy transition context: A technology review". In: *Renewable and sustainable energy reviews* 65 (2016), pp. 800–822.

[107] Poul Alberg Østergaard. "Reviewing optimisation criteria for energy systems analyses of renewable energy integration". In: *Energy* 34.9 (2009), pp. 1236–1245.

[108] Chun Sing Lai and Malcolm D. McCulloch. "Sizing of Stand-Alone Solar PV and Storage System With Anaerobic Digestion Biogas Power Plants". In: *IEEE Transactions on Industrial Electronics* 64.3 (2017), pp. 2112–2121.

[109] ELV Eriksson and E MacA Gray. "Optimization of renewable hybrid energy systems–A multi-objective approach". In: *Renewable energy* 133 (2019), pp. 971–999.

[110] Jijian Lian et al. "A review on recent sizing methodologies of hybrid renewable energy systems". In: *Energy Conversion and Management* 199 (2019), p. 112027.

[111] Raul Banos et al. "Optimization methods applied to renewable and sustainable energy: A review". In: *Renewable and sustainable energy reviews* 15.4 (2011), pp. 1753–1766.

[112] Hongxing Yang, Lin Lu, and Wei Zhou. "A novel optimization sizing model for hybrid solar-wind power generation system". In: *Solar Energy* 81.1 (2007), pp. 76–84.

[113] Bogdan S Borowy and Ziyad M Salameh. "Methodology for optimally sizing the combination of a battery bank and PV array in a wind/PV hybrid system". In: *IEEE Transactions on energy conversion* 11.2 (1996), pp. 367–375.

[114] Abdul Qayoom Jakhrani et al. "A novel analytical model for optimal sizing of standalone photovoltaic systems". In: *Energy* 46.1 (2012), pp. 675–682.

[115] Claudia Valéria Távora Cabral et al. "A stochastic method for stand-alone photovoltaic system sizing". In: *Solar Energy* 84.9 (2010), pp. 1628–1636.

[116] Xiangqi Zhu, Jiahong Yan, and Ning Lu. "A probabilistic-based PV and energy storage sizing tool for residential loads". In: *2016 IEEE/PES Transmission and Distribution Conference and Exposition (T&D)*. IEEE, 2016, pp. 1–5.

[117] Lorenzo Bartolucci et al. "Hybrid renewable energy systems for renewable integration in microgrids: Influence of sizing on performance". In: *Energy* 152 (2018), pp. 744–758.

[118] Yijie Zhang et al. "A techno-economic sizing method for grid-connected household photovoltaic battery systems". In: *Applied Energy* 269 (2020), p. 115106.

[119] Tao Ma, Hongxing Yang, and Lin Lu. "A feasibility study of a stand-alone hybrid solar–wind–battery system for a remote island". In: *Applied Energy* 121 (2014), pp. 149–158.

[120] Laith M. Halabi and Saad Mekhilef. "Flexible hybrid renewable energy system design for a typical remote village located in tropical climate". In: *Journal of Cleaner Production* 177 (2018), pp. 908–924.

[121] Ozan Erdinc and Mehmet Uzunoglu. "Optimum design of hybrid renewable energy systems: Overview of different approaches". In: *Renewable and Sustainable Energy Reviews* 16.3 (2012), pp. 1412–1425.

[122] Yuhui Shi et al. "Particle swarm optimization: developments, applications and resources". In: *Proceedings of the 2001 congress on evolutionary computation (IEEE Cat. No. 01TH8546)*. Vol. 1. IEEE. 2001, pp. 81–86.

[123] Melanie Mitchell. *An introduction to genetic algorithms*. MIT press, 1998.

[124] Junqin Xu and Jihui Zhang. "Exploration-exploitation tradeoffs in metaheuristics: Survey and analysis". In: *Proceedings of the 33rd Chinese control conference*. IEEE. 2014, pp. 8633–8638.

[125] Hongxing Yang, Zhou Wei, and Lou Chengzhi. "Optimal design and techno-economic analysis of a hybrid solar–wind power generation system". In: *Applied Energy* 86.2 (2009), pp. 163–169.

[126] Yang Zhang et al. "Comparative study of hydrogen storage and battery storage in grid connected photovoltaic system: Storage sizing and rule-based operation". In: *Applied Energy* 201 (2017), pp. 397–411.

[127] Yang Zhang et al. "Battery sizing and rule-based operation of grid-connected photovoltaic-battery system: A case study in Sweden". In: *Energy Conversion and Management* 133 (2017), pp. 249–263.

[128] Masoume Shabani et al. "Techno-economic comparison of optimal design of renewable-battery storage and renewable micro pumped hydro storage power supply systems: A case study in Sweden". In: *Applied Energy* 279 (2020).

[129] Pawan Saini and Lata Gidwani. "An investigation for battery energy storage system installation with renewable energy resources in distribution system by considering residential, commercial and industrial load models". In: *Journal of Energy Storage* 45 (2022), p. 103493.

[130] Dalila Fares, Mohamed Fathi, and Saad Mekhilef. "Performance evaluation of metaheuristic techniques for optimal sizing of a stand-alone hybrid PV/wind/battery system". In: *Applied Energy* 305 (2022), p. 117823.

[131] Akbar Maleki, Morteza Gholipour Khajeh, and Mehran Ameri. "Optimal sizing of a grid independent hybrid renewable energy system incorporating resource uncertainty, and load uncertainty". In: *International Journal of Electrical Power & Energy Systems* 83 (2016), pp. 514–524.

[132] Ruben Zieba Falama et al. "A techno-economic comparative study of renewable energy systems based different storage devices". In: *Energy* 266 (2023), p. 126411.

[133] Murtaza Farsadi, Tohid Sattarpour, and Amin Yazdani Nejadi. "Optimal placement and operation of BESS in a distribution network considering the net present value of energy losses cost". In: *2015 9th International Conference on Electrical and Electronics Engineering (ELECO)*. IEEE. 2015, pp. 434–439.

[134] Mohammad Rasol Jannesar et al. "Optimal placement, sizing, and daily charge/discharge of battery energy storage in low voltage distribution network with high photovoltaic penetration". In: *Applied energy* 226 (2018), pp. 957–966.

[135] Samart Salee and Paramet Wirasanti. "Optimal siting and sizing of battery energy storage systems for grid-supporting in electrical distribution network". In: *2018 International ECTI Northern Section Conference on Electrical, Electronics, Computer and Telecommunications Engineering (ECTI-NCON)*. IEEE. 2018, pp. 100–105.

[136] Mohamed Hashem et al. "A Bi-level optimizer for reliability and security assessment of a radial distribution system supported by wind turbine generators and superconducting magnetic energy storages". In: *Journal of Energy Storage* 51 (2022), p. 104356.

[137] Bogdan Constantin Neagu et al. "Optimal placement of energy storage systems in microgrids using a PSO based approach". In: *2019 IEEE PES Innovative Smart Grid Technologies Europe (ISGT-Europe)*. IEEE. 2019, pp. 1–5.

[138] Abolfazl Ghaffari, Alireza Askarzadeh, and Roohollah Fadaeinedjad. "Optimal allocation of energy storage systems, wind turbines and photovoltaic systems in distribution network considering flicker mitigation". In: *Applied Energy* 319 (2022), p. 119253.

[139] Farihan Mohamad, Jiashen Teh, and Ching-Ming Lai. "Optimum allocation of battery energy storage systems for power grid enhanced with solar energy". In: *Energy* 223 (2021), p. 120105.

[140] Mostafa Nick et al. "Optimal location and sizing of distributed storage systems in active distribution networks". In: *2013 IEEE grenoble conference*. IEEE, 2013, pp. 1–6.

[141] Kyri Baker, Gabriela Hug, and Xin Li. "Energy storage sizing taking into account forecast uncertainties and receding horizon operation". In: *IEEE Transactions on Sustainable Energy* 8.1 (2016), pp. 331–340.

[142] S. X. Chen, H. B. Gooi, and M. Q. Wang. "Sizing of Energy Storage for Microgrids". In: *IEEE Transactions on Smart Grid* 3.1 (2012), pp. 142–151.

[143] Raji Atia and Noboru Yamada. "Sizing and Analysis of Renewable Energy and Battery Systems in Residential Microgrids". In: *IEEE Transactions on Smart Grid* 7.3 (2016), pp. 1204–1213.

[144] Loiy Al-Ghussain et al. "Sizing renewable energy systems with energy storage systems in microgrids for maximum cost-efficient utilization of renewable energy resources". In: *Sustainable Cities and Society* 55 (2020), p. 102059.

[145] Subhonmesh Bose et al. "Optimal placement of energy storage in the grid". In: *2012 IEEE 51st IEEE Conference on Decision and Control (CDC)*. IEEE. 2012, pp. 5605–5612.

[146] Mohamed T Elsir et al. "Sizing and allocation for solar energy storage system considering the cost optimization". In: *2019 8th International Conference on Renewable Energy Research and Applications (ICRERA)*. IEEE, 2019, pp. 407–412.

[147] Chandrabhanu Opathella et al. "MILP formulation for generation and storage asset sizing and sitting for reliability constrained system planning". In: *International Journal of Electrical Power & Energy Systems* 116 (2020), p. 105529.

[148] Alvaro Avendaño Peña, David Romero-Quete, and Camilo A Cortes. "Sizing and siting of battery energy storage systems: A Colombian case". In: *Journal of Modern Power Systems and Clean Energy* 10.3 (2021), pp. 700–709.

[149] Mostafa Nick, Rachid Cherkaoui, and Mario Paolone. "Optimal allocation of dispersed energy storage systems in active distribution networks for energy balance and grid support". In: *IEEE Transactions on Power Systems* 29.5 (2014), pp. 2300–2310.

[150] Srinivas Bhaskar Karanki and David Xu. "Optimal capacity and placement of battery energy storage systems for integrating renewable energy sources in distribution system". In: *2016 National Power Systems Conference (NPSC)*. IEEE. 2016, pp. 1–6.

[151] Arun Rathore and NP Patidar. "Optimal sizing and allocation of renewable based distribution generation with gravity energy storage considering stochastic nature using particle swarm optimization in radial distribution network". In: *Journal of Energy Storage* 35 (2021), p. 102282.

[152] Tomas Markvart. "Sizing of hybrid photovoltaic-wind energy systems". In: *solar energy* 57.4 (1996), pp. 277–281.

[153] Minjian Cao et al. "Engineering energy storage sizing method considering the energy conversion loss on facilitating wind power integration". In: *IET Generation, Transmission & Distribution* 13.9 (2019), pp. 1693–1699.

[154] Pedro Bezerra Leite Neto, Osvaldo R Saavedra, and Luiz Antonio de Souza Ribeiro. "A dual-battery storage bank configuration for isolated microgrids based on renewable sources". In: *IEEE Transactions on Sustainable Energy* 9.4 (2018), pp. 1618–1626.

[155] P. Arun, Rangan Banerjee, and Santanu Bandyopadhyay. "Optimum Design of Diesel Generator Integrated Photovoltaic-Battery System". In: *Energy & Fuels* 24.12 (2010), pp. 6565–6575.

[156] Sonam Norbu and Santanu Bandyopadhyay. "Power Pinch Analysis for optimal sizing of renewable-based isolated system with uncertainties". In: *Energy* 135 (2017), pp. 466–475.

[157] Santanu Bandyopadhyay. "Design and optimization of isolated energy systems through pinch analysis". In: *Asia-Pacific Journal of Chemical Engineering* 6.3 (2011), pp. 518–526.

[158] Yasser F Nassar et al. "Dynamic analysis and sizing optimization of a pumped hydroelectric storage-integrated hybrid PV/Wind system: A case study". In: *Energy Conversion and Management* 229 (2021), p. 113744.

[159] Sofiane Kichou et al. "A simple and effective methodology for sizing electrical energy storage (EES) systems based on energy balance". In: *Journal of Energy Storage* 49 (2022), p. 104085.

[160] Panyawoot Boonluk et al. "Optimal Siting and Sizing of Battery Energy Storage Systems for Distribution Network of Distribution System Operators". In: *Batteries* 6.4 (2020).

[161] Tianming Gu et al. "Placement and capacity selection of battery energy storage system in the distributed generation integrated distribution network based on improved NSGA-II optimization". In: *Journal of Energy Storage* 52 (2022), p. 104716.

[162] KA Khan et al. "PKL electrochemical cell and the Peukert's law". In: *IJARIIE* 4.2 (2018), pp. 4219–4227.

[163] Ioannis Hadjipaschalis, Andreas Poullikkas, and Venizelos Efthimiou. "Overview of current and future energy storage technologies for electric power applications". In: *Renewable and Sustainable Energy Reviews* 13.6-7 (2009), pp. 1513–1522.

[164] Binson Babu. "Self-discharge in rechargeable electrochemical energy storage devices". In: *Energy Storage Materials* (2024), p. 103261.

[165] Pauli Virtanen et al. "SciPy 1.0: fundamental algorithms for scientific computing in Python". In: *Nature methods* 17.3 (2020), pp. 261–272.

[166] G Vennam, A Sahoo, and S Ahmed. "A survey on lithium-ion battery internal and external degradation modeling and state of health estimation". In: *Journal of Energy Storage* 52 (2022), p. 104720.

[167] John Wang et al. "Cycle-life model for graphite-LiFePO4 cells". In: *Journal of power sources* 196.8 (2011), pp. 3942–3948.

[168] Reza Fallahifar and Mohsen Kalantar. "Optimal planning of lithium ion battery energy storage for microgrid applications: Considering capacity degradation". In: *Journal of Energy Storage* 57 (2023), p. 106103.

[169] Greg Albright, Jake Edie, and Said Al-Hallaj. "A comparison of lead acid to lithium-ion in stationary storage applications". In: *Published by AllCell Technologies LLC* (2012).

[170] E Cabrera Castillo. "Standards for electric vehicle batteries and associated testing procedures". In: *Advances in Battery Technologies for Electric Vehicles*. Elsevier, 2015, pp. 469–494.

[171] Elexon. *Elexon Load Profile*. 2019. URL: `https://data.ukedc.rl.ac.uk/browse/edc/efficiency/residential/LoadProfile`.

[172] Department for Business Energy and Industrial Strategy. *Regional and local authority electricity consumption statistics*. 2023. URL: `https://www.gov.uk/government/statistics/regional-and-local-authority-electricity-consumption-statistics`.

[173] Office for National Statistics. *UK business; activity, size and location: 2019*. 2019. URL: `https://www.ons.gov.uk/businessindustryandtrade/business/activitysizeandlocation/bulletins/ukbusinessactivitysizeandlocation/2019`.

[174] BEIS. *Energy Consumption in the UK (ECUK) 1970 to 2021*. Report. Department for Business, Energy & Industrial Strategy, 2022.

[175] Vincenzo Bianco, Oronzio Manca, and Sergio Nardini. "Electricity consumption forecasting in Italy using linear regression models". In: *Energy* 34.9 (2009), pp. 1413–1421.

[176] Mark Z Jacobson and Vijaysinh Jadhav. "World estimates of PV optimal tilt angles and ratios of sunlight incident upon tilted and tracked PV panels relative to horizontal panels". In: *Solar Energy* 169 (2018), pp. 55–66.

[177] Han Kun Ren et al. "An analytical method for sizing energy storage in microgrid systems to maximize renewable consumption and minimize unused storage capacity". In: *Journal of Energy Storage* 68 (2023), p. 107735.

[178] National Renewable Energy Laboratory. *2021 Annual Technology Baseline (ATB) Cost and Performance Data for Electricity Generation Technologies*. 2021. URL: `https://data.openei.org/submissions/4129`.

[179] Open Power System Data. *Load, wind and solar, prices in hourly resolution*. 2019. URL: `https://data.open-power-system-data.org/time_series`.

[180] Stephen Frank and Steffen Rebennack. "An introduction to optimal power flow: Theory, formulation, and examples". In: *IIE transactions* 48.12 (2016), pp. 1172–1197.

[181] Kong Soon Ng et al. "Enhanced coulomb counting method for estimating state-of-charge and state-of-health of lithium-ion batteries". In: *Applied energy* 86.9 (2009), pp. 1506–1511.

[182] Probability Methods Subcommittee. "IEEE reliability test system". In: *IEEE Transactions on power apparatus and systems* PAS-98.6 (1979), pp. 2047–2054.

[183] Christos Ordoudis et al. "An updated version of the IEEE RTS 24-bus system for electricity market and power system operation studies". In: *Technical University of Denmark* 13 (2016).

[184] Ray Daniel Zimmerman, Carlos Edmundo Murillo-Sánchez, and Robert John Thomas. "MATPOWER: Steady-state operations, planning, and analysis tools for power systems research and education". In: *IEEE Transactions on power systems* 26.1 (2010), pp. 12–19.

[185] Iain Staffell and Stefan Pfenninger. "Using bias-corrected reanalysis to simulate current and future wind power output". In: *Energy* 114 (2016), pp. 1224–1239.

[186] Leon Thurner et al. "pandapower—an open-source python tool for convenient modeling, analysis, and optimization of electric power systems". In: *IEEE Transactions on Power Systems* 33.6 (2018), pp. 6510–6521.

[187] Han Kun Ren, Malcolm McCulloch, and David Wallom. "Optimal sizing of solar photovoltaic and lithium battery storage to reduce grid electricity reliance in buildings". In: *2022 ECEEE Summer Study*. Ed. by Horia Petran. ECEEE, 2022, pp. 1199–1208.

[188] Paul Denholm and Maureen Hand. "Grid flexibility and storage required to achieve very high penetration of variable renewable electricity". In: *Energy Policy* 39.3 (2011), pp. 1817–1830.

[189] Thomas H Cormen et al. *Introduction to algorithms*. MIT press, 2022.

[190] Hussein Baher. *Analog and digital signal processing*. John Wiley & Sons, 2001.

[191] Thongchart Kerdphol, Yaser Qudaih, and Yasunori Mitani. "Battery energy storage system size optimization in microgrid using particle swarm optimization". In: *IEEE PES Innovative Smart Grid Technologies, Europe*. IEEE. 2014, pp. 1–6.

[192] Xuebing Han et al. "A review on the key issues of the lithium ion battery degradation among the whole life cycle". In: *ETransportation* 1 (2019), p. 100005.

[193] Chang Liu, Yujie Wang, and Zonghai Chen. "Degradation model and cycle life prediction for lithium-ion battery used in hybrid energy storage system". In: *Energy* 166 (2019), pp. 796–806.

[194] Asmae Berrada and Khalid Loudiyi. "Operation, sizing, and economic evaluation of storage for solar and wind power plants". In: *Renewable and sustainable energy Reviews* 59 (2016), pp. 1117–1129.

[195] Anita Seervi et al. "Renewable Energy Forecasting for Energy Storage Sizing: A Review". In: *2021 IEEE International Conference on Intelligent Systems, Smart and Green Technologies (ICISSGT)*. IEEE. 2021, pp. 134–139.

[196] Lu Peng et al. "Effective long short-term memory with differential evolution algorithm for electricity price prediction". In: *Energy* 162 (2018), pp. 1301–1314.

[197] Stephen P Boyd and Lieven Vandenberghe. *Convex optimization*. Cambridge University Press, 2004.

[198] Haifeng Liu, Leigh Tesfatsion, and AA Chowdhury. "Locational marginal pricing basics for restructured wholesale power markets". In: *2009 IEEE Power and Energy Society General Meeting (PESGM)*. IEEE. 2009, pp. 1–8.

[199] Jun Hao et al. "Locational marginal pricing in the campus power system at the power distribution level". In: *2016 IEEE Power and Energy Society General Meeting (PESGM)*. IEEE. 2016, pp. 1–5.

[200] Ling Ai Wong et al. "Review on the optimal placement, sizing and control of an energy storage system in the distribution network". In: *Journal of Energy Storage* 21 (2019), pp. 489–504.